Exploring the Role of Neuropilin Receptors and Semaphorin-3F in Oral Squamous Cell Carcinoma

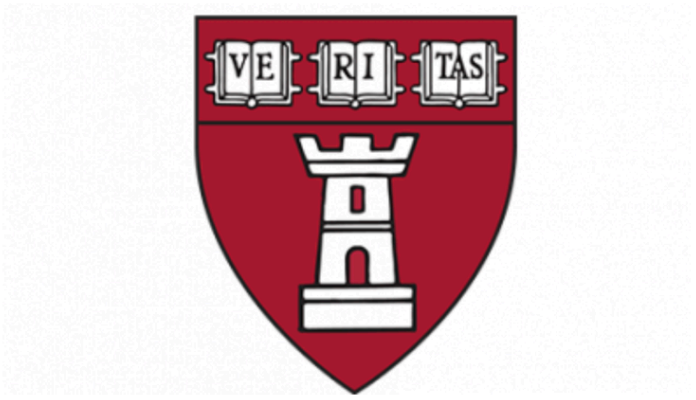

HARVARD UNIVERSITY
SCHOOL OF DENTAL MEDICINE
DEPARTMENT OF ORAL MEDICINE, INFECTION AND IMMUNITY

A Thesis Presented by

Asma Almazyad

to
The Faculty of Medicine
In partial fulfillment of the requirements
for the degree of
Doctor of Dental Medicine

Research Mentor: Dr. Diane R. Bielenberg, Ph.D.
Boston Children's Hospital/Harvard Medical School

Harvard School of Dental Medicine
Boston, Massachusetts

April 21, 2020

Table of Contents

To my mother and my sister Khawlah;
Your sacrifices are the reason I got here!

“Exploring the Role of Neuropilin Receptors and Semaphorin-3F in Oral Squamous Cell Carcinoma”

Abstract: Oral squamous cell carcinoma (OSCC) is the most common cancer in the oral cavity with a 5-year survival rate of only 38% in metastatic cases. OSCC dissemination is correlated with enhanced tumor angiogenesis and lymphangiogenesis. Neuropilin 1 and 2 are membrane receptors in endothelial cells (EC) that bind to angiogenic factors (VEGF-A) and lymphangiogenic factors (VEGF-C and VEGF-D), respectfully, and complex with VEGFR1-3 to stimulate the sprouting of blood and lymphatic vessels during developmental angiogenesis and lymphangiogenesis. In addition to EC, tumor cells also express Neuropilin (NRP) receptors but whether NRPs can signal via VEGF ligands in tumor cells lacking VEGFRs and what role either NRP1 or NRP2 plays in the tumorigenesis process is unclear. I hypothesize that NRP1 expression in oral epithelial cells promotes survival in physiologic conditions and tumor initiation or tumor growth (either directly or indirectly by enhancing angiogenesis) during pathologic (carcinogenic) conditions. I hypothesize that NRP2 expression promotes carcinoma progression either directly by increasing tumor cell motility or indirectly by increasing microvessel density in the tumor microenvironment thereby increasing the chances of dissemination. Our laboratory has reported NRP1 upregulation in human and mouse oral dysplasia and OSCC samples. One of my aims is to expand our analysis to examine NRP2 expression in human and mouse normal oral mucosa, oral dysplasia and OSCC samples. NRP2 has an alternative ligand called Semaphorin-3F (SEMA3F) that competes with VEGF binding and inhibits angiogenesis, lymphangiogenesis, and cell

motility. Another aim will examine the expression of SEMA3F in human and mouse normal oral mucosa and OSCC samples with the prediction that SEMA3F will be lost during tumor progression. In order to characterize the necessity of the *Nrp1*, *Nrp2*, or *Sema3F* genes in keratinocytes during the tumorigenesis process, Cre-Lox technology will be used to conditionally delete each gene in the oral mucosa followed by chemical (4-NQO) induction of carcinogenesis in mice. Lastly, novel preclinical trials using SEMA3F protein for the first time will be examined in human and mouse OSCC models. Taken together, my results demonstrate that normal oral epithelium expresses both NRP1 receptor and SEMA3F ligand in the suprabasal layers and lacks expression of NRP2. During dysplasia and OSCC, NRP1 and NRP2 are both upregulated and SEMA3F expression is downregulated. *In vivo* carcinogenesis experiments in specific knockout mice revealed striking findings and demonstrated that Nrp1 expression was essential to cancer initiation in the oral epithelium as K14Nrp1iKO mice failed to develop any dysplasia or OSCC in the 4-NQO model. Nrp2 expression appeared to contribute more to tumor growth and progression as K14iNrp2KO mice developed fewer and smaller OSCC than control groups. My results surrounding the effects of SEMA3F suggest that its bioactivity may be more complex than initially anticipated. *In vitro,* exogenous SEMA3F inhibited the migration and invasion of Nrp2-expressing mouse OSCC cells (WT3). *In vivo*, slow-release mini osmotic pumps releasing exogenous SEMA3F systemically (0.3 mg/kg/day) inhibited human OSCC tumor-associated angiogenesis and lymphangiogenesis compared to control treated tumors. Over the course of just 2 weeks, systemic exogenous SEMA3F protein therapy induced complete regression in immunocompetent mice in the majority of mice with established mouse OSCC. In

contrast, SEMA3F therapy did not induce regression of OSCC in immunodeficient mice, but did slow OSCC growth and progression. Results examining the role of endogenous Sema3F in keratinocytes were more confounding. Whereas oral epithelial cells in wildtype mice undergoing carcinogenesis were found to downregulate endogenous Sema3F expression during dysplasia, mice depleted in *Sema3F* fail to develop OSCC tumors after 4-NQO treatment. These results suggest that endogenous *Sema3F* expression actually promotes carcinogenesis, likely via an indirect paracrine effect on another cell type in expressing Nrp2 in the oral mucosa such as melanocytes, dendritic cells, or T cells. Overall, I have identified NRP2 as a novel target in OSCC and its associated vasculature. Our 4-NQO models in transgenic mice showed both NRPs and SEMA3F to play key roles in OSCC initiation and progression. SEMA3F is a promising anti-tumor therapy specifically targeting the NRP2 axis in carcinoma cells and stromal cells, but future studies will be needed to uncover its role in tumor immunity.

Introduction:

Oral Squamous Cell Carcinoma:

Oral cancer is a relatively common compared to other sites of the head and neck region, e.g., hypopharynx, nasopharynx and lip.(1) The majority of oral cancers (90%) are OSCC.(2) OSCC is the 6th most common cancer worldwide with the highest incidence rate in southern Asia and one of the leading causes of cancer death in men in some countries such as India and Sri Lanka.(3) In the United States, OSCC is a serious health issue with an estimate of 35,130 new cases and 7,100 deaths in 2020.(4) OSCC occurs in patients mainly in their 6th to 8th decades with a male predilection (2:1); however, there is an increased incidence in the younger population and female gender in recent years.(2, 5) The most recognized risk factors for OSCC is tobacco smoking and alcohol use.(6) Other risk factors of OSCC include areca nut habit (a common practice in part of South East Asia where individuals chew areca nuts wrapped in betel leaf for 16-24 hours daily), history of caner, radio/chemotherapy, family history, history of autoimmune diseases, and prolonged immunosuppression.(7) Additionally, patients with Plummer-Vinson syndrome, a rare iron deficiency anemia disorder associated with esophageal webs, glossitis, and cheilitis, are at high risk of developing OSCC as well as pharyngeal carcinoma. Genetic disorders such as Fanconi anemia and dyskeratosis congenita predispose affected patients to develop OSCC at young age.(7) OSCC commonly occurs in the nonkeratinizing mucosa of the oral cavity such as ventral/lateral tongue, floor of the mouth and soft palate.(8, 9) Premalignant lesions such as leukoplakia or erythroplakia usually proceed the development of OSCC (**Figure 1**).(10) For example, studies found about 8-60% of leukoplakia have epithelial dysplasia, carcinoma in situ or invasive OSCC at the

first biopsy with about 1-3% annual malignant transformation.(11, 12) OSCC is diagnosed initially by visual examination; however, histopathology examination is necessary to confirm the diagnosis and imaging (Computed Tomography and Magnetic Resonance Imaging scans) is essential for tumor staging.(2)

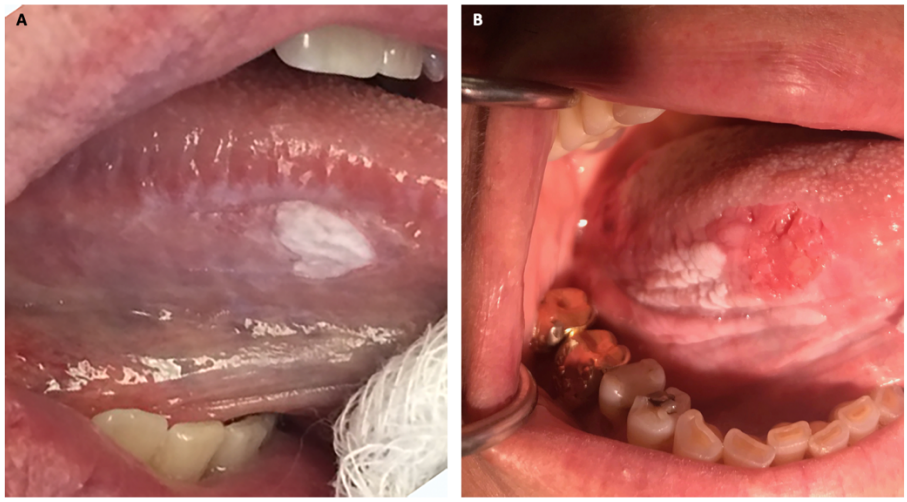

Figure 1. A. Well demarcated leukoplakia present in the right lateral tongue; biopsy was obtained and showed dysplasia. **B.** Both leukoplakia and erythroplakia (erythroleukoplakia) present in the right lateral tongue; biopsy was obtained and showed OSCC. Photos taken with patient consent (Almazyad, unpublished 2020).

Recently, the 8th edition of the American Joint Committee on Cancer Staging System updated the staging for oral cancer, which includes Tumor size (T), lymph node status (N) and distant metastasis (M). Some of the most significant changes in oral cancer staging include taking into account the depth of invasion in terms of tumor size and the extra-capsular extension of tumor cells in a positive lymph node.(13) The standard treatment of operable head and neck squamous cell carcinoma (HNSCC) is surgical resection with post-operative radiotherapy. However, concomitant chemotherapy-enhanced radiation was found to be beneficial for patients with positive microscopic surgical margin or positive lymph node with extra-capsular extension.(14) Until recently, first-line treatment of recurrent or metastatic HNSCC consisted of platinum-based

chemotherapy and Cetuximab (EGFR monoclonal antibody); while immune checkpoint inhibitors such as Nivolumab or Pembrolizumab (both anti-PD1 monoclonal antibodies) were only used for refractory cases. However, in 2019, the U.S. Food and Drug Administration (FDA) approved pembrolizumab for un-operable recurrent or metastatic HNSCC as first-line treatment, in combination with platinum and fluorouracil chemotherapy.(15)

Despite the advancements in treatment modalities, there has been only moderate improvement in the mean overall survival rate for all stages of OSCC, from 68% to 52% over the last 40 years.(16) In addition, the survival rate drops to 39% with regional and distant metastasis. Unfortunately, the majority of OSCC patients (67%) present with regional or distant metastasis.(17) Numerous studies have shown that cervical lymph node metastasis is the preferential route of tumor dissemination and a major negative prognostic factor for OSCC.(18) In fact, clinico-pathological studies suggested that node status is the most important prognostic factor for HNSCC.(19) A large series of HNSCC were reviewed to study the significance of lymph node density (ratio between the number of positive lymph nodes to the number of total excised lymph nodes) in relation to patients' prognosis and survival. High lymph node density of cut point value range of 6-14% is inversely related to overall survival and disease-specific survival rates.(20-22) Moreover, one study concluded that a cut point of value > 20% is highly suggestive of patients' death, locoregional recurrence as well as subclinical residual disease.(23) As such, addition of neoadjuvant targeted therapy to prevent or shrink local lymph node metastasis will likely improve mortality and morbidity of OSCC patients.

Tumor Angiogenesis:

Tumor angiogenesis is the process of sprouting new blood vessels from existing vessels within and around the tumor mass and is essential for substantial tumor growth and metastasis.(24) It has been established that tumor growth beyond 1-2 mm^3 in volume is angiogenesis dependent.(25) Even before the first angiogenesis factor was isolated, Judah Folkman theorized that tumor cells secreted a factor to attract blood vessels and if this factor could be blocked then tumor growth could be inhibited.(26) After the subsequent isolation and purification of specific angiogenesis factors (such as basic fibroblast growth factor (bFGF) and Vascular endothelial growth factor (VEGF)) in the 1980s, research on tumor angiogenesis and angiogenesis blockers bloomed with thousands of publications now available.(27) The fact that solid tumor growth is angiogenesis dependent is now dogma and seldom disputed.(25) This has led to the development of many angiogenesis inhibitors. Although not the first angiogenesis inhibitor, bevacizumab (humanized antibody against VEGF-A) is one of the most recognized angiogenesis inhibitors that was FDA-approved first for colon cancer and subsequently for other cancers.(28) Like all malignant tumors, OSCC requires angiogenesis to grow and disseminate.(29) Many studies confirm that VEGF levels are increased in OSCC and correlate with metastasis and worse prognosis.(30) Many clinical trials have tested angiogenesis inhibitors in combination with chemotherapy, radiation, or targeted therapy such as EGFR inhibitors in metastatic and recurrent HNSCC.(31-34) However, most trials to date have shown low to modest overall benefit. In addition, most of the published or ongoing studies have focused on VEGF antibodies or VEGF receptor

tyrosine kinase inhibitors. As such, there is still an urgent need for improved anti-angiogenesis drugs for OSCC.(35)

Tumor Lymphangiogenesis:

The lymphatic system and lymphangiogenesis has gained attention in cancer and vascular biology fields in the past 20 years. Since the identification of specific markers for lymphatic endothelial cells (such as podoplanin, Prox1 and LYVE1), both clinical and experimental research in this field has been growing tremendously.(36-38) Previously, tumor-associated lymphatic vessels were thought to be bystanders and have no active role in tumor metastasis. However, animal models and experiments with human cell lines have shown that tumor cells induce lymphangiogenesis in numerous cancer types.(39, 40) Additionally, studies of tumor dissemination have revealed a key role for cancer cell trafficking through lymphatic vessels.(41) Tumor lymphangiogenesis is the sprouting or enlargement of lymphatic capillaries into the tumor bed or around the tumor periphery.(42) High intra-tumoral lymphatic vessel density was found to be associated with positive lymph node status, aggressive tumor behavior and low survival rate in OSCC.(43) Additionally, peri-tumoral lymphatic endothelial cells often proliferate to increase their vessel luminal diameter even if they do not sprout into the tumor parenchyma.(44) Unlike blood capillaries, lymphatic capillaries lack a basement membrane and have gaps within the endothelium to allow the influx of fluid and cells (either immune cells or metastatic tumor cells).(42) Collectively, there is convincing evidence that tumor-associated lymphangiogenesis has a significant impact on tumor metastasis in many human cancers including OSCC. There are many promising agents that target mainly lymphatic pathway

(such as VEGF-C) tested in different cancer models *in vivo* and *in vitro* but none of them were approved to patient care.(45, 46) Thus, development of anti-lymphangiogenic agents may be a potential targeted therapy that could be used along with anti-angiogenic drugs to improve therapeutic outcome.

Neuropilin Receptors:

The Neuropilins (NRPs) are transmembrane glycoproteins that are abundantly expressed in ECs during embryogenesis, inflammation and cancer.(47, 48) There are two NRP proteins: NRP1 and NRP2. The human *NRP* genes share 45% homology and are located on chromosome 10 and 2 respectively.(49) Both NRPs have similar protein structure with 5 extracellular domains (a1, a2, b1, b2, and c), a transmembrane domain and a short cytoplasmic domain (**Figure 2**).(47) The a and b domains are thought to be involved in ligand binding while the c domain aids in dimerization. In ECs, NRPs are well known for binding different members of the VEGF family and complexing with VEGF receptor tyrosine kinases (VEGFR1-3), thereby enhancing both angiogenic and lymphagiogenic signaling (**Figure 3**).(50) NRPs cannot signal directly upon binding to VEGFs and do not possess tyrosine kinase activity on their own. NRP1 and NRP2 have primarily non-overlapping expression patterns in tissues. For instance, NRP1 is expressed in arterial ECs while NRP2 is expressed in venous and lymphatic ECs.(47) Although NRP1 is expressed in epithelial cells and carcinoma cells in addition to endothelial cells, (51, 52) NRP2 expression is not well characterized, and the function of either NRP in epithelial cells is unclear.

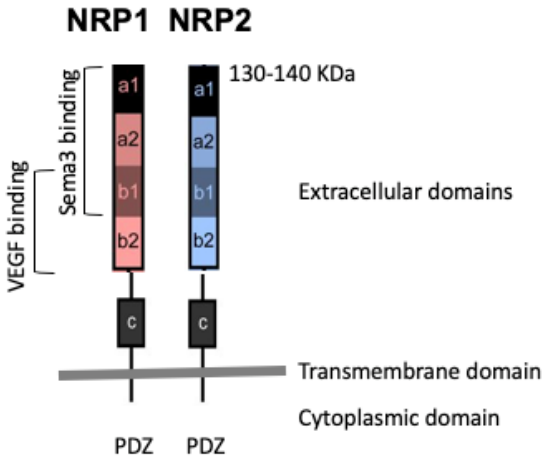

Figure 2. Illustration of the extracellular domain structure of Neuropilin 1 and 2. The two NRP receptors share high homology and share some ligands such as VEGFA, while they differ in other ligands. For example, NRP1 binds SEMA3A and NRP2 binds SEMA3F.

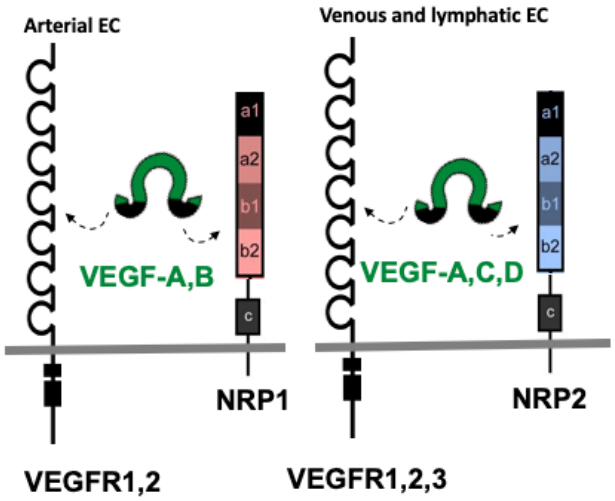

Figure 3. Neuropilins act as co-receptors for VEGF family proteins with VEGFRs. NRP1 can bind VEGF-A or –B, while NRP2 binds VEGF-A, -C or –D.

NRP1 was first identified by Fujisawa in 1987 as an antigen that binds to A5 monoclonal antibody located in the cell surface in the optic tectum of Tadpole brain.(53) Subsequently, Nrp1 was considered as a growth-promoting factor and adhesion molecule in the developing nervous system in xenopus and chicken.(54, 55) Further studies found the critical role Nrp1 plays in neural and cardiovascular development; as both overexpression and knock down models in mice were embryonic lethal with neural and cardiovascular anomalies.(56, 57) Soker, et. al., were the first to clone NRP1 from tumor cells and recognize the ability of NRP1 to bind to VEGF-A_{165} and to enhance VEGFR2 phosphorylation.(50) Additionally, NRP1 was found to be a receptor to other growth factors such as placenta growth factor 2, HGF and VEGF-B.(58) NRP1 is expressed in both sensory and sympathetic neurons and arterial ECs during development to mediate

the guidance of axons and vessels.(47) Other cells expressing NRP1 include skin and oral keratinocytes and carcinomas of the breast, kidney and prostate.(51, 52, 59-61) Clinicopathological studies showed correlation between NRP1 expression and worse prognosis using human samples or the Cancer Genome Atlas in gastric cancer, cervical cancer, hepatocellular carcinoma as well as glioma.(62-65) Previous studies in the Bielenberg lab indicated that NRP1 is expressed in both epidermis and epithelium of the oral cavity in the differentiated keratinocytes.(52) Additionally, NRP1 expression was upregulated in cutaneous squamous cell carcinoma as well as OSCC.(51, 66) There are no solid clinicopathological studies correlating NRP1 expression with OSCC tumor behavior. However, one study showed human OSCC cell lines transfected with NRP1 exhibited increased epithelial-to-mesenchymal transition.(67) Consistent with that, treating human OSCC cell lines *in vitro* with the NRP1 inhibitory ligand, Semaphorin-3A, resulted in reduced tumor cell motility.(51) Although there is abundant descriptive data using immunohistochemistry (IHC) to suggest that NRP1 expression correlates with tumor stage in different cancers, there are few functional studies investigating the mechanism for this correlation. To my knowledge, only one study has investigated tumor initiation in *Nrp1*-deficient mice. The study showed that when *Nrp1* was knocked out in epidermal cells (using a constitutive Keratin-14 promoter driven cre) and then exposed to a single dose of carcinogen (DMBA) followed by 25 weeks of the tumor promoter TPA, only 20 % of mice developed skin tumors compared to 100% of control mice.(68) Another study found that silencing of NRP1 in a human cutaneous squamous cell carcinoma cell line inhibited cell proliferation suggesting an autocrine function for the VEGF/NRP1 axis in cancer cells.(69) Additionally, their data suggested that VEGF-A signaling through

NRP1 (in the absence of VEGF RTK) in human skin cancer cells was mediated through GIPC1/Syx complex and RhoA activation.(69)

Ten years after the discovery of NRP1, NRP2 was discovered as a class 3 Semaphorin (SEMA3) receptor in embryonic mouse and rat tissues.(70, 71) Similar to NRP1, NRP2 mediates axonal guidance and is expressed in sympathetic neurons during development. (72, 73) NRP2 is unique in that it is expressed in lymphatic and venous ECs during development and binds the angiogenic ligand, VEGF-A, as well as the lymphangiogenic ligands VEGF-C and VEGF-D.(47) *Nrp2*-deficient mice are viable but smaller in size at birth and have reduced lymphatic vessel numbers.(74, 75) Other cells express NRP2 as well including melanocytes, visceral smooth muscle cells, and many tumor cells such as melanoma, glioblastoma and neuroblastoma.(42, 47) Recently, many studies have demonstrated NRP2 expression in epithelial malignancies as well. NRP2 overexpression was associated with advanced tumor stage and poor prognosis in breast carcinoma, bladder carcinoma, hepatocellular carcinoma, and gastric carcinoma.(76-79) Interestingly, Zhang, et. al., reported NRP2 overexpression correlated with advanced tumor stage, lymph vessel density and lymph node metastasis in OSCC.(80) Although NRP1 expression has been investigated in epithelial cells in various tissues including the oral cavity specifically, little attention has been given to NRP2 expression in normal oral epithelium or OSCC.(51, 81) In normal cutaneous epidermis, Nrp2 expression was restricted to melanocytes in the hair follicle in mice and was absent in keratinocytes.(47) To my knowledge, in the literature there are no published data regarding NRP2 expression in normal oral epithelium. Recent clinicopathological studies have shown that

a large subset of OSCC express NRP2, which was significantly associated with high metastatic potential.(80, 82) Although the data presented in these studies are promising, there were no controls (normal oral epithelium VS OSCC) and neither of the studies take in account NRP2 expression in oral dysplasia (pre-malignant condition). As such, differential NRP2 expression in normal oral epithelium, oral dysplasia and OSCC in mouse and human models is not well studied and needs further characterization.

Many preclinical studies have suggested that molecular signal transduction pathways contributing to lymphangiogenesis can be targeted to prevent lymph node metastasis as an alternative or additional therapy.(83) The most extensively investigated lymphangiogenic signal transduction pathway in cancer metastasis is the VEGF-C/VEGF-D/VEGFR3 signaling axis.(84) VEGF-C and VEGF-D were found to be overexpressed in many cancer models and significantly contribute to lymph node metastasis.(40, 85) Clinicopathological studies link overexpression of VEGF-C or VEGF-D in several human cancers such as breast, colorectal and ovarian cancer with negative prognostic impact and increased tumor metastatic potential.(86-88) Mortia, et. al., found that approximately 50% of OSCC express VEGF-C and its expression positively correlated with lymph node metastasis.(89) The growth factors VEGF-C and VEGF-D bind to VEGFR3 and induce survival, proliferation and migration of lymphatic endothelial cells via mitogen activated protein (MAP) kinase and phosphatidylinositol 3 (PI3) kinase intercellular signaling pathways.(90) Therefore, the VEGF-C/VEGF-D/VEGFR3 signaling axis is an attractive cascade to target to block lymphangiogenesis. Humanized IgG antibody against VEGFR3 (IMC-3C5) and fully humanized VEGF-C neutralizing antibody (VGX-100) showed

reduced tumor lymphangiogenesis and metastasis in preclinical studies. (91) NRP2 is a co-receptor in the VEGF-C/VEGF-D/VEGFR3 signaling axis and essential for lymphangiogenesis.(92) The coupling action of NRP2 with VEGF-C and -D increases affinity to VEGFR-3, enhances VEGFR3 phosphorylation and provokes pronounced lymphangiogenic response.(93) VEGFR3 is ubiquitously expressed on all lymphatic endothelial cells, therefore targeting this receptor may show side effects in normal lymphatic vessels. NRP2, on the other hand, is downregulated after birth and adult vascular and lymphatic capillaries do not express NRP2 constitutively. However, NRP2 is dramatically upregulated during inflammation (48), ischemia (94), and during tumor (lymph)angiogenesis [Bielenberg lab, unpublished data] (**Figure 4**).

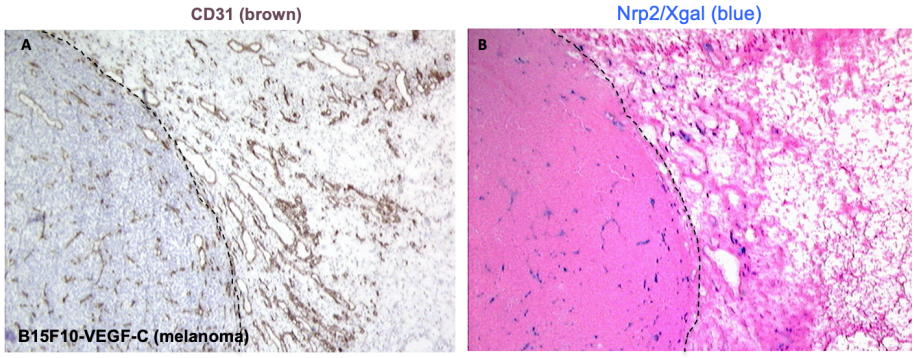

Figure 4: A. IHC of CD31 (an endothelial cell marker) highlights blood vessel infiltration in melanoma cell line (B15F10-VEGF-1C) implanted in $Nrp^{+/-}$ transgenic adult mice**. B.** X-gel staining for Nrp2 shows a subset of blood vessels express Nrp2 in the same section of melanoma (B15F10-VEGF-1C) in **4A**. [Bielenberg lab, unpublished data].

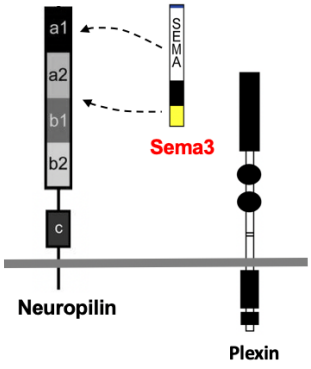

Figure 5. Neuropilins also bind the class 3 semaphorin (SEMA3) proteins. SEMA3 proteins bind to the a and b domains of NRPs and the SEMA3/NRP complex then signals through Plexin receptors.

Semaphorins:

Another family of ligands for NRPs are the class 3 Semaphorins (SEMA3).(47) In total, the whole Semaphorin family consists of eight different classes (consisting of 22 proteins) with only classes 3-7 found in vertebrates.(95) SEMA3 is the only class that exists in a secreted form; other semaphorins are membrane-bound proteins that require proteolytic cleavage to be shed.(96) SEMA3 proteins consist of multiple domains including a 500 amino acid N-terminal sema domain, a plexin-semaphorin-integrin domain, an immunoglobulin-like domain and a C-terminal basic domain.(95) The NRP/SEMA3 complex then interacts with another receptor family called plexins to transmit the signal into the cell (**Figure 5**).(95) There are seven SEMA3 proteins (SEMA3A-G) which vary in ligand binding specificity to either NRP1 or NRP2 and in their tissue distribution pattern. SEMA3A exclusively binds to NRP1. SEMA3F binds to NRP1 and NRP2, but is only functional through NRP2.(70) Both VEGF and SEMA3 bind to NRPs in competitive manner due the overlapping binding sites of SEMA3 and VEGF in NRPs-domain B with similar affinity.(97, 98) Both SEMA3A and SEMA3F have been reported to have an inhibitory effect on EC proliferation and migration.(97, 99, 100) SEMA3 can inhibit EC in two ways: it can compete with VEGFs to block their stimulatory function or it can directly bind NRP and Plexin (regardless of the presence of VEGF) and signal to inhibit EC.(101) SEMA3F, for example, binds directly to NRP2, then the SEMA3F/NRP2 complex signals through PlexinA1 to inhibit AKT phosphorylation and RhoA activation and inhibits EC or tumor cell motility (**Figure 6**).(102) Additionally, studies that have sought to elucidate the cellular source of endogenous SEMA3F agree that the epithelium appears to be the primary cell type to secrete this ligand.(48, 103)

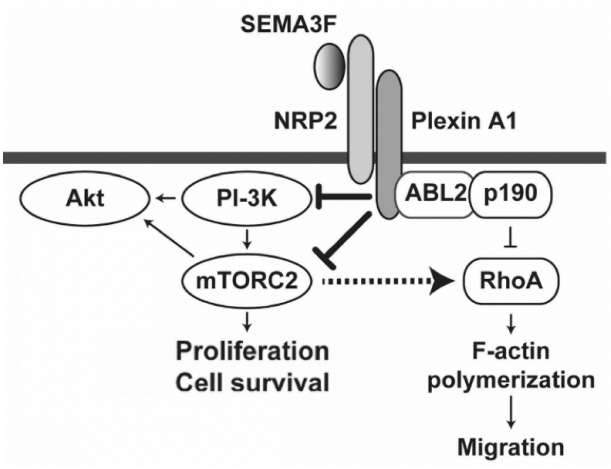

Figure 6. Schematic cartoon illustrating SEMA3F binds to NRP2-Plexin-A1 complex and associates with PTEN to inactivate PI-3K /Akt to block cell survival and proliferation. In addition, inactivation PI-3K/mTORC3 mediate cytoskeleton stress fiber (F-actin) and inhibit migration via RhoA. (Modified from 102)

SEMA3F was originally identified as a tumor suppressor gene located on chromosome 3p21.3, which is frequently deleted in small cell lung cancer and downregulated in many metastatic cancer cell lines.(104, 105) Overexpression (transfection) of SEMA3F in tumor cells resulted in reduced tumor growth, migration and invasion mediated via downregulation of MMPs, integrins and pro-angiogenic genes.(106) SEMA3F may similarly act as a tumor suppressor gene in OSCC. Recently, it was found to be significantly downregulated in human OSCC tissue and cell lines.(107) In addition, SEMA3F transfected OSCC cell lines show reduced cellular proliferation, migration and invasion in vitro compared to control transfected cells.(108) Several preclinical studies suggest that SEMA3F acts as a lymphangiogenesis inhibitor via NRP2.(105, 109) As such, SEMA3F is a promising agent to target NRP2 and inhibit both angiogenesis and lymphangiogenesis in OSCC.

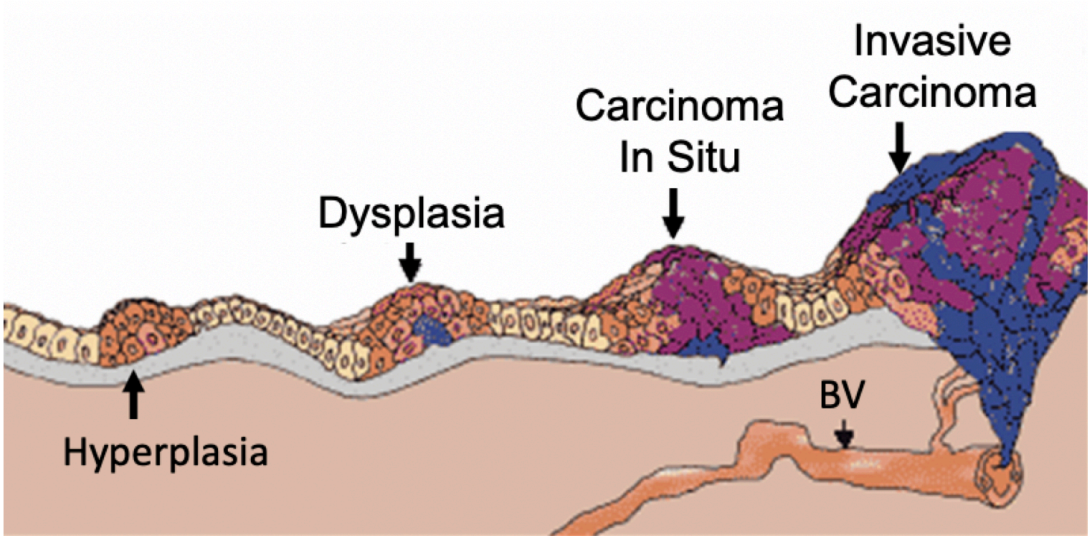

Figure 7. Diagram illustrating multistep progression of OSCC: **Hyperplasia:** Benign epithelial proliferation; **Dysplasia:** Premalignant transformed epithelial cells with variable degree with epithelial involvement. **Carcinoma in situ:** Cancerous cells involving the full thickness of the epithelium without basement membrane invasion. **Invasive carcinoma**: Diffuse cancerous cells infiltration with basement membrane invasion. (Adapted and modified from ndhealthfacts.org)

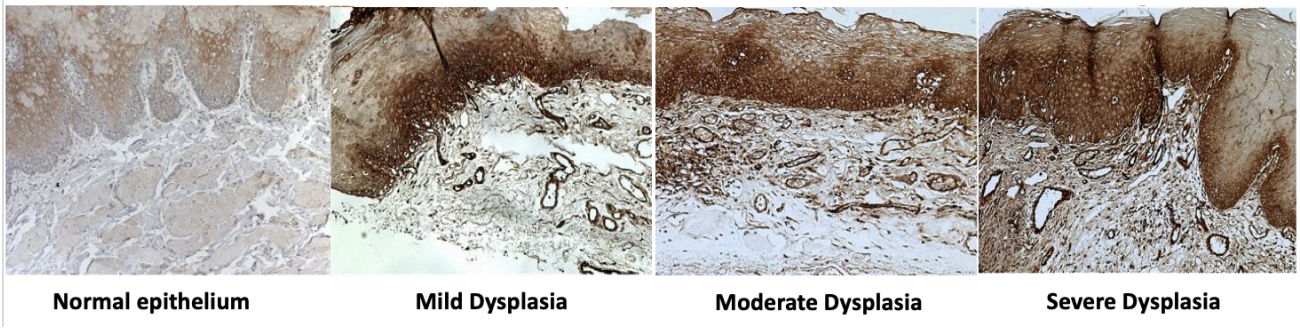

Figure 8. Pattern of NRP1 expression in normal human oral epithelium and different grades of dysplasia. NRP1 is expressed at all stages but it's expression pattern changes from moderate expression in suprabasal, differentiated cells in normal epithelium (far left) to high expression in the basal cell layer in all stages of dysplasia (three right images). This image was obtained from Dr. Bielenberg. (51)

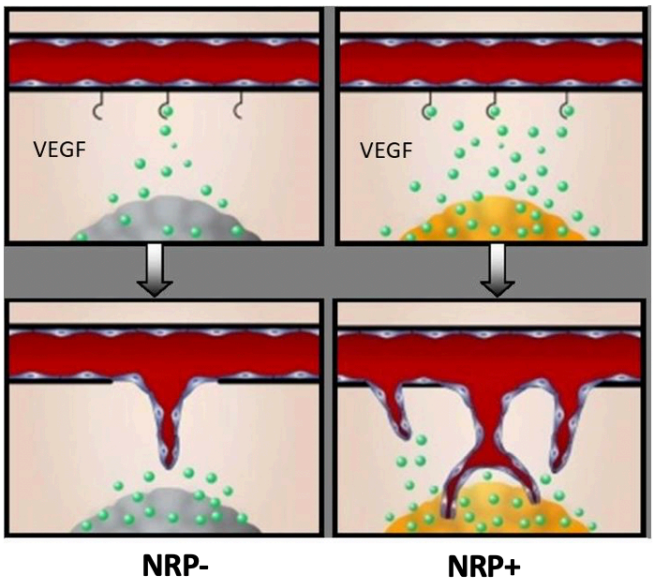

Figure 9. Illustration depicting my hypothesis of VEGF sequestration in NRP-expressing tumor cells. Tumors can grow to 1 mm^3 but then become hypoxic as their distance from blood vessels increases. Hypoxia upregulates VEGF, and VEGF secreted from tumor cells recruits surrounding blood vessels to grow (top panels). However, tumor cells that express NRP (yellow color) sequester more VEGF locally (bottom right) and recruit more neovessels. The result is that tumor cells with higher NRP expression have higher tumor vessel density and increased chances to metastasize.

<u>Aim 1:</u> The Role of NRP1 Receptor in Oral Squamous Cell Carcinoma

One of the goals in my current study is to investigate the role of the NRP1 receptor in the oral epithelium and in OSCC tumor cells, which has yet to be explained. The expression of NRP1 in normal oral epithelium and OSCC was studied previously in the Bielenberg Laboratory. Shahrabi-Farahani, et. al., found that NRP1 expression is localized to suprabasal cells (differentiated epithelial cells) in normal oral epithelium. However, different grades of oral dysplasia and OSCC exhibited up-regulation of NRP1 expression in proliferating epithelial cells including basal cells in both human samples and mice models (**Figure 7-8**).(51) Interestingly, there was a correlation between areas with high NRP1 expression in tumor cells and areas with high blood vessel infiltration, suggesting

a link between NRP1 in OSCC cells and tumor angiogenesis. Additionally, when tumor cells were transfected with NRP1, the resulting tumors had increased microvessel density in mice although they expressed the same amount of VEGF mRNA as control tumors. (61, 110) NRP1 is not expected to signal directly through VEGF family members in epithelial cells because they lack the expression of VEGF receptor tyrosine kinases (RTKs). Rather, tumor cell derived-NRPs have been assumed to bind VEGF on the cell membrane and increase the gradient of VEGF within the tumor microenvironment and therefore recruit surrounding blood vessels to sprout toward the tumor and follow the gradient of VEGF. In essence, the NRP1 receptor on cancer cells' surface may act like heparan sulfate proteoglycans to sequester VEGF in the tumor compartment and attract neovessels. An illustration of this "depot effect" or "VEGF sequestration effect" is shown in **Figure 9**. My **hypothesis** is that NRP1 expression in epithelial cells promotes tumor initiation and enhances tumor growth, angiogenesis, and metastasis.

I will address my hypothesis in the following specific aims:

- **Specific Aim 1A:** To determine the role that Nrp1 plays in OSCC tumorigenesis and metastasis. I used cre-lox technology to knockout Nrp1 expression in epithelial cells in mice. Oral tissues were harvested from control (CO) and inducible, tissue-specific *Nrp1*-knockout (KO) mice at various stages from normal to carcinoma in a carcinogenesis model of OSCC.
    - K14Cre^{ERT} mice were bred to *Nrp1*-floxed mice. The cre enzyme is tamoxifen-inducible and expressed after the keratin 14 promoter and therefore only induced in epithelial cells.(111, 112) K14-Nrp1 mice are normal until the *Nrp1* gene is ablated following tamoxifen treatment.

CO and K14iNrp1KO mice were compared for Nrp1 expression and the incidence of tumors following oral carcinogen (4NQO) treatment. Paraffin-embedded biopsies from various time points including normal oral epithelium, hyperplastic and dysplastic tissues and OSCC were analyzed and stained for proliferative markers (ki67), and vessel density (CD31). I predict that mice lacking Nrp1 in the oral epithelium will develop fewer OSCC than CO mice with decreased blood vessel density.

- **Specific Aim 1B:** To determine the mechanistic function that Nrp1 plays in OSCC tumorigenesis.
  - The effect of silencing NRP1 in human OSCC cell line with and without VEGF protein was tested *in vitro* using 3D soft agar colony formation assays and 2D cell viability assays (MTT). I predict that loss of Nrp1 in OSCC cells will affect tumor growth and tumor cell viability.

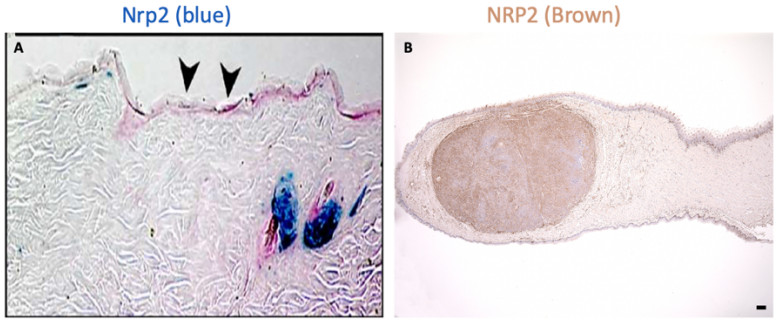

Figure 10. A. Adult mouse skin shows no Nrp2 expression in keratinocytes (arrowheads) in Nrp2LacZ reporter mouse. (47) **B.** Mouse tongue injected orthotopically with human OSCC xenograft in nude mouse demonstrated high NRP2 expression in the tumor cells (Scale bar =100 μm).

Aim 2: The Expression and Role of NRP2 Receptor in Oral Squamous Cell Carcinoma

Another goal of my study is to investigate the expression and role of the NRP2 receptor in the oral epithelium and in OSCC tumor cells, which has yet to be explored. Based on our previously published data, normal keratinocytes lack the expression of Nrp2 protein in both newborn and adult mice (**Figure 10A**). (47, 113) Additionally, my preliminary data showed high expression of NRP2 protein in a human OSCC xenograft injected in nude mice (**Figure 10B**). My **hypothesis** is that normal oral epithelium and quiescence blood vessels do not express NRP2, while epithelial dysplasia and OSCC express NRP2 protein in both squamous cells and endothelial cells; as such, NRP2 expression may be upregulated during tumor progression. NRP2 expression on the tumor cell membrane is expected to bind and sequester VEGFA, C or D proteins. NRP2 is not expected to signal directly through VEGF family members on epithelial cells because they lack the expression of VEGF RTKs. We predict tumor cell derived-NRPs enhance VEGF sequestration within the tumor microenvironment and recruit blood and lymphatic vessels to sprout within and around the tumor (**Figure 9**). I further hypothesize that the NRP2 expression in OSCC cells leads to increased tumor growth due to angiogenesis and increased metastatic capacity due to lymphangiogenesis.

I will address my hypothesis in the following specific aims:

- **Specific Aim 2A:** To determine the expression of the NRP2 receptor in normal oral epithelial tissue, pre-malignant lesions and OSCC.

- NRP2 expression in different human epithelial (normal, pre-malignant, malignant) tissues in paraffin-embedded sections were evaluated using IHC.
- Nrp2 expression will be evaluated in paraffin-embedded sections from a C57Bl/6 mouse treated with 4NQO to induce oral carcinoma. Biopsies from various stages including hyperplasia, dysplasia and OSCC were evaluated using IHC.

- **Specific Aim 2B:** To determine the role that Nrp2 plays in OSCC tumorigenesis and metastasis. Similar to that described above in Aim 1, I used cre-lox technology to knockout *Nrp2* expression in epithelial cells in mice. Oral tissues were harvested from CO and inducible, tissue-specific Nrp2-KO mice at various stages from normal to carcinoma in a carcinogenesis model of OSCC.
    - $K14Cre^{ERT}$ mice were bred to Nrp2-floxed mice.(75, 111) K14-Nrp2 mice should be normal until the Nrp2 gene is ablated following tamoxifen treatment. CO and K14iNrp2KO mice were compared for Nrp2 expression and the incidence and size of tumors following oral 4NQO treatment. Paraffin-embedded biopsies from various time points including normal oral epithelium, hyperplastic and dysplastic tissues and OSCC were analyzed and stained as described above for ki67, CD31, or the lymphatic endothelial marker, podoplanin. I predict that mice lacking Nrp2 in the oral epithelium will develop smaller and fewer tumors than CO mice with decreased lymphatic vessel density.

- **Specific Aim 2C:** To determine the role that NRP2 plays in tumor-derived blood and lymphatic vessels during lymphangiogenesis and metastasis. I examined the tumorigenicity and (lymph)angiogenic potential of orthotopic, syngeneic OSCC isografts in *Nrp2*-deficient and wildtype (WT) mice.
    - C57Bl/6J Nrp2-KO mice that lack the Nrp2 receptor globally and constitutively were used in this aim.(75) WT-3 Luc, a luciferase-transduced OSCC cell line originally isolated from an OSCC tumor after 4NQO treatment in C57Bl/6 mice, were injected into the tongue in age- and sex-matched (littermates) WT and Nrp2-KO mice. Following injection, mice were monitored using non-invasive bioluminescent imaging (Xenogen IVIS). Tumor incidence and size were recorded at necropsy. Cryosections from tumor isografts were analyzed for vessel density (CD31 or Lyve-1). I predict that mice lacking Nrp2 in EC and LEC will develop smaller tumors with fewer metastases than WT mice due to a decreased blood and lymphatic vessel density.

<u>Aim3:</u> The Expression and Role of SEMA3F in Oral Squamous Cell Carcinoma.

The final goal of the current study is to investigate the expression and role of the Nrp2 inhibitory ligand, Sema3F, in normal epithelium, oral dysplasia and OSCC. Sema3F is constitutively expressed in the epidermis of adult mouse skin, suggesting that normal oral epithelium may also express endogenous Sema3F.(48) SEMA3F was originally isolated as a tumor suppressor gene from lung cancer cells (104, 114). Our lab previously

demonstrated that cancer cell lines (bladder cancer, prostate cancer, and melanoma) lose expression of SEMA3F during tumor progression (105). Based on these data, I **hypothesize** that normal oral epithelium expresses SEMA3F protein, while SEMA3F expression will be lost during oral cancer progression in epithelial dysplasia and/or OSCC. Mice lacking endogenous Sema3F were found to have increased lymphatic networks in the skin, suggesting that Sema3F secreted from epidermal cells can act in a paracrine fashion on dermal LEC and inhibit lymphangiogenesis.(103) Exogenous SEMA3F competes with VEGFA/C/D in binding to NRP2 and inhibits endothelial cell proliferation *in vitro*.(100) Tumor cells transfected with SEMA3F showed reduced tumor angiogenesis when implanted in mice compared to controls.(101, 105) Additionally, when NRP2-positive tumor cells were transfected with SEMA3F, their motility was inhibited *in vitro*.(105) Functionally-active SEMA3F protein is not commercially available; however, our laboratory has isolated and purified SEMA3F protein.(115) There are currently no published reports using purified SEMA3F protein in preclinical trials of any cancer. Since most epithelial cells express NRP1 but not NRP2, targeting the NRP2 pathway is predicted to be less toxic than targeting NRP1.(47) In fact, clinical trials using anti-NRP1 in combination with Bevacizumab were stopped prematurely due to severe proteinuria (likely caused by the drug targeting NRP1 in podocytes of the kidney).(116) I hypothesize that exogenous SEMA3F will have an inhibitory effect on NRP2-expressing OSCC tumor migration and invasion *in vitro* and be a powerful anti-tumor and anti-metastatic drug *in vivo* in OSCC mouse models.

I will address these hypotheses in the following specific aims:

- **Specific Aim 3A:** To determine the expression of SEMA3F in normal oral epithelial tissue, pre-malignant lesions and OSCC.
    - SEMA3F expression in different human epithelial (normal, pre-malignant, malignant) tissue in paraffin-embedded sections were evaluated using IHC.
    - Sema3F expression will be evaluated in paraffin-embedded sections from mouse oral carcinogenesis models. Biopsies from various stages including hyperplasia, dysplasia and OSCC were evaluated using IHC.
- **Specific Aim 3B:** To determine the role that Sema3F plays in OSCC tumorigenesis and metastasis. We used cre-lox technology to knockout Sema3F expression in epithelial cells in mice. Oral tissues were harvested from CO and inducible, tissue-specific Sema3F-KO mice at various stages from normal to carcinoma in a carcinogenesis model of OSCC.
    - K14Cre^{ERT} mice were bred to Sema3F-floxed mice.(111, 117) K14-Sema3F mice should be normal until the Sema3F gene is ablated following tamoxifen treatment. CO and K14iSema3FKO mice were compared for Sema3F expression and the incidence and size of tumors following oral 4NQO treatment. Paraffin-embedded biopsies from various time points including normal oral epithelium, hyperplastic and dysplastic tissues and OSCC were analyzed and stained for ki67, CD31 and podoplanin. I predict that mice lacking Sema3F in the oral

epithelium will develop OSCC earlier than CO mice with increased lymphatic vessel density.

- **Specific Aim 3C:** To explore the effect of exogenous Sema3F as a treatment for OSCC.
    - The effect of Sema3F protein on NRP2-expressing OSCC (WT-3 Luc) were tested in vitro using migration, invasion, and proliferation assays. I predict that Sema3F will inhibit migration and invasion but not proliferation.
    - Orthotopically injected WT-3 Luc and HSC3 were treated with Sema3F purified protein in slow-release osmotic pumps for two weeks. I predict that Sema3F-treated tumors will be smaller in size with decreased blood and lymphatic vessel densities compared to vehicle-treated tumors.

In summary, there is a strong premise and rationale regarding the NRP1 and NRP2 impact on tumorigenesis, angiogenesis and lymphangiogenesis in several cancer types. SEMA3F shows promising preclinical data. This thesis is designed to test the overall hypothesis: **"NRP1 and NRP2 are overexpressed in OSCC which indirectly induce angiogenesis and lymphangiogenesis. SEMA3F is anti-angiogenic and anti-lymphangiogenic via competition of the NRP2/VEGF-A/VEGFR2 and NRP2/VEGF-C/VEGFR3 axes and direct SEMA3F/NRP2/plexinA1 signaling".** The goals of this project are threefold: 1) to study the functional role of the NRP1 receptor in regard to OSCC tumorigenesis and angiogenesis, 2) to characterize NRP2 and SEMA3F expression in normal oral epithelium, oral epithelial dysplasia and OSCC, and

3) to test the functional effect or requirement of NRP2 or SEMA3F in OSCC regarding tumor and endothelial cell proliferation and metastatic potential.

Innovation:

I believe the aims mentioned above provide a substantial novelty in the vascular and cancer biology fields and will establish NRP1/2 as a mediator of OSCC progression. This project is innovative because:

1. We determined the localization and function of NRP2 in normal oral epithelium, oral epithelial dysplasia, and OSCC, which to my knowledge, has never been published in the literature.
2. I used genetically modified C57Bl/6 mice (K14iNrp1KO, K14iNrp2KO and K14iSema3FKO mice). To my knowledge, this is the first attempt to study Nrp1, Nrp2 or Sema3F in OSCC in an immunocompetent transgenic mouse model.
3. The establishment of the role of NRP1, NRP2 and/or SEMA3F in OSCC will provide insight and a strong rationale to target this pathway using novel strategies for oral cancer.
4. SEMA3F protein as a drug has never been reported previously in preclinical cancer trials in any model. Our data strongly suggest that SEMA3F inhibits and possibly regresses established oral cancer.

Materials and Methods:

Cell culture

The following oral human cell lines were analyzed: NOK, DOK, HSC3, HSC4, SCC9, SCC68, OSCC1 and 5PT (**Table 1**). HSC3 was obtained from Dr. Kyoko Hida (Department of Vascular Biology, Hokkaido University of Graduate School of Dental Medicine, Hokkaido, Japan). HSC4 was obtained from Dr. Chia-Cheng Li (Department of periodontics and oral medicine, University of Michigan, Ann Arbor, MI). SCC9 and SCC68 were kind gifts from Dr. Karl Munger (Department of Pathology and Harvard Center for Cancer Biology, Harvard Medical School, Boston, MA). OSCC1 and 5PT were protein lysates obtained from Dr. Daniela-Elena Costea (Department of Clinical Medicine and Centre for Cancer Biomarkers, University of Bergen, Bergen, Norway). Mouse oral cancer cell lines were analyzed including: WSSC2, WSCC5, WT3, WT4 (**Table 2**). WSCC2, WSCC5, WT3 and WT4 were obtained from Dr. Dipak Panigrahy (Department of Pathology, Beth Israel Deaconess Medical Center and Harvard Medical School, Boston, MA). Human umbilical vein endothelial cells (HUVEC) were purchased from Lonza (Walkersville, MD). Porcine aortic endothelial (PAE) cells were obtained from Lena Claesson-Welsh (Uppsala University, Sweden). PAE cells transfected with NR2 (PAE/NRP2) were created in the Bielenberg laboratory. All cell lines obtained from secondary parties were obtained as kind gifts.

All the cell lines stored in liquid nitrogen were transferred first to dry ice briefly, then thawed quickly at 37º C in a water bath and plated on 10 cm tissue culture dishes. HSC3, HSC4, WSCC2, WSCC5, WT3, WT4 were maintained in Dulbecco's Modified Essential

Media (DMEM, Thermo Fisher Scientific). SCC9, SCC68, PAE/NRP2, and PAE were maintained in Ham's F12/DMEM (1:1) (Thermo Fisher Scientific). Lastly, HUVEC was maintained in Endothelial Cell Growth Medium-2 (EGM-2, Lonza). All media was supplemented with 10% Fetal Bovine Serum (FBS) (Thomas Scientific), Penicillin (100 units), Streptomycin (100ug), and L-Glutamine (0.29 mg/ml) (100X GPS, Thermo Fisher Scientific). All the cells were maintained as a monolayer and stored in humidified incubators at 37ºC and 5% CO_2. At a confluency of 80-90%, cells were split into multiple 10 cm tissue culture dishes using 0.05% Trypsin-EDTA (Thermo Fisher Scientific) and resuspended in 10 mL of full media. Cell lines were typically only passaged 3-5 times in culture. Cells were frozen down for long-term storage.

Table 1. Different human cell lines to be examined via western for NRP2 expression

Name of cell line	Feature of cell line
NOK	Human normal oral keratinocytes
DOK	A piece of dorsal tongue showing epithelial dysplasia(118)
HSC3	Tongue SCC cell line with TP53 gene mutation and invasive phenotype(119)
HSC4	Metastatic Tongue SCC derived from cervical lymph node(119)
SCC9	Tongue SCC cell line (T2N1M0)(120)
SCC68	Tongue SCC cell line (T4N1M0)(121)
OSCC1	OSCC in 41 YO male (122); lysate from Norway
5PT	Cisplatin resistant OSCC (123); lysate from Norway
HUVEC	Human umbilical venous endothelial cells; positive control
PAE/NRP2	Positive control cell line transfected with NRP2(105)
PAE	Negative control cell line devoid of NRP1, NRP2, and VEGFRs

Table 2. Different murine cell lines/tissues to be examined via western for Nrp2 expression.

Name of cell line	Feature of cell line
WSCC-2 and WSCC5	4NQO-induced OSCC in wildtype C57Bl/6 mice (124)
WT3 and WT4	Isolated from mice that were injected subcutaneously with WSCC-5
WT skin biopsy from Nrp2+/+ mice	Positive control; melanocytes in the skin should express Nrp2
Nrp2KO skin biopsy from Nrp2-/- mice	Negative control; all cells should be devoid of Nrp2

Freezing and storage of the cells: Cells were trypsinized and resuspended in full media, and centrifuged for 5 minutes at 1000 rpm in 4^{o}C. Media was suctioned off and the cell pellet was resuspended in a freezing solution (70% regular media of each cell line, 20% FBS, and 10% dimethylsulfoxide). Then, partitioned in 1mL CryoTube vials (Nalgene Labware) and multiple cryotubes were stored in a container insulated with isopropanol ("Mr. Frosty", Nalgene Labware) and were kept at -80^{o}C overnight then transferred to liquid nitrogen.

Whole cell protein lysis (from cell lines): Cultured cells were placed on ice and washed twice with phosphate buffered saline (PBS). Then cells were lysed with lysis buffer (10mM Tris-HCL PH 7.4, 1% NP-40 detergent, 1mM EDTA, and protease inhibitor). Whole cell lysate was collected with a cell scraper, incubated on ice for 15 minutes, and centrifuged at 14000 rpm for 10 minutes at 4^{o}C. The supernatants were removed and collected in eppendorf tubes then stored at -20^{o}C.

Protein assay: Concentrations of whole cell lysates were determined by comparison to serial dilutions of a control protein, Bovine Serum Albumin (Purified BSA 100×, Biolabs, 10mg/ml), using a 96-well flat bottom plate (Corning). Twenty-five microliter of 2% Protein Assay Solution S (Biorad) in Protein Assay Solution A (Biorad) and 200µl of Protein Assay Solution B (Biorad) was added to each 5µl sample. The plate was read in a spectrophotometer plate-reader at 650 nm using the program Softmax pro 48. BSA values were graphed in Excel as a function of protein concentration. Protein lysate concentrations were calculated using the line of best-fit formula obtained from this graph. This formula was used to calculate the protein concentration of lysates obtained from our cell lines.

7.5% SDS-PAGE Gel: The "home-made" 7.5% SDS-PAGE gel was composed of a resolving gel and stacking gel. The solution of resolving gel was made using of 1.875 ml H_2O, 3.25 ml of 12% ProtoGel Quick-Cast, 9.32 ml of 4X Tris-HCl/SDS at pH 8, 0.1 ml of 10% ammonium persulfate, and 0.01 ml TEMED. This solution was allowed to polymerize in a gel cast for 30 minutes. The solution of stacking gel was made using 2.08 ml H2O, 1.25 ml of 12% ProtoGel Quick-Cast, 1.62 ml of 4X Tris-HCl/SDS at pH 6.8, 0.05 ml of 10% ammonium persulfate, and 0.005 ml TEMED, added above the separating gel layer of the gel cast containing a 10- or 15-well comb. The gel was allowed to polymerize. If necessary, the gel was stored in 4^{o}C.

Western Blotting: Whole cell lysates were used for western blotting. The samples were adjusted to equal concentration, mixed with reducing sample buffer, boiled for 5-10

minutes, then loaded onto a 7.5% SDS-PAGE gel. The gel was immersed in 1X Running Buffer (10 X Running Buffer; 250mM Tris base, 1.92M glycine, 1% SDS, pH 8.3, Boston BioProducts). The gel was run at 100 V for 2 hours. Resolved proteins were transferred at 300 mA for 2 hours to a nitrocellulose membrane (Biorad) in 1X Transfer Buffer (10 X Transfer Buffer; 250mM Tris base, 1.92M glycine, pH 8.5, Boston BioProducts) with 20% methanol. After transferring, the membrane was blocked with 3% non-fat milk diluted in Tris-buffered saline (TBS: 100mM Tris-HCL, 1.5M NaCl, pH 7.4) containing 0.1 % Tween-20 (TBST) for 60 minutes. Membranes were incubated overnight at 4ºC with the following primary antibodies diluted in TBST (**Table 3**). After incubation in primary antibody, the membrane was washed 3 times in TBST (10 minutes each time) followed by incubation in HRP-conjugated secondary antibodies for one hour at room temperature. The membrane was washed 3 times in TBST and then incubated in a mixture of Western Lighting plus-ECL (Perkin Elmer) Oxidizing and Enhancing Luminol Reagent (1:1 ratio) for 3 minutes and exposed to Kodak BioMax light film (Sigma Aldrich) for 1-10 minutes. Then the film was developed in a Kodak X-omat 2000 A processor.

Membrane stripping: In order to incubate the membrane for another antibody, after developing, the membrane was washed in TBST, and then immersed in Restore Western Blot Stripping Buffer (Thermo Scientific) for 15 minutes. The stripped membrane was blocked for 1 hour at room temperature before proceeding with the next antibody.

Table 3. Antibodies used for western blotting

Antigen	Host animal	Clonality	Source	Dilution	Secondary Antibody
NRP1 (mouse and human)	Rabbit	Monoclonal	Abcam	1:800	Peroxidase labeled anti-rabbit IgG
Mouse Nrp2	Rabbit	Monoclonal	Cell Signaling	1:800	Peroxidase labeled anti-rabbit IgG
Human NRP2 (C-9)	Mouse	Monoclonal	Santa Cruz	1:1000	Peroxidase labeled anti-mouse IgG
Peroxidase labeled-Actin	Mouse	Monoclonal	Sigma-Aldrich	1:10000	N/A

Human Specimens: Institutional review board approval was obtained from the University of Tennessee Health Science Center. Twenty-three total cases were obtained, including normal (2) and oral dysplasia (21) samples, from Dr. Shokoufeh Shahrabi-Farahani (Department of Diagnostic Sciences, University of Tennessee Health Science Center, College of Dentistry, Memphis, TN) and 5 human OSCC sections were obtained from Dr. Daniela-Elena Costea (Department of Clinical Medicine and Centre for Cancer Biomarkers, University of Bergen, Bergen, Norway).

Immunohistochemistry (IHC) /Immunofluorescent (IF) staining: Formalin-fixed paraffin embedded sections as well as frozen sections of normal oral mucosa, oral dysplasia and OSCC from human and mice models were used for immunohistochemical evaluation. Formalin-fixed paraffin embedded sections (4-5 μm) were placed on a slide warmer at 58^{o}C for a minimum of 20 minutes and deparaffinized in xylene, rehydrated through a series of alcohols (from 100% ethanol to 50% ethanol), then placed in PBS, pH 7.4 for 5 minutes. Depending on the antigen of interest, corresponding antigen retrieval procedures were performed (**Table 4**). Cyosections were fixed in cold acetone or

methanol for 10 minutes, and then washed in PBS. No antigen retrieval was performed on frozen sections. Following antigen retrieval, the slides were washed in PBS. In order to quench endogenous peroxidase, 3% hydrogen peroxide in methanol was added to slides for 12 minutes. After washing in PBS, the blocking agent of TNB (0.1 mol/L Tris-HCl, pH7.5; 0.15 mol/L NaCl, 0.5% blocking reagent) (Perkin Elmer FP1012) was be added for 15-30 minutes and the slides were incubated with primary antibody overnight (Table 4) at 4^{o}C, washed, and then incubated in biotinylated-secondary antibody at room temperature for 1 hour. For amplification of antigen-antibody reaction, based on the antigen and the antibody of interest and corresponding protocol, either Avidin-HRP (ABC Vectastain Elite Kit PK-6100, Vector Labs) for 30 minutes was used or biotinylated-Tyramide (1:50 Tyramide in amplification diluent, Perkin Elmer) for 4-7 minutes in combination with Streptavidin-HRP (SA-HRP, Perkin Elmer) diluted in TNB for 30 minutes was used. The slides amplified with Tyramide were washed in TNT (Tris-NaCl-Tween) instead of PBS. Finally, staining was visualized either with Alexa Fluor-congugated antibodies for IF or diaminobenzidine (DAB, Vector Labs) for IHC. Slides were counterstained with Hoechst (Sigma) or Mayer's Hematoxylin (Sigma) and Tacha's bluing solution (Biocare Medical), then mounted with antifade mounting media (Fluoro-Gel, Electron Microscopy Sciences) for IF or permount (Fisher) for IHC.

Microvessel density analysis (MVD): Blood vessel density ($CD31^+$ vessels/mm^2) and lymphatic vessel density (LVD; $podoplanin^+$ or $Lyve1^+$ vessels/mm^2) was counted with the use of imageJ. Tumor sections photographed at X100 or X200 magnification (10 to 20 fields) were counted, adjusted to square millimeters, and averaged.

Table 4. Primary antibodies used for IHC.

Antigen	Clonality	Source	Antigen retrieval	Dilution	Secondary Antibodies	Additional Reagents
Nrp1	Monoclonal	Abcam	Na citrate (10mM 1×, pH 6) boiling in microwave, 5 minutes	1:200	Biotinylated anti-rabbit IgG (Vectastain)	ABC (Avidin HRP kit); Vectastain PK6100
Mouse Nrp2	monoclonal	Cell signaling	Na citrate (10mM 1×, pH 6) boiling in microwave, 5 minutes	1:200	Biotinylated anti-rabbit IgG (Vectastain)	ABC (Avidin HRP kit); Vectastain PK6100
Human NRP2	polyclonal	Sigma	Na citrate (10mM 1×, pH 6) boiling in microwave, 5 minutes	1:200	Biotinylated anti-rabbit IgG (Vectastain)	ABC (Avidin HRP kit); Vectastain PK6100
Mouse Podoplanin	monoclonal	ReliaTech	PK (20 µg/ml), 10 minutes at warm room	1:200	Biotinylated Syrian Hamster (Jackson immunoresearch)	Tyramide/SA-HRP
Mouse lyve-1	Monoclonal	ReliaTech	No antigen retrieval	1:200	Biotinylated anti-rabbit IgG (Vectastain)	ABC (Avidin HRP kit); Vectastain PK6100
Semaphorin 3F	polyclonal	In-house design, GeneScript	Na citrate (10mM 1×, pH 6) boiling in microwave, 5 minutes	1:200	Biotinylated anti-rabbit IgG (Vectastain)	ABC (Avidin HRP kit); Vectastain PK6100
Mouse ki67	Monoclonal	Abcam	PK (20 µg/ml), 10 minutes at warm room	1:100	Biotinylated anti-rabbit IgG (Vector)	ABC (Avidin HRP kit); Vectastain PK6100

Mouse models:

NRP2 Knockout/GFP Knockin model (Nrp2KO): These mice are global and constitutive knockout of Nrp2 in the C57Bl/6J strain. A gfp reporter is inserted into exon 1 upstream of the initiation start site. These mice were originally created by Peter Mombaerts (75) and purchased from Jackson Labs (stock # 006700). These mice already exist in the Bielenberg laboratory and have been bred at Boston Children's Hospital for more than 5 years. These *Nrp2*-deficient mice (Nrp2-/-) are viable and fertile but smaller in size than heterozygous and wildtype littermates. Wild type (WT) littermates will be used as controls.

Transgenic models: The Cre-LoxP recombination system is a gene editing technique that can enable the deletion of a gene (or portions of a gene flanked by loxP sites) of interest in specific cells or tissue types based on the Cre driver. Cre-ERT is a tamoxifen-inducible Cre recombinase that will be used to knockout a gene of interest in cells expressing Keratin 14 (K14), which is specific to keratinocytes in the skin and oral mucosa.

Nrp1iKO mice model:

K14-cre^{ERT} mice: have a tamoxifen-inducible cre recombinase inserted downstream of the K14 promoter and were developed by Elaine Fuchs.(111) These mice were originally purchased from Jackson Labs (stock # 005107) and are in the CD1 strain.

Nrp1-floxed mice: These mice possess *loxP* sites flanking exon 2 of the *Nrp1* gene and were developed by David Ginty (HMS).(112) These mice were originally purchased from Jackson Labs (stock # 005247) and are in the C57Bl/6 strain.

Nrp2iKO mice model:

K14-cre^{ERT} mice: discussed above.

Nrp2-floxed mice: These mice possess *loxP* sites flanking exon 1 of the *Nrp2* gene and were developed by Peter Mombaerts.(75) These mice were originally purchased from Jackson Labs (stock # 006697) and are in the C57Bl/6 strain.

Sema3FiKo mice model:

K14-cre^{ERT} mice: discussed above.

Sema3F-floxed mice: These mice possess *loxP* sites flanking exon 1 of the *sema3F* gene and were developed by David Ginty (HMS).(117) These mice were originally purchased form Jackson Labs (stock # 00357) and are in the C57Bl/6 strain.

Breeding: The Bielenberg laboratory keeps all strains breeding as both original strains and mixed strains. The breeding strategy to generate experimental and CO mice is depicted below (**Figure 11**)

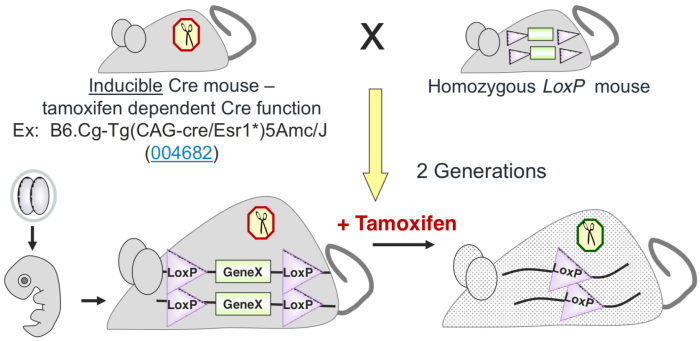

Figure 11: Breeding strategy: cross-breeding between homozygous K14-cre^{ERT} and homozygous Nrp1-floxed mice results in all heterozygous offspring for both alleles (K14+/cre;Nrp1+/f) in the F1 generation. Next, the F1 offspring are bred with homozygous Nrp1-floxed mice and the resultant F2 offspring are a mix of: **K14+/cre;Nrp1f/f (Nrp1iKO experimental)**, **K14cre/+ or Nrp1f/f (control)**, K14+/+;Nrp1+/f (heterozygous, not used), K14+/cre, Nrp1+/f (heterozygous, not used). Deletion of floxed Nrp1 allele will take place only after tamoxifen treatment.

Genotyping: Mice are weaned at 3 weeks of age and separated by sex. A small piece of ear tissue is biopsied and used for determining genotype. Ear tissue is dissolved in NaOH for at least one hour at 37 ^{o}C and then neutralized in HCl (final pH 7) to extract genomic DNA. DNA, primers (**Table 5**), and GoTaq Green master mix (containing *Taq* DNA polymerase, dNTPs, $MgCl_2$ and reaction buffers; Promega) are combined and standard PCR reactions were performed using a thermocycler. PCR cycling consists of 42 cycles with touch-down temperature of 63^{o}C repeated for 10 cycles. PCR products are separated by size on 2% agarose gels and visualized using ethidium bromide. A representative genotyping for each Cre-LoxP model is shown in (**Figure 12**).

Table 5. List of Primers and size bands of different mice strains used

Gene (stock #)	Primers sequence 5'----> 3'	Primary type	Band sizes
K14 cre (005107)	CGC ATC CCT TTC CAA TTT AC	Forward	Cre transgene= 169 bp
	GGG TCC ATG GTG ATA CAA GG	Reverse	
NRP1floxed (005247)	AAG GAG TGG CAC AGC ATC TT	Forward	Mutant= 398 bp
	TCA CAC CCA AAC TTC CTT CC	Reverse	Wildtype= 183 bp
NRP2 floxed (006697)	CAG GTG ACT GGG GAT AGG GTA	Wildtype forward	Mutant= 350 bp
	AGC TTT TGC CTC AGG ACC CA	Common	Wildtype= 200 bp
	CCT GAC TCC CAG TCA TAG	Mutant forward	
Sema3f floxed (005357)	TTC TGT CTT GGC CAT CCT CT	Forward	Mutant= 450 bp
	GGC CCT TAA GAA CCA GAA CC	Reverse	Wildtype= 296 bp
NRP2 KO (006700)	GGG AAA CCC TCG TGA TGT TGT	Common	Mutant=175 bp
	TGA AAT GAG CAA AGA GGG AGC	Wildtype	Wildtype= 125 bp
	ATC TTC CAT CAC GTC GAA CTC	Mutant	

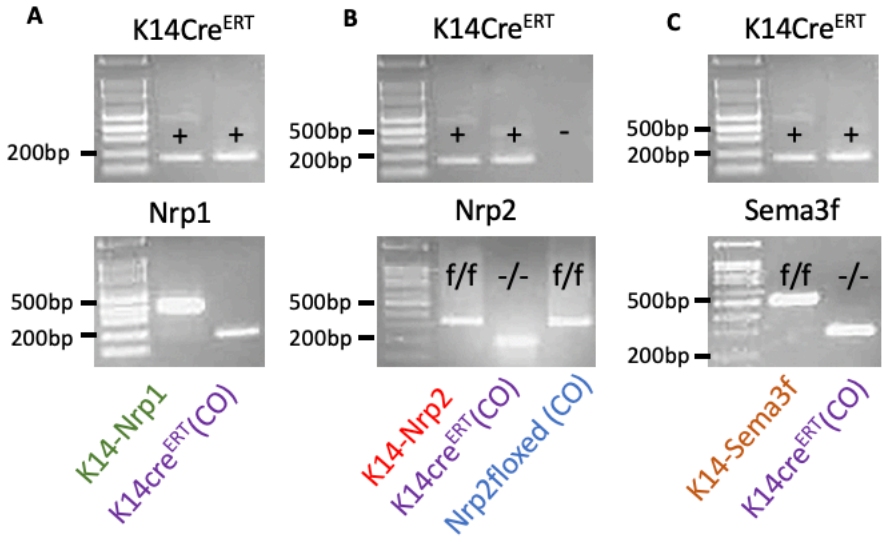

Figure 12: Agarose gels illustrate band size for each mouse used in the experiments. **A.** Upper agarose gel illustrates a band size of 169 bp indicating Cre is present in both lanes. Lower agarose gel illustrates a band size of 398 bp indicating Nrp1 gene is floxed. **B.** Upper agarose gel illustrates a band size of 169 bp indicating Cre is present in first two lanes. Lower agarose gel illustrates a band size of 350 bp indicating Nrp2 gene is floxed. **C.** Upper agarose gel illustrates a band size of 169 bp indicating Cre is present in both lanes. Lower agarose gel illustrates a band size of 450 bp indicating Sema3f gene is floxed.

Gene deletion: Age-matched, sex-matched (littermates when possible) experimental and CO mice (cre only or floxed only) will be injected intraperitoneally with 4-hydroxytamoxifen (4OHT, Sigma-Aldrich) dissolved in methanol and peanut oil at a concentration of 1 mg/ml (0.2 ml/dose) for 5 consecutive days.

Gene deletion confirmation: In order to confirm the gene deletion after 4OHT, our laboratory designed primers (**Table 6**) to detect the recombined DNA after deletion for each gene of interest (Nrp2 and Sema3F). Another small piece of ear tissue was biopsied from the mice after 1 week of treatment with 4OHT. DNA extraction, PCR and product size visualization were done for each ear similar to genotyping above. For Nrp1, deletion

in the epithelial compartment was confirmed using Nrp1 immunostaining on biopsied tissues (**Figure 13**).

Table 6. List of primers and size bands for recombinant DNA after 4QHT

Gene of interest	Primers sequence 5'----> 3'	Primary type	Band sizes
Nrp2	AAG GAG TGG CAC AGC ATC TT	Forward	Deletion= 500 500 bp
	TCA CAC CCA AAC TTC CTT CC	Reverse	
Sema3F (ref)	GAA TGC CCG GGT AAA CAC CA	Forward (P1)	No deletion = 400 bp
	TCG AAG CGT ACC CTG GCT CT	Reverse (P2)	Deletion =200 bp

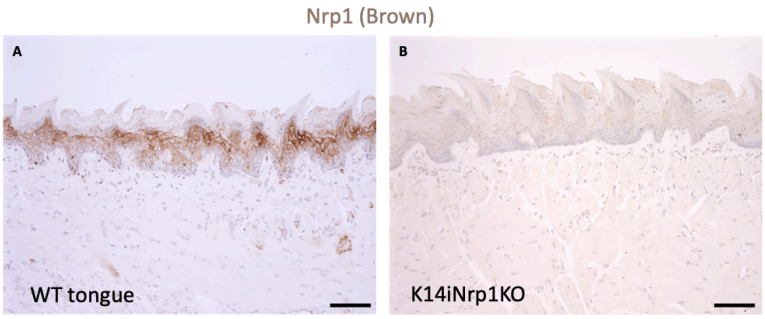

Figure13: Comparison between Nrp1 expression in K14iNrp1KO and WT after Tamoxifen injection (1 mg/mg) for 5 consecutive days. WT mouse tongue mucosa (A) show Nrp1 expression in the epithelium while Nrp1 expression is lost in K14iNrp1KO mouse tongue mucosa (B). Scale bar =100 μm.

4NQO carcinogenesis model:

4-Nitroquinoline-1-oxide (4NQO, Sigma-Aldrich) stock solution was diluted in drinking water (100 microgram/milliliter).(125) Mice were given 4NQO-containing water ad libitum for 16 weeks. Fresh 4NQO-containing water was changed every week. After 16 weeks, mice were returned to normal drinking water. Within 9 weeks after 4NQO cessation, the oral cavity (especially the tongue) is expected to develop hyperplasia, oral dysplasia and OSCC (**Figure 14**). Mice will be monitored semi-weekly by direct observation of the tongue as well as weight measurements. The mice will be sacrificed at week 9 post-carcinogen to measure the incidence of different stages of tumor development. Tongue specimens will be photographed, fixed overnight in 10% buffered formalin, then processed and embedded in paraffin (**Table 7**).

Table 7. Illustration of 4NQO carcinogenesis model timeline (weeks after birth)

Mice group	3 weeks	4-5 weeks	16 weeks	9 weeks				
CO n = 10	Genotype mice	4OHT	4NQO in drinking water	Tongue observation and weight measurement. After euthanasia, mice will be necropsied and tongues will be analyzed histologically to evaluate different stages of tumor development.				
				Expected stages to be observed in CO and KO				
KO n = 10				Normal	Hyperplasia	Dysplasia	papilloma	OSCC

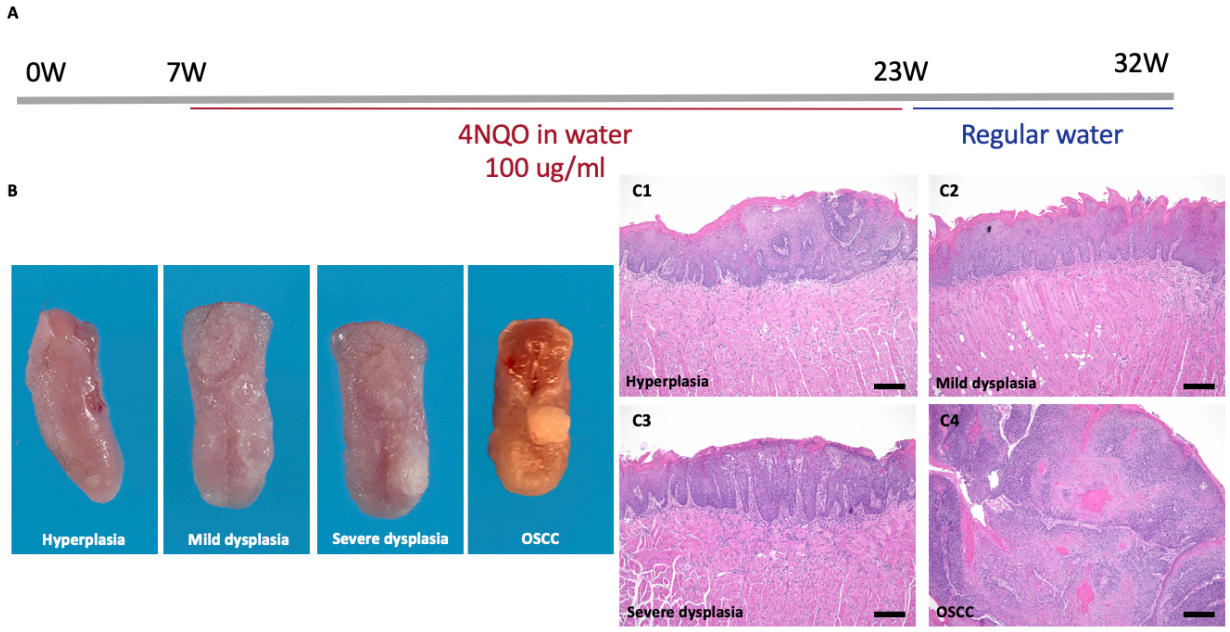

Figure14: **A.** 4NQO model timeline. At age of 7 week, mice will be drinking water containing 4NQO (100 ug/ml) for 16 weeks. Tongues and mouse weight will be under observation for a period of 9 weeks. **B-** Gross images of different stages of tumor development. **C**. Histological examination shows different stages of tumor development; hyperplasia (C1), mild dysplasia (C2), Severe dysplasia (C3) and OSCC (C4). Scale bar =100 μm.

In vitro assays:

Mouse luciferase-transduced OSCC cell line: The mouse OSCC cell line determined by western blotting to have the highest expression of Nrp2 protein, WT3, was subsequently infected with a retroviral construct expressing luciferase. Virus was first amplified in HEK293T cells and the conditioned-medium containing virus was then added to WT3 with 1 mg/ml neomycin. Cells were tested for transduction by adding luciferin substrate in the culture media and imaging the bioluminescence via IVIS.

Migration assay: Transwell migration chambers (Corning) with 8.0 μm pore size in a 24-well plate were used to compare the migration of Sema3F treated and untreated WT3. At first, to analyze basal migration the upper chambers containing 10,000 cells/0.2 ml, 20,000 cells/0.2 ml or 40,000 cells/0.2 ml in full media (DMEM/low glucose, 10% FBS, 1% GPS) were inserted in a lower chamber containing the same media and incubated at 37ºC and 5% CO_2. After 10h, the media was removed from the upper chamber and the membrane was fixed and stained using the Diff Quick kit. After counting and evaluation of the number of the cells which had migrated and were visible on the lower membrane, the best concentration of 20,000 cells/0.2 ml was chosen for subsequent tests. Then the same procedure was repeated, three upper migration chambers were used per dose of Sema3F: 0, 300 μg/ml, and 600μg/ml. After 10 h, each membrane was fixed and stained similar to the baseline experiment and the migrated cells were counted using imageJ.

Invasion assay: Matrigel invasion chambers (Corning) with 8.0 µm pore size in a 24-well plate were used to compare the invasion of Sema3F treated and untreated WT3. Chambers and inserts were hydrated with (DMEM/low glucose, 10% FBS, 1% GPS) and incubated at 37ºC and 5% CO_2 for 2 hours. WT3 cell suspension was added into the insert at 40,000 cells /0.2 ml. Three invasion chambers were considered which contained: full media, full media with 300 µg/ml Sema3F, or full media with 600 µg/ml Sema3F. After 22 hours, each membrane was fixed and stained and the invaded cells were counted using imageJ.

Proliferation assay: Proliferation assay was performed on WT3-Luc and HSC3 cell lines. In the first step, cell suspensions of 10,000 cells/well (WT3-Luc) or 40,000 cells/well (HSC3). Cells were plated in glass inserts of 24- or 12- well dishes containing media with 10% serum and incubated at 37 ^{0}C and 5% CO_2 overnight. Media was switched to 1% serum to briefly starve the cells and synchronize the cycles. Some wells were fixed and counted at this stage to establish the cell attachment number prior to ligand addition. On the 3rd day, Sema3F (200 - 800 ng/ml) or Vegf (50 - 100 ng/ml) protein was added to the cells in different concentrations. After 48 hours, the glass insert was fixed and Hoechst staining. Microscopic images at 100X-200X magnification were obtained randomly across the insert (5-10 fields/insert) and cells were counted using imageJ.

Transfection: The transfection of expression vectors into HSC3 was performed with Lipofectamine^{TM} 3000 Reagent were used for all siRNA treatments as directed in the instruction manual (ThermoFisher, Waltham, MA, USA).

Soft agar colony formation assay: Colony formation assay was performed on HSC3 Luc, isControl HSC3 Luc and siNRP1 HSC3 Luc. 2 ml of full DMEM containing 0.7% agar was prepared and used as the bottom base. Cells were suspended in 2 ml of full DMEM containing 0.3% agar. After 30 days, colonies were fixed in cold methanol for 15 minutes and stained with 0.005% crystal violet for 1 hour. The colonies in each well were scanned and analyzed by image J software.

In vivo assays:

Orthotopic syngeneic mouse OSCC isografts: Female, 12-week-old, *Nrp2*-deficient and WT littermates (n=5/group) were injected directly into the lateral border of the tongue (20ul) with $2x10^6$ WT3-Luc cells resuspended in growth factor-reduced Matrigel (BD Biosciences) in a ratio of 1 volume matrigel: 4 volume cells in HBSS. Tumor growth was monitored by visual inspection and IVIS Xenogen imaging. After approximately 1-2 weeks, mice were sacrificed and necropsied. The tongue tumors were analyzed by gross and histological evaluation. MVD, LVD and cellular proliferation were evaluated.

SEMA3F preclinical trials: Tongues were injected as described above with WT3-Luc in female C57Bl/6 mice (N=4-6/group) or in female (12 week) Balb/c Nu/Nu (nude) athymic mice (purchased from MGH; N=5/group). Additionally, $1x10^6$ human HSC3 cells in female (12 week) Balb/c Nu/Nu (nude) athymic mice (N=3/group). After 7 days, mice were randomized and implanted with mini osmotic pumps (Alzet) containing SEMA3F or vehicle (HBSS). Pumps released a dose of

0.3 mg/kg/day SEMA3F. Tumor growth was monitored via visual inspection or Xenogen imaging and euthanized and necropsied after 14 days on drug (21 days post tumor injection). The tongue tumors were evaluated by gross and histological examination. MVD, LVD and cellular proliferation were evaluated. Experiments were repeated three times.

Results:

Aim 1A:

Our laboratory previously found that Nrp1 was upregulated in the basal (dividing) epithelial cells of the tongue during dysplasia whereas normal basal epithelial cells in the tongue lacked Nrp1 expression.(51) In order to understand the role of Nrp1 in oral carcinogenesis, mice with conditional deletion of Nrp1 in keratinocytes (K14-Nrp1 mice; **Figure 15A**) were created. K14Cre^{ERT} mice were used as controls (**Figure 15 A-B**). Mice lacking *Nrp1* in keratinocytes after 4-OHT were viable with normal epidermis and oral mucosa. Nrp1 depletion was confirmed by IHC on oral biopsies (**Figure 13**). Carcinogen (4-NQO) was given to both groups, K14Cre^{ERT} and K14iNrp1KO mice, in the drinking water, ad libitum, from 7 to 23 weeks of age (16 weeks in total) to generate premalignant lesions and OSCC. Weight measurements were taken once a week after 4-NQO termination for 9 weeks. In general, both male and female K14iNrp1KO mice were smaller in size (weight), compared to K14Cre^{ERT} mice; but the weight differences were more significant in the male group. However, the rate of weight of loss in both K14Cre^{ERT} and K14iNrp1KO mice were similar and never exceeded 20% of body mass (**Figure 16**).

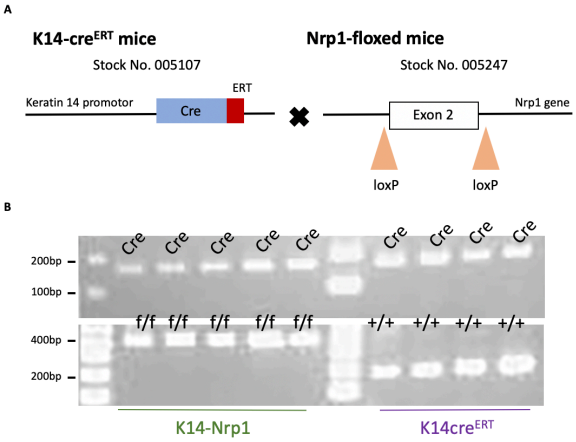

Figure 15: A. Genetic strategy used to study the necessity of Nrp1 in keratinocytes during OSCC tumorigenesis. **B.** Representative agarose gels of both K14-Nrp1 and K14Cre^{ERT} genotyping. Agarose gel illustrates a band size of 169 bp indicating Cre is present in both groups (top panel). Agarose gel illustrates a band size of 398 bp indicate Nrp1 gene is floxed in the first group on the left and a band size of 183 bp indicate Nrp1 gene is not floxed in the second group on the right (bottom panel).

At the end of the 9-week observation period, mice were sacrificed, necropsied and their tongues were harvested from K14Cre^{ERT} and K14iNrp1KO. Grossly, all K14Cre^{ERT} mice (10/10) showed formation of one or more tumors, as well as white plaques on the tongue, gingiva and palatal mucosa (**Figure 17 A-B**). Only one female K14iNrp1KO mouse had one small white horn on the tongue, which is more consistent with excessive keratinization or early benign papilloma (**Figure 17 C**). None of the male K14iNrp1KO mice developed lesions or white plaques (**Figure 17 D**). The number of tumors per mouse was quantified in each group. On average, K14Cre^{ERT} mice developed 1.5 lesions/mouse, while K14iNrp1KO mice developed only 0.1 lesions/mouse (**Figure 17 E**).

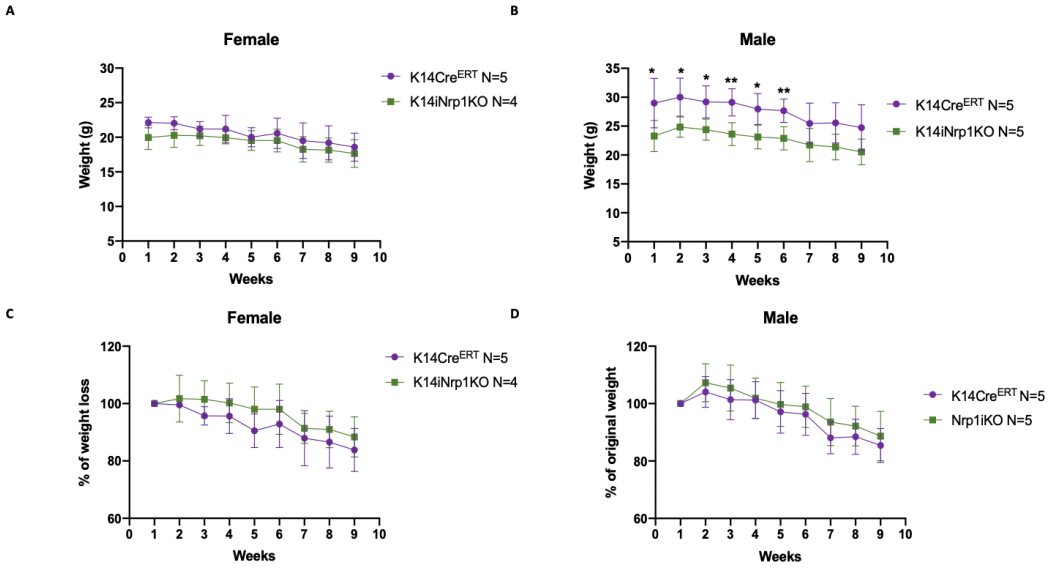

Figure 16: Quantification of mice weight following carcinogen treatment. **A-B.** K14Cre^{ERT} (purple) and K14iNrp1KO (green) mice were followed for 9 weeks after 4NQO termination and weights were recorded weekly. Weights from each group were averaged for each time point. **A, C.** Female mice. **B, D.** Male mice. **B.** K14iNrp1KO male mice were significantly smaller than controls from week 1 to week 6 following carcinogen (*p<0.01, **p<0.001). **C-D.** The percent of original body weight was calculated for each group and averaged. Neither of the groups exceeded 20% loss in body mass during this observation period.

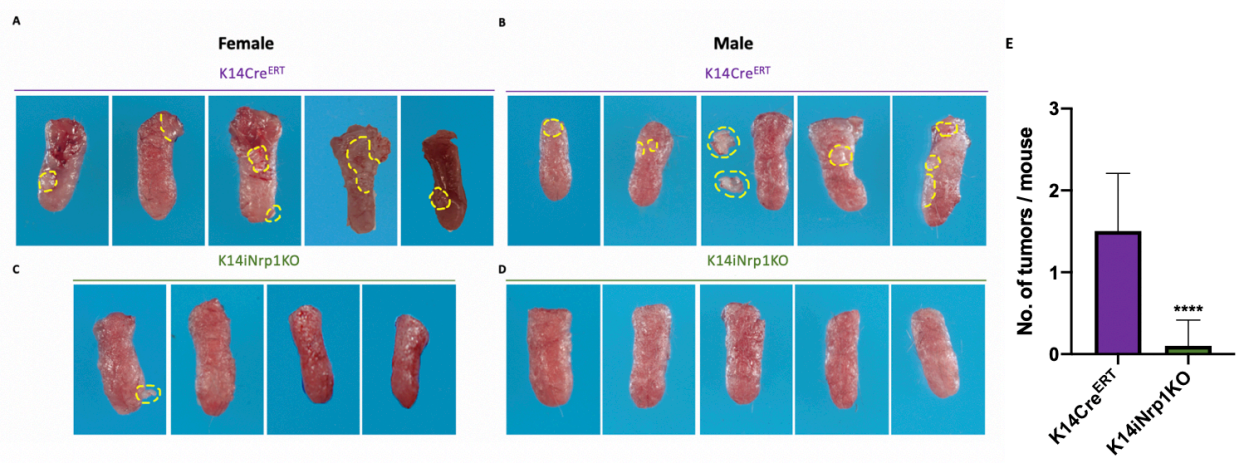

Figure 17: A. Gross images of female K14Cre^{ERT} tongues showing one or more tumors present in all mice. **B.** Gross images of male K14Cre^{ERT} tongues showing one or more tumors present in all mice, with 2 exhibiting multiple lesions in the tongue as well as gingival and palatal mucosa. **C.** Gross images of female K14iNrp1KO tongues showing that one out of four mice developed a mass. **D.** Gross images of male K14iNrp1KO tongues are devoid of any tumor or mass formation. **E.** Number of tumors per mouse was graphed for each group; the mean number of tumors per mouse was significantly less in K14iNrp1KO mice (n=9) compared to K14Cre^{ERT} (n=10) (****p<0.0001).

Histological examination of K14Cre^{ERT} tongues showed 100% of mice developed carcinoma in situ (CIS) and/or invasive OSCC. Mice lacking Nrp1 in keratinocytes did not develop CIS or OSCC. However, three mice deficient in *Nrp1* showed epithelial hyperplasia and one had a papilloma (a benign epithelial proliferation) (select images shown in **Figure 18**). Note: At the writing of this thesis, 6/10 control tongues and 6/9 K14iNrp1KO tongues have been returned from the pathology core; as samples continue to arrive, graphs will be updated. Deletion of the Nrp1 protein in the epithelial compartment of K14Nrp1iKO was confirmed using Nrp1 immunostaining in the harvested tongues (**Figure 19**).

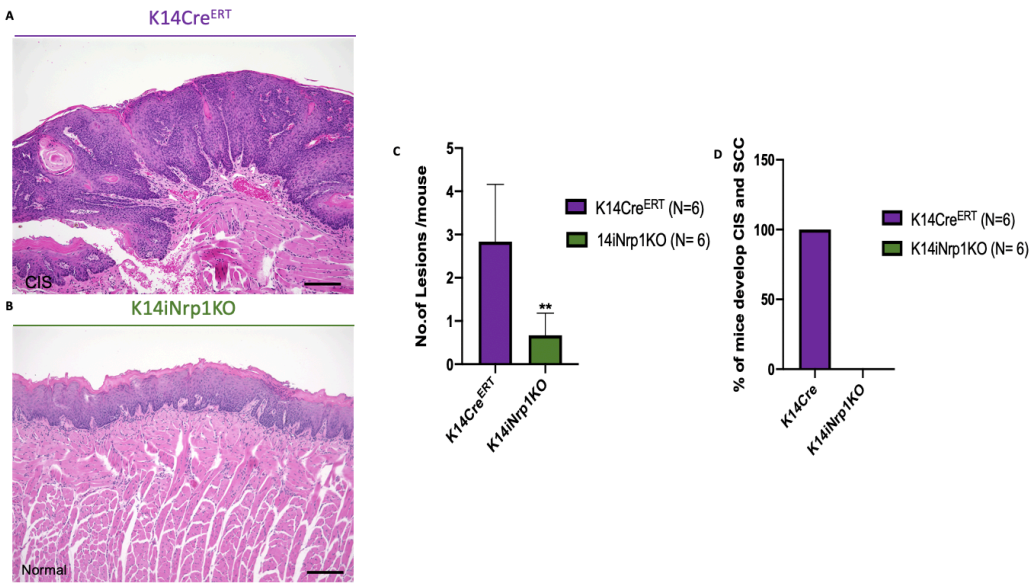

Figure 18: A. Representative hematoxylin and eosin stain of K14Cre^{ERT} tongue shows carcinoma in situ. **B.** Representative hematoxylin and eosin stain of K14iNrp1KO tongue shows normal tongue mucosa. **C.** The number of lesions per mouse was graphed for each group; the mean numbers of lesions per mouse was significantly less in K14iNrp1KO mice (n=6) compared to K14Cre^{ERT} (n=6) (**p<0.01). **D.** The percent of mice developing CIS or OSCC was graphed for each group; K14iNrp1KO mice did not develop any malignancies.

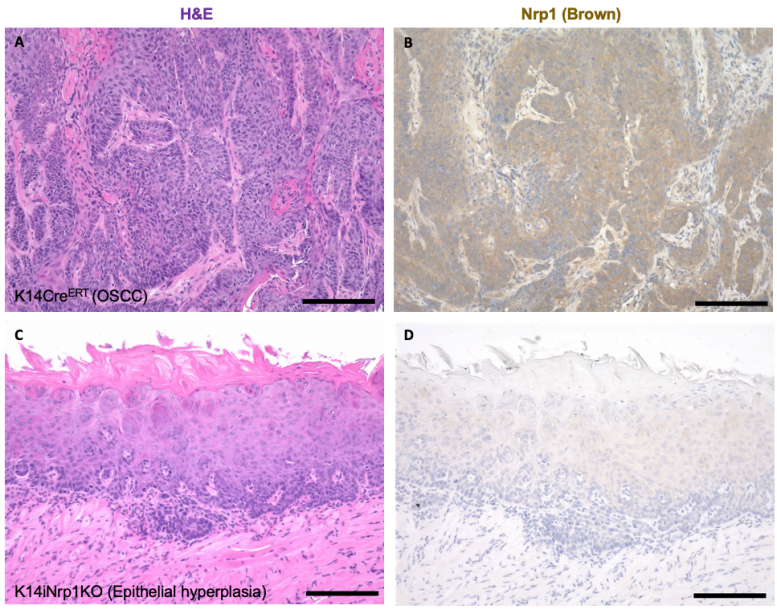

Figure 19: A. Hematoxylin and eosin stain of K14Cre^{ERT} tongue shows invasive OSCC. **B.** Immunostain of antibody directed against Nrp1 (Abcam) shows Nrp1 expression in carcinoma cells of K14Cre^{ERT} mice. **C.** Hematoxylin and eosin stain of K14iNrp1KO tongue shows epithelial hyperplasia. **D.** Immunostain of antibody directed against Nrp1 (Abcam) confirms the absence of Nrp1 expression in tongue oral mucosa of K14iNrp1KO mice.

Aim 1B:

We found that Knocking down of NRP1 in human HSC3 (HSC3 siNRP1) cells reduced cell viability (**Figure 20 B**) and inhibited colony formation in soft agar, compared to controls (HSC3 siControl) (**Figure 20 C-D**) The addition of both known ligands (SEMA3A and VEGF) that bind to NRP1 separately *in vitro* showed cell growth difference in VEGF proliferation (**Figure 20 E**) assay but not SEMA3A (**Figure 20 F**).

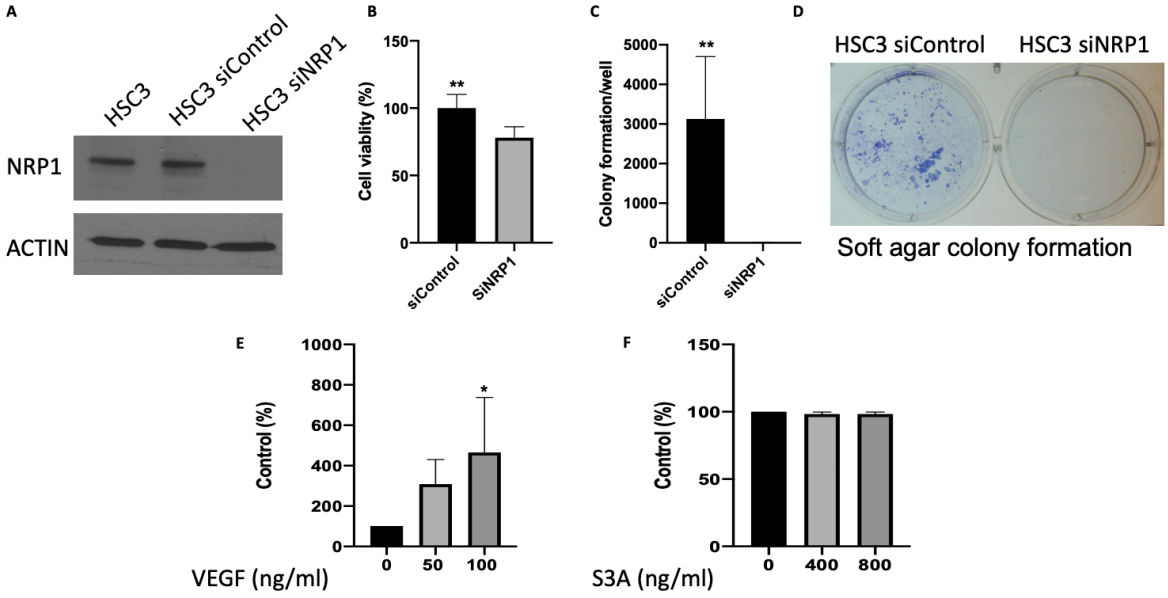

Figure 20: A. Immunoblotting confirms that HSC3 expresses NRP1. HSC3 cells treated with (siControl) still express NRP1 and HSC3 cells treated with (siNRP1) show no expression of NRP1 protein**. B.** Mean of the cell viability measured using MTT assay is significantly reduced in HSC3 siNRP1 cells compared to HSC3 siControl (**p<0.001) **C.** Representative colony formation of HSC3 treated with siControl and SiNRP1 were seed in soft agar. **D.** Mean colony formation per well of each group was graphed. Number of colonies in HSC3 siNRP1 is significantly less than HSC3 siControl. (**p<0.001). **E.** VEGF protein show significant increase in HSC3 proliferation in high dose (*p<0.01) **F.** SEMA3A protein didn't affect HSC3 proliferation.

Aim 2A:

We examined 21 human samples of oral epithelial dysplasia of different stages and 2 normal mucosa (one benign fibroma covered by normal mucosa and reactive mucosa adjacent to traumatic ulcer) for NRP2 expression. We found normal oral mucosa was devoid of NRP2 expression in both epithelium and quiescent endothelium (n=2) (**Figure 21 B**). During the early stages of oral epithelial dysplasia (aka. mild), NRP2 is only expressed in the underlying endothelium but not the epithelium (n= 4) (**Figure 22 B**). However, it is highly upregulated in moderate dysplasia (n=6) and severe dysplasia (n=11), in both the epithelium and the subjacent blood vessels as well as some inflammatory cells (**Figure 23 B, D**).

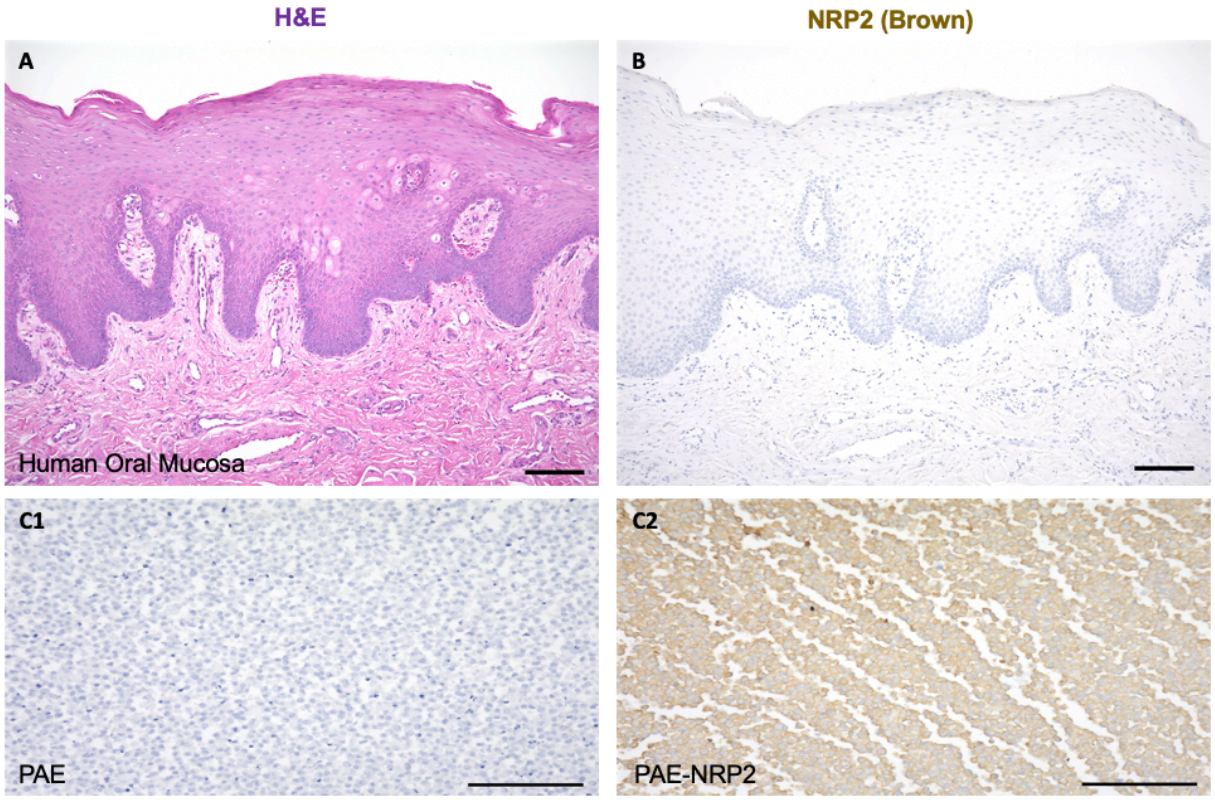

Figure 21: A. Hematoxylin and eosin stain of human oral mucosa. **B.** Immunostain of human oral mucosa using antibody directed against human NRP2 (Sigma) show absence of NRP2 expression in both epithelium and blood vessels. **C1-2:** Porcine aortic endothelial cells (PAE) **(C1)** and PAE transfected with NRP1 (not shown) were used as negative controls and PAE transfected with NRP2 (PAE-NRP2) **(C2)** was used as a positive control. NRP2 reactivity is seen as a brown color; all slides are counterstained with hematoxylin (blue color). Scale bar =100 μm.

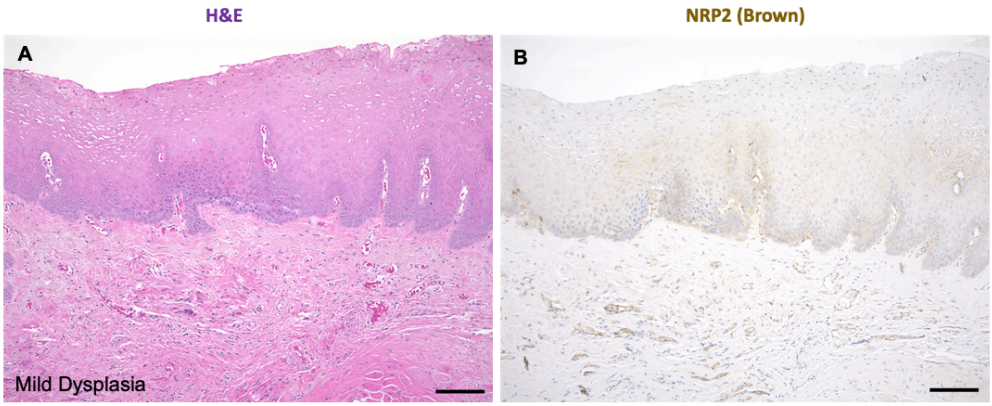

Figure 22: A. Hematoxylin and eosin stain of mild dysplasia that exhibits focal basal cell hyperplasia and hyperchromasia limited to the lower third of the epithelial thickness. **B.** Immunostain using NRP2 (Sigma) shows faint and focal NRP2 expression in the endothelium. Scale bar =100 μm.

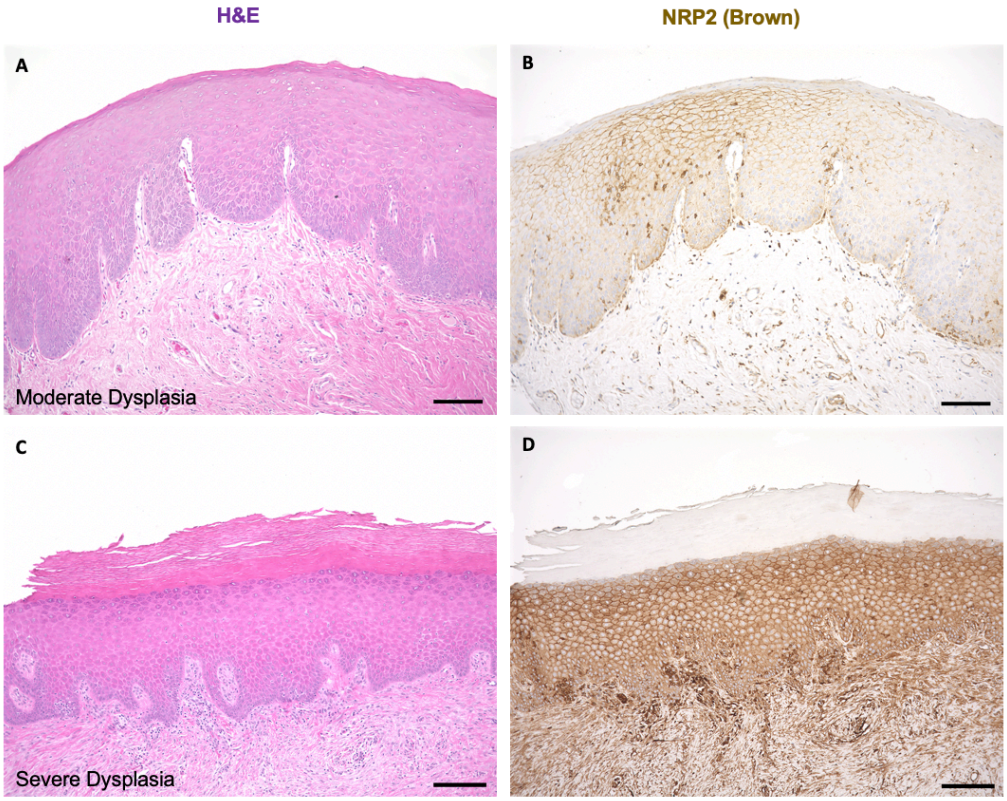

Figure 23: A. Hematoxylin and eosin stain of moderate dysplasia that exhibits acanthosis, basal cell hyperplasia, hyperchromasia and cells with increased nuclear to cytoplasmic ratio involving half of the epithelial thickness. **B.** Immunostain of using NRP2 (sigma) shows membranous staining in the layers of the epithelium and subjacent blood vessels. **C.** Hematoxylin and eosin stain of severe dysplasia that exhibits basal cell hyperplasia, dyskeratosis and hyperchromasia involving more than half of the epithelial thickness. **D.** Immunostain of using NRP2 (sigma) shows strong, membranous expression in the epithelium in all the layers and subjacent blood vessels. Scale bar =100 μm.

Similar findings were seen in mouse normal tongue mucosa (n=5); Nrp2 expression is not found in either epithelium nor endothelium (**Figure 24 B**).

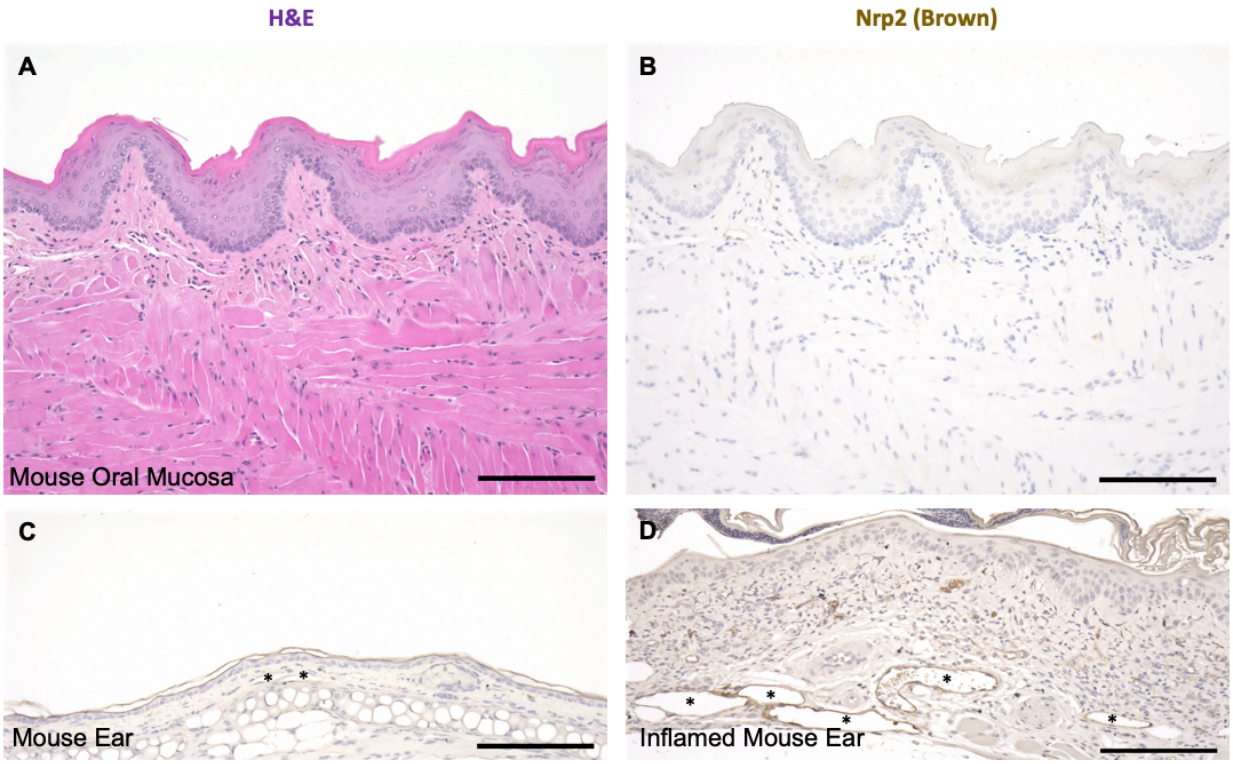

Figure 2-4: A. Hematoxylin and eosin stain of normal mouse tongue mucosa. **B.** Immunostain of mouse oral mucosa using antibody directed against mouse Nrp2 (Cell Signaling) show absence of Nrp2 expression in both epithelium and endothelium. **C.** Normal mouse ear was used as a negative control where quiescent endothelial cells do not express Nrp2 (asterisk denotes negative vessels). **D.** Inflamed mouse ear where endothelial cells upregulate Nrp2 expression was used as a positive control (asterisk denotes positive vessels). Scale bar =100 μm.

Nrp2 expression was also examined in different stages of the mouse model of 4NQO oral carcinogenesis. The results paralleled NRP2 expression in human samples. Early stages of carcinogenesis (epithelial hyperplasia) showed low and faint Nrp2 expression only in the endothelial cells (**Figure25 B**). High-grade dysplasia showed Nrp2 upregulation in both epithelial and endothelial cells (**Figure 25 D**).

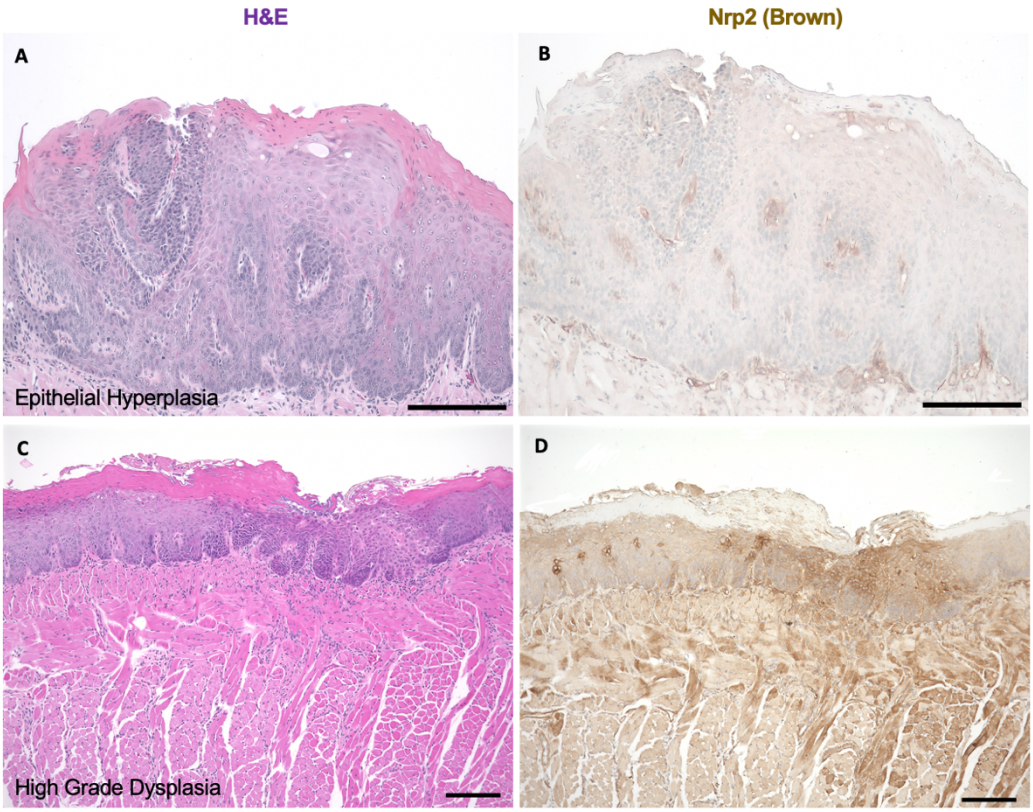

Figure 25: A. Hematoxylin and eosin stain of mouse epithelial hyperplasia (induced by 4NQO) that exhibits acanthosis and focal basal cell hyperplasia. **B.** Immunostain of Nrp2 (Cell Signaling) shows faint and focal NRP2 expression in the endothelium. **C.** Hematoxylin and eosin stain of mouse high grade dysplasia (induced by 4NQO) exhibits basal cell hyperplasia, dyskeratosis, cells with increased nuclear to cytoplasmic ratio and cellular pleomorphism involving the full epithelium thickness. **D.** Immunostain of Nrp2 (Cell Signaling) shows strong, membranous expression in the epithelium in all the layers and subjacent blood vessels in the dysplastic area. Adjacent normal epithelium is devoid of Nrp2 expression except for melanocytes. Scale bar =100 μm.

NRP2 expression was analyzed in human OSCC xenograft models as well as in human biopsies of OSCC. Human OSCC cell lines (HSC3, SCC9) were injected orthotopically into immunodeficient (nude) mice, and the human OSCC tumor cells showed strong immunoreactivity to NRP2 by IHC (HSC3 shown in **Figure 26 B**; SCC9 data not shown). OSCC samples from human subjects showed high NRP2 expression in both well- and poorly-differentiated OSCC (**Figure 27 B, D**).

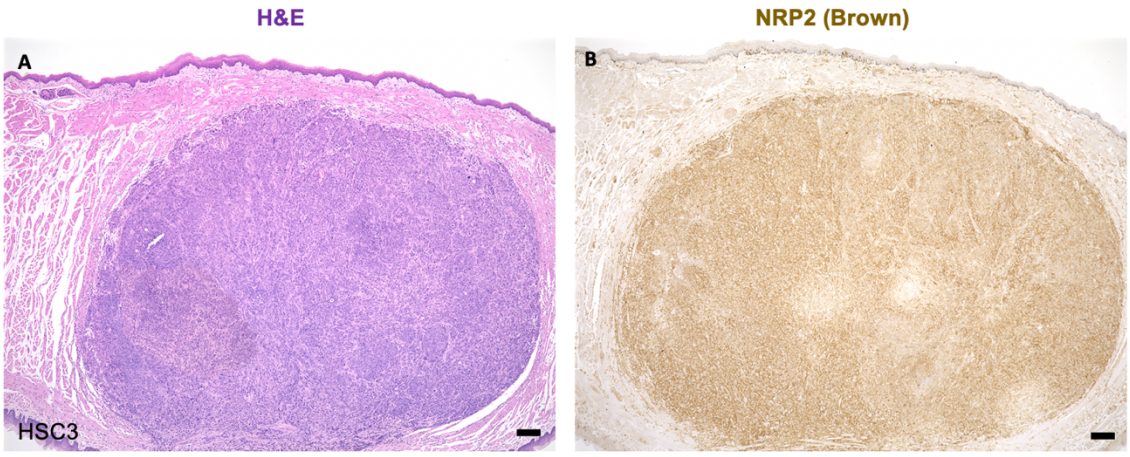

Figure 26: A. Hematoxylin and eosin stain of human OSCC (HSC3) xenograft implanted in immunodeficient mouse tongue. **B.** Immunostain of NRP2 (Sigma) shows membranous staining in carcinoma cells. Scale bar =100 μm.

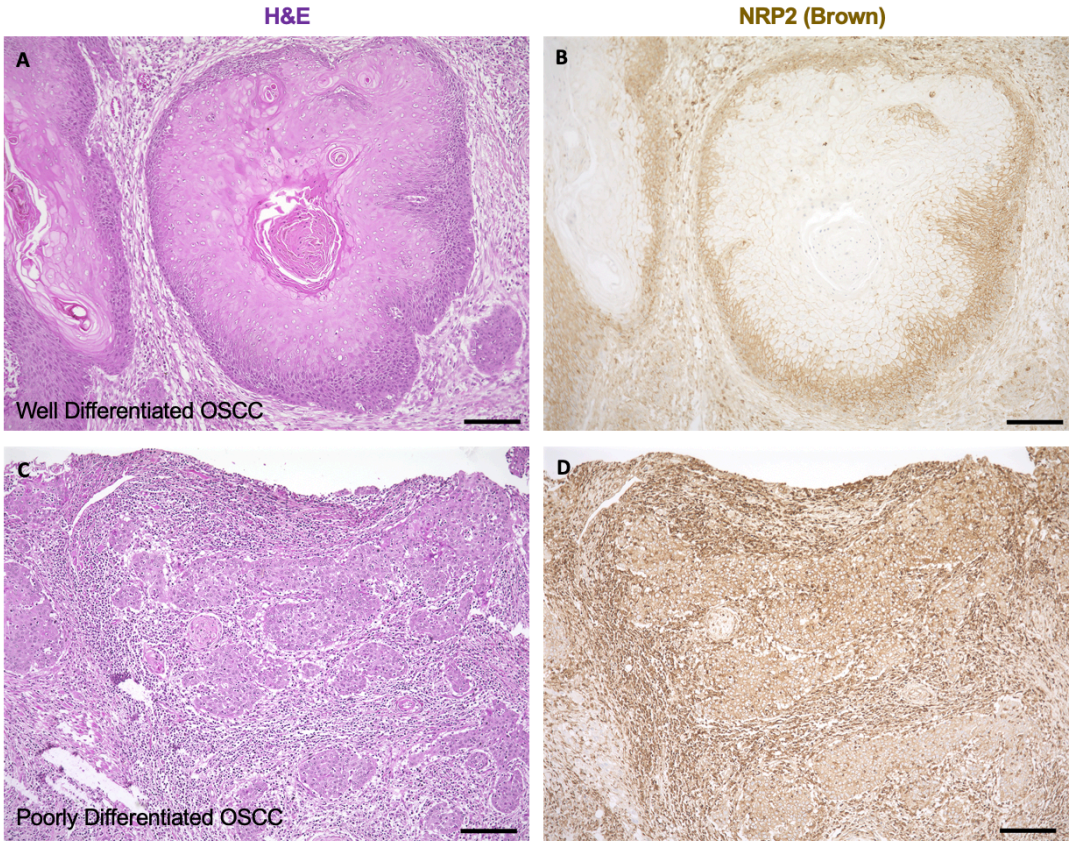

Figure 27: A. Hematoxylin and eosin stain of human well-differentiated OSCC. **B.** Immunostain of NRP2 (Sigma) shows membranous staining of carcinoma cells especially in the basal layers of the tumor islands. **C.** Hematoxylin and eosin stain of human poorly differentiated OSCC. **D.** Immunostain of NRP2 (Sigma) shows diffuse, membranous staining of carcinoma cells, inflammatory cells and endothelial cells. Scale bar =100 μm.

Orthotopic mouse OSCC (WT3-Luc) isografts grown in syngeneic C57Bl/6 mice also highly express Nrp2 in both carcinoma cells and associated blood vessels (**Figure 29**). Lastly, mouse spontaneous OSCC from the 4NQO oral carcinogenesis model exhibited similar findings (**Figure 30 B)**.

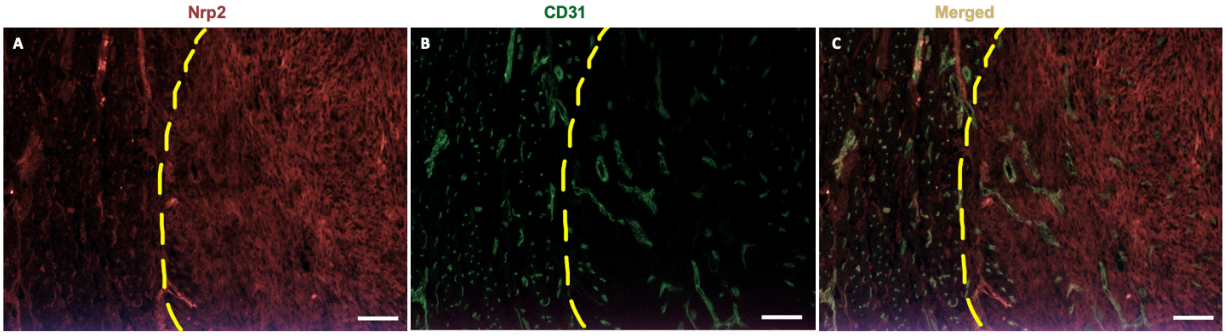

Figure 29: A. Immunofluorescent stain using Nrp2 (Cell Signaling) shows that both carcinoma cells and endothelial cells express Nrp2 (red color) in WT3-Luc tongue tumors. **B.** Immunofluorescent stain using CD31 (green color, BD Pharminogen) highlights blood vessels in WT3-Luc tumors and surrounding stroma. **C.** Merged CD31 and Nrp2 immunofluorescent staining shows Nrp2 expression in carcinoma cells (red) and blood vessels (overlay color is yellow).

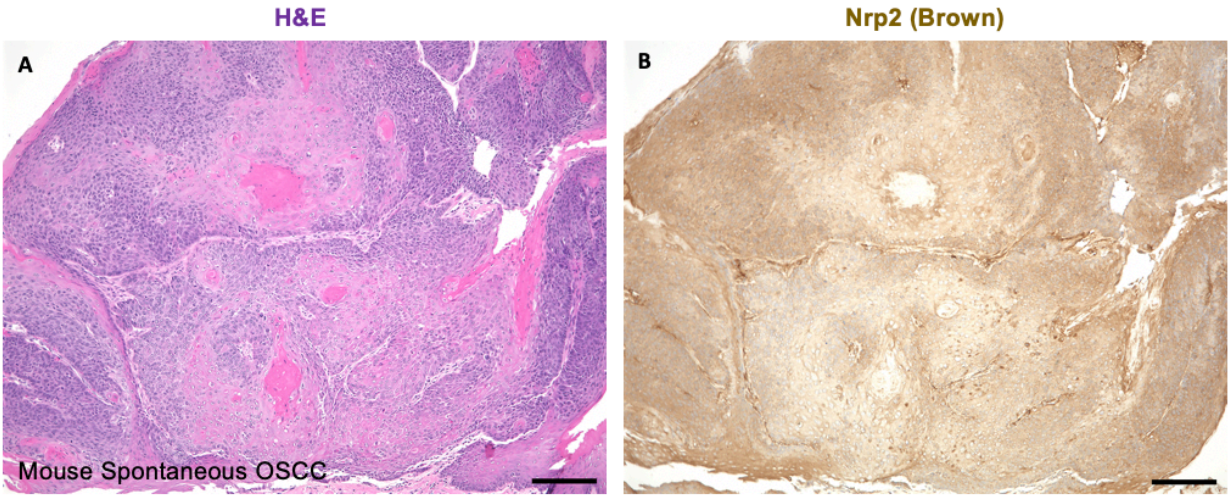

Figure 2-30: A. Hematoxylin and eosin stain of mouse OSCC from the 4NQO (spontaneous) oral carcinogenesis model. **B.** Immunostain of Nrp2 (Cell Signaling) shows membranous staining of carcinoma cells as well as endothelial cells. Scale bar = 100 μm.

Aim 2B:

Conditional deletion of Nrp2 in keratinocytes (K14-Nrp2 mice; **Figure 31 A**) was used to understand the role of the Nrp2 receptor in OSCC tumorigenesis. Nrp2-floxed and K14Cre^{ERT} mice were used as controls (**Figure 31 A and B**). Mice lacking Nrp2 in keratinocytes after 4-OHT were viable with normal epidermis and oral mucosa. After 4-OHT administration, confirmation of *Nrp2* gene deletion was analyzed using specific PCR primers to detect the recombined DNA sequence (**Figure 31 C**). The 4-NQO carcinogen was given to the mice in the drinking water, ad libitum, for 16 weeks to generate premalignant lesions and OSCC in Nrp2-floxed, K14Cre^{ERT} and K14iNrp2KO mice. Mouse weight was quantified once a week after 4-NQO termination for 9 weeks. In general, both male and female K14iNrp2KO mice were larger in size, compared to Nrp2-floxed and K14Cre^{ERT} mice. However, the rate of weight of loss in all groups were similar and no group lost more than 20% of body mass (**Figure 32**).

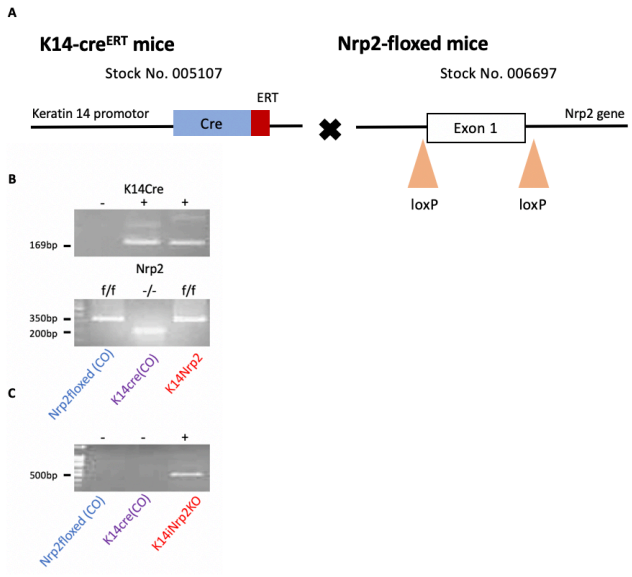

Figure 31: A. Genetic strategy used to study the role of Nrp2 in keratinocytes during OSCC tumorigenesis. **B.** Representative agarose gels of Nrp2-floxed, K14Cre^{ERT} and K14-Nrp2 genotyping. Agarose gel illustrates a band size of 169 bp that indicates *Cre* is present in 2nd and 3rd lanes (top panel). Agarose gel illustrates a band size of 350 bp that indicates the *Nrp2* gene is floxed in the 1st and 3rd lanes and a band size of 200 bp indicates the *Nrp2* gene is not floxed in the 2nd lane (bottom panel). **C.** Agarose gel illustrates a band size of 500 bp, which confirms that the *Nrp2* gene was recombined (loss of exon 1) after 4-OHT administration in the 3rd lane.

At the end of the 9-week observation period, mice were sacrificed, necropsied and their tongues were harvested from Nrp2-floxed, K14Cre^{ERT} and K14iNrp2KO mice. Grossly, Nrp2-floxed (n=7) and K14Cre^{ERT} mice (n=10) showed formation of at least one or two masses per mouse, as well as white plaques on the tongue, gingiva and palatal mucosa (**Figure 33 A-D**). *Note: the same K14Cre^{ERT} mice were used as controls in all Aims 1-3. Five out of nine K14iNrp2KO mice formed one tumor; one mouse had 2 tumors in the tongue; and 3 mice did not develop any tumors (**Figure 33 E-F**).

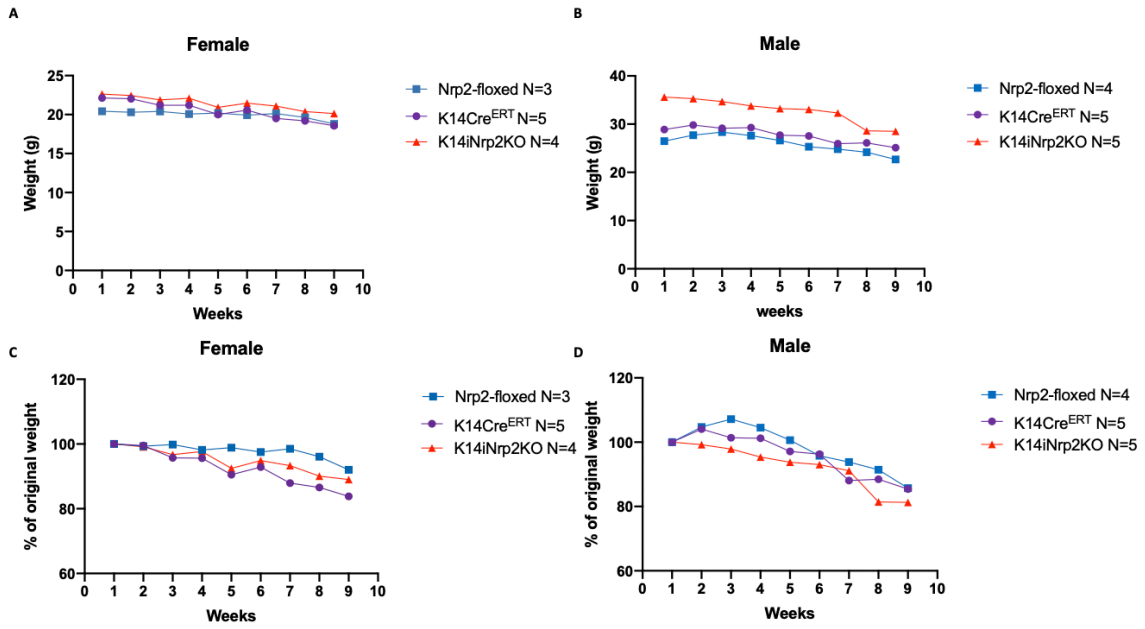

Figure 32: Quantification of mice weight following carcinogen treatment. **A-B.** Nrp2-floxed (blue), K14Cre^{ERT} (purple) and K14iNrp2KO (red) mice were followed for 9 weeks after 4NQO termination and weights were recorded weekly. Weights from each group were averaged for each time point and none of the groups differed significantly at any time point. **A, C.** Female mice. **B, D.** Male mice. **C-D.** The percent of original body weight was calculated for each group and averaged. None of the groups exceeded 20% loss in body mass during this observation period. *Note: error bars were removed to make the graphs easier to read.

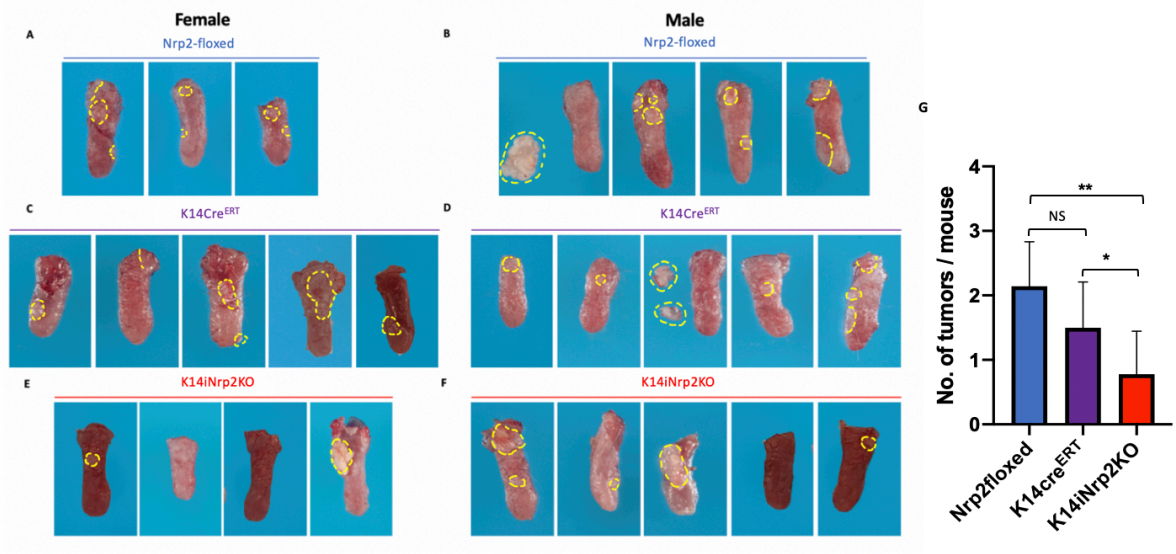

Figure 33: Gross images of female Nrp2-floxed **(A)**, K14-Cre^{ERT} **(C)**, and K14iNrp2KO **(E)** tongues showing one or more tumors present in all Nrp2-floxed and K14Cre^{ERT} but only 2/4 mice develop single tumor in the K14iNrp2KO group. Gross images of male Nrp2floxed **(B)** K14Cre^{ERT} **(D)**, and K14iNrp2KO **(F)** tongues showing multiple tumors present in all Nrp2-floxed and K14Cre^{ERT}; 3/5 K14iNrp2KO mice have only single tumor; 1/5 had 2 tumors and 1/5 did not develop any tumors. **G.** Number of tumors per mouse was graphed for each group; the mean number of tumors per mouse was significantly less in K14iNrp2KO mice (n=9) compared to Nrp2floxed (n=7) and K14Cre^{ERT} (n=10) mice (**p<0.001; *p<0.01).

Histological examination of Nrp2-floxed (2/2) and K14Cre^{ERT} (6/6) mice showed that 100% of examined tongues developed CIS and invasive OSCC (**Figure 34 A-B, E**). Mice lacking *Nrp2* in keratinocytes showed reduced incidence of malignancy with only 22% (2/9) of the mice developing CIS or invasive OSCC (**Figure 34 E**). However, some K14iNrp2KO mice that did not appear to have lesions in the gross images, did show early stages of carcinogenesis including oral dysplasia when examined histologically (**Figure 34 C**). Note: At the writing of this thesis, 6/10 K14Cre^{ERT} control tongues, 2/7 Nrp2-floxed control tongues, and 9/9 K14iNrp2KO tongues have been returned from the pathology core and examined histologically; as samples continue to arrive, graphs will be updated.

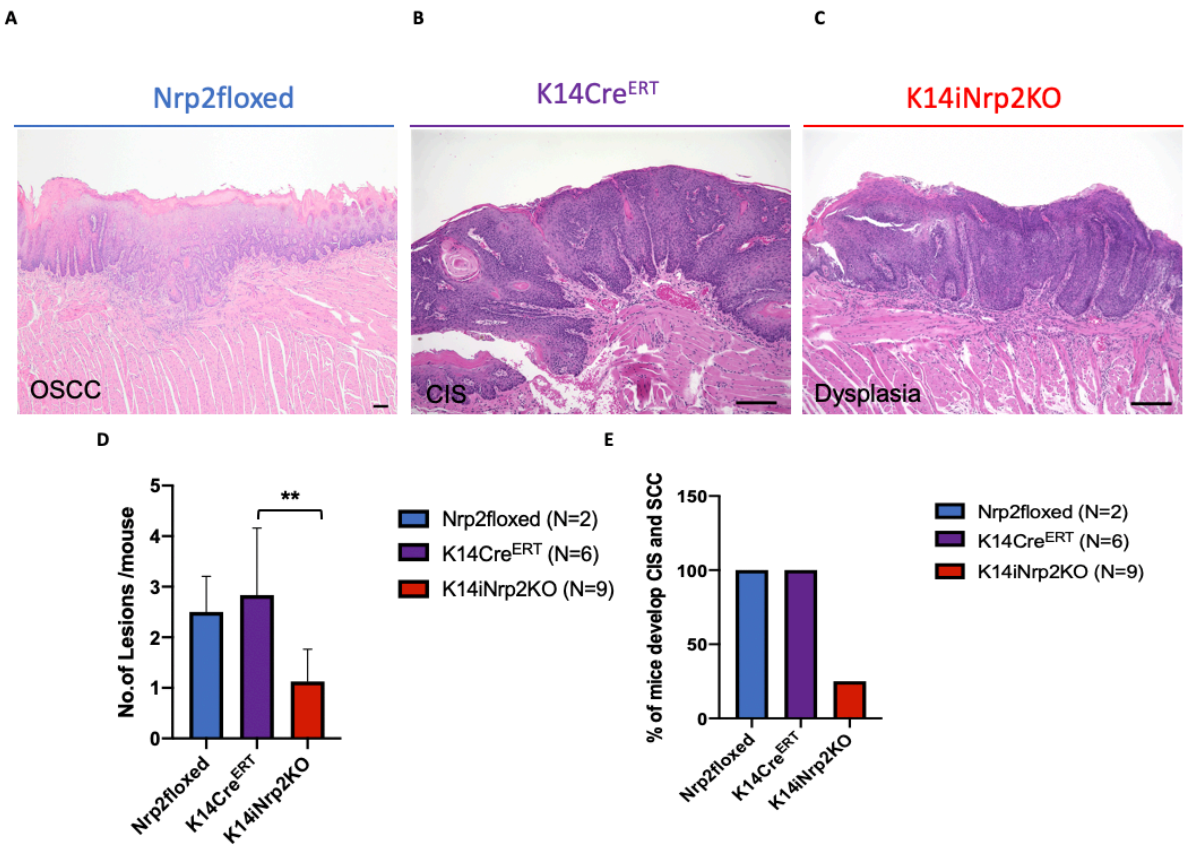

Figure 34: A. Representative image from hematoxylin and eosin stain of Nrp2-floxed tongue showing invasive OSCC. **B.** Representative hematoxylin and eosin stain of K14Cre^{ERT} tongue shows carcinoma in situ (CIS). **C.** Representative hematoxylin and eosin stain of K14iNrp2KO tongue shows dysplasia. **D.** Number of lesions per mouse was averaged and graphed for each group; the mean number of lesions per mouse was significantly less in K14iNrp2KO mice (N=9) compared to K14Cre^{ERT} (N=6) (**p<0.01). **E.** The percent of mice developing CIS or OSCC was calculated and graphed for each group; only 25% of K14iNrp2KO developed CIS or OSCC.

Aim 2C:

To study the role of Nrp2 in the tumor microenvironment (mainly blood vessels), syngeneic mouse OSCC (WT3-Luc) that express Nrp2 (**Figure 2-35 A**) were implanted into the tongues of C57Bl/6 wildtype (*Nrp2*$^{+/+}$) and *Nrp2*-deficient (*Nrp2*$^{-/-}$) mice. The incidence of WT3-Luc isografts was not significantly different between *Nrp2*$^{+/+}$ (5/5) and *Nrp2*$^{-/-}$ (4/5) mice after 10 days of tumor growth *in vivo* (**Figure 35 B**). Additionally, tumor size in both groups was comparable when visualized and measured using a bioluminescence *in vivo* imaging system (IVIS) (**Figure 35 C**); following euthanasia and necropsy, histological examination of the tongues corroborated the imaging results (**Figure 35 D-E**). Incidentally, we did not observe the WT3-luc model to metastasize to regional lymph nodes or distant organs in any of our trials. Mice were imaged using IVIS after primary tumor removal but no additional signals were seen.

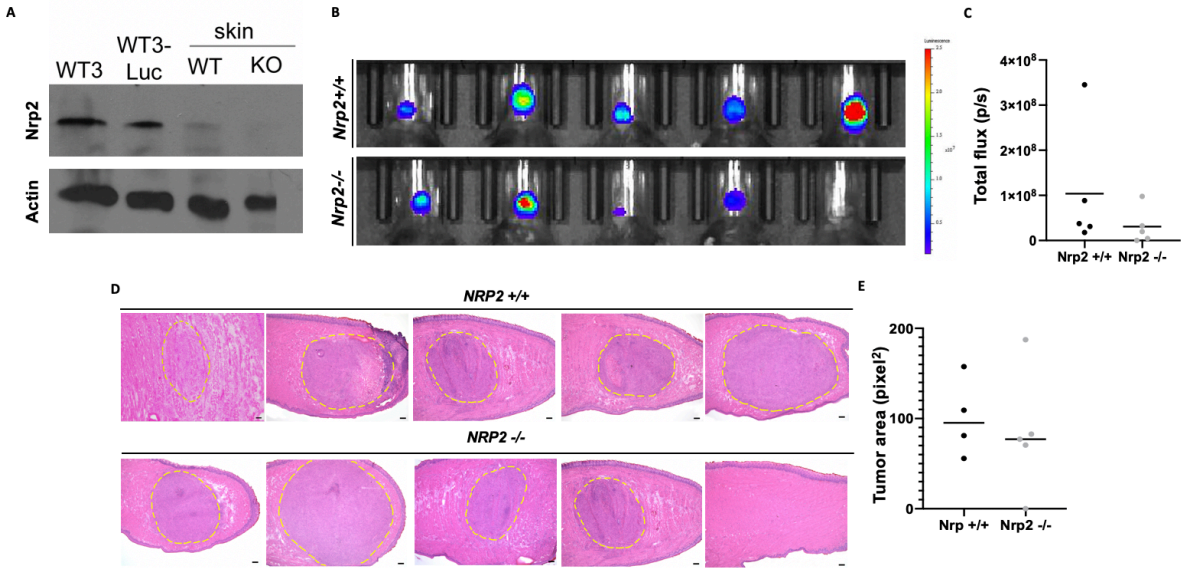

Figure 35: A. Immunoblotting confirms WT3 and WT3-Luc cells express Nrp2 protein. Protein lysates from Nrp2+/+ (WT) or Nrp2-/- (KO) mouse skin served as positive and negative controls, respectively. **B.** After 10 days of growth in vivo, Xenogen IVIS images of WT3-Luc isografts in Nrp2$^{+/+}$ and Nrp2$^{-/-}$ mice demonstrate tumor presence and relative luciferase activity (where red is high, dark blue is low). Tumor incidence: Nrp2$^{+/+}$ = 5/5, Nrp2$^{-/-}$ = 4/5). **C.** Total flux/tumor is graphed for each group; mean tumor flux was not significantly different between the groups. **D.** Hematoxylin and eosin stain of mouse tongue tumors from both Nrp2$^{+/+}$ and Nrp2$^{-/-}$ mice confirm tumor size and incidence. (Nrp2$^{+/+}$ = 5/5, Nrp2$^{-/-}$ = 4/5). **E.** Tumor cross sectional area is graphed for each group; mean tumor size was not significantly different between the groups. Scale bar =100 μm.

Interestingly, although overall tumor size did not differ significantly between WT and Nrp2-KO mice, IHC examination using CD31 staining revealed a 46% reduction in microvessel density per field in *Nrp2*$^{-/-}$ mice compared to *Nrp2*$^{+/+}$ controls (**Figure 2-36 A**). Additionally, Lyve1 staining showed a 74% reduction in peri-tumoral lymphatic vessels in *Nrp2*-deficient mice compared to *Nrp2*-intact control mice (**Figure 2-36 B**).

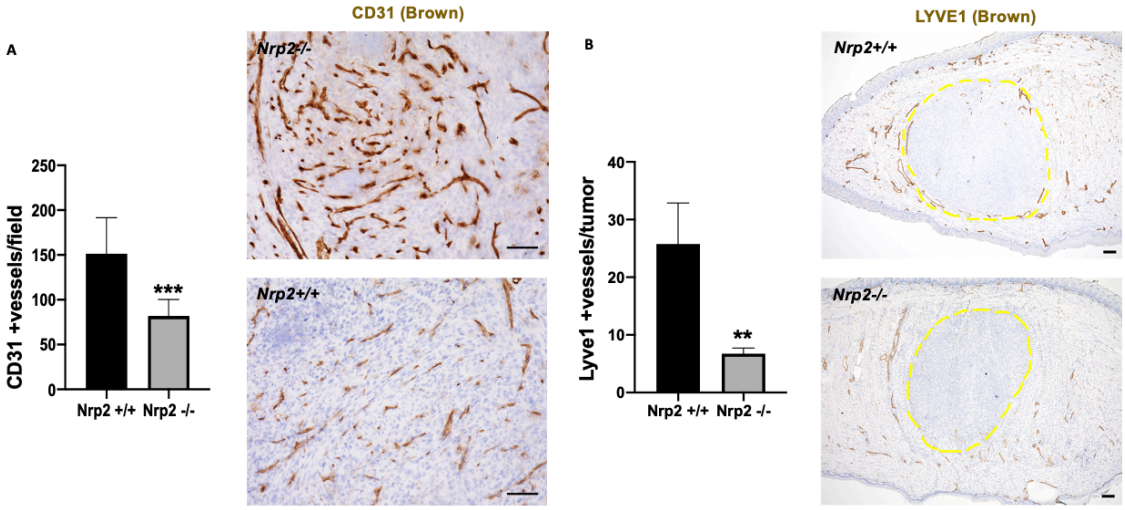

Figure 36: A. Intra-tumoral blood vessel density was significantly lower in *Nrp2*$^{-/-}$ mice compared to *Nrp2*$^{+/+}$ mice (***p<0.001). Panels to the right of the graph show representative IHC images of CD31 (brown color) staining and hematoxylin counterstaining (blue color) in each group. Blood vessels in WT mice were thicker and more branched than in Nrp2-KO mice. **B.** Peri-tumoral lymphatic vessel numbers were significantly lower in *Nrp2*$^{-/-}$ mice compared to *Nrp2*$^{+/+}$ mice (**p<0.01). Panels to the right of the graph show representative IHC images of Lyve1 (brown color) staining and hematoxylin counterstaining (blue color) in each group. Scale bar =100 μm.

Since the vessel density was lower in the OSCC injected tongue tumors in *Nrp2*-deficient mice compared to wildtype littermates, we tested whether the normal tongue vessel density was already lower prior to tumor implantation. Blood and lymphatic vessels were compared between normal adult tongues from *Nrp2*$^{+/+}$ *and Nrp2*$^{-/-}$ mice using IHC. There was no significant difference between the two groups in terms of blood vessel number or size (cross sectional area) (**Figure 37 A-B**). However, lymphatic capillary vessel numbers

(identified by Lyve1 staining) were 25% lower in *Nrp2*$^{-/-}$ mice compared to *Nrp2*$^{+/+}$ group (**Figure 37 C**), consistent with published reports.(48, 74)

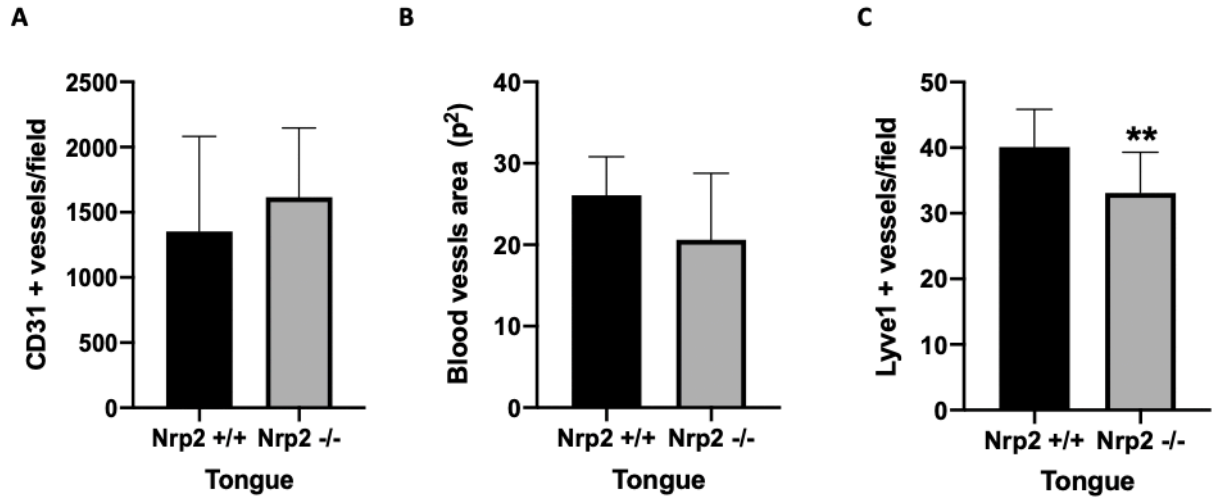

Figure 37: A. Blood vessel numbers (CD31+) per field in normal tongue mucosa were similar in *Nrp*$^{-/-}$ and *Nrp2*$^{+/+}$ mice. ***B.*** Blood vessel area (pixels^2) per field in normal tongue mucosa was similar in *Nrp*$^{-/-}$ and *Nrp2*$^{+/+}$ mice. **C.** Lymphatic vessel numbers (Lyve1+) per field were significantly lower in *Nrp2*$^{-/-}$ compared to *Nrp2*$^{+/+}$ mice (**p<0.01). Blood vessel images were taken at 100X magnification and lymphatic vessel images were taken at 200X magnification.

Aim 3A:

Normal mouse tongue mucosa (n=5) expresses SEMA3F protein, as determined by IHC, in the suprabasal layers of the epithelium sparing the basal cell layer (**Figure 38 B**). The pattern of SEMA3F staining in the epithelium of the tongue was similar to that previously reported by our laboratory in normal mouse epithelium in the skin.(48) The peptide used to immunize rabbits to create the anti-SEMA3F antibody (contracted through GeneScript) was designed to the Sema domain of Sema3F and does not cross react with other SEMA3 proteins.(126) Controls for SEMA3F staining included SEMA3F-transfected melanoma tumor sections (positive control), depletion of staining by pre-incubation of antibody with pure SEMA3F protein prior to IHC incubation (competition control), and staining of constitutive *Sema3F*-deficient mice tissue sections (negative control) (data not shown).

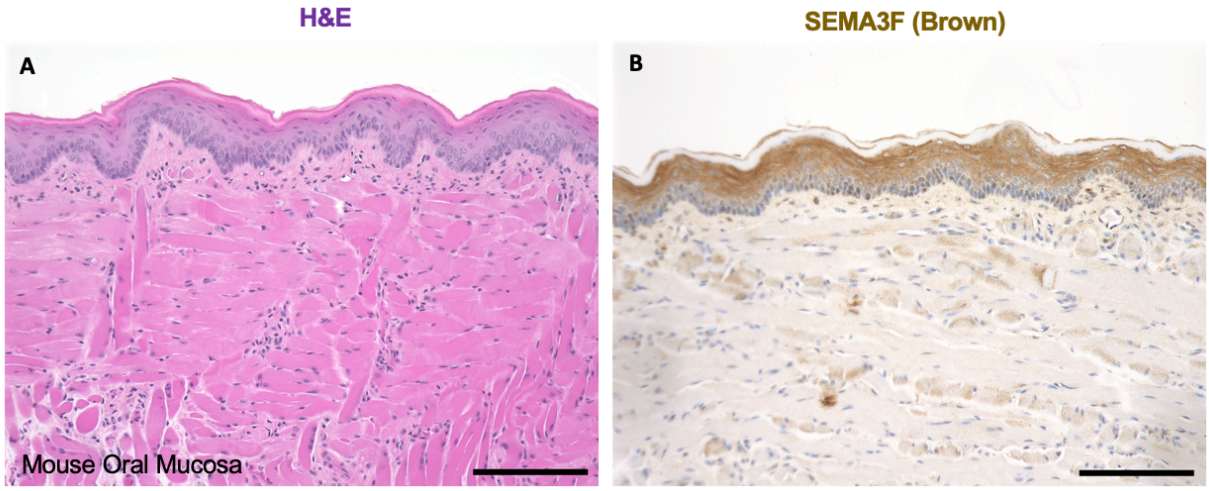

Figure 38: **A.** Hematoxylin and eosin stain of mouse tongue normal mucosa (ventral side). **B.** Immunostain of mouse oral mucosa using SEMA3F antibody (GeneScript) shows that Sema3F protein is present in the keratinocytes in the suprabasal layers of the epithelium. Scale bar =100 μm.

SEMA3F immunostaining showed diminished expression or at least partial loss in the epithelium during early stages of oral dysplasia, mainly in the severely transformed cells (**Figure 39 B**). In contrast, SEMA3F exhibited complete loss of expression in severe dysplasia and carcinoma cells in OSCC while the adjacent normal mucosa continued to express SEMA3F (**Figure 39 D**).

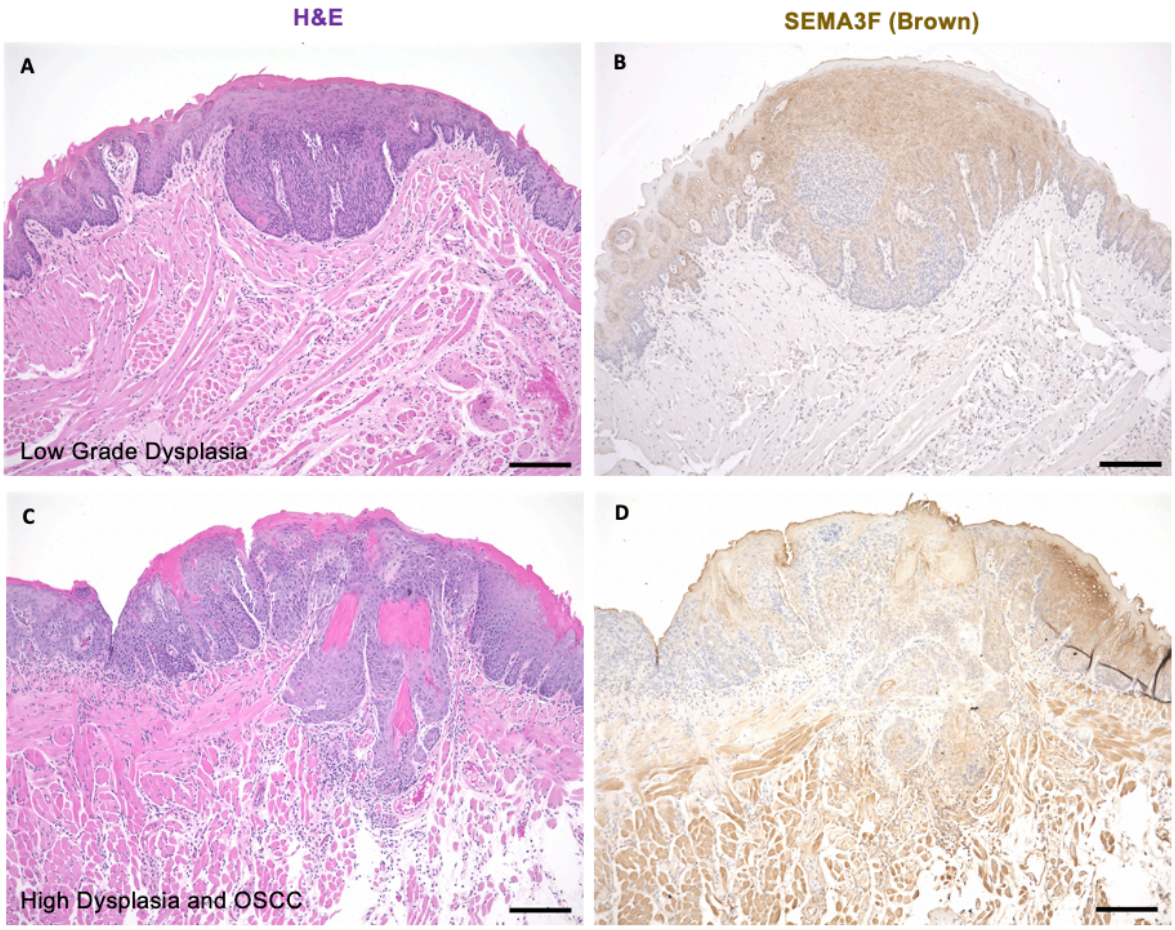

Figure 39: A. Hematoxylin and eosin stain of mouse low grade dysplasia that exhibits acanthosis, hyperchromasia with dyskeratosis. **B.** Immunostain for SEMA3F (Genescript) shows one focus of cells that exhibits loss of Sema3F protein expression. **C.** Hematoxylin and eosin stain of mouse invasive OSCC shows cells with increased nuclear to cytoplasmic ratio, cellular pleomorphism and dyskeratosis arising from high grade dysplasia (right side of section). **D.** Immunostain for SEMA3F shows loss of SEMA3F protein in the area of high dysplasia and invasive OSCC. Adjacent normal epithelium retained SEMA3F expression in the suprabasal layer. Scale bar =100 μm.

Aim 3B:

Mice with a conditional deletion in the *Sema3F* gene in keratinocytes (K14-Sema3F mice; **Figure 40 A-B**) were created and bred to understand the role of the Sema3F protein during OSCC tumorigenesis. K14Cre^{ERT} mice were used as controls (**Figure 15 B**). Mice lacking Sema3F in keratinocytes after 4-OHT were viable with normal epidermis and oral mucosa but one mouse developed malocclusion. After 4-OHT administration, confirmation of *Sema3F* gene deletion was analyzed using specific PCR primers designed to detect the recombined DNA sequence (**Figure 40 C**). The 4-NQO carcinogen was given in the drinking water, ad libitum, for 16 weeks to generate premalignant lesions and OSCC in K14Cre^{ERT} and K14iSema3FKO mice. Mouse weight was quantified once a week for 9 weeks after 4-NQO termination. In general, K14iSema3FKO mice were smaller in size than K14Cre^{ERT}mice, however their average weights were not statistically different based on our small sample size (**Figure 41 A-B**). Weights of individual female K14iSema3FKO mice were more variable than female K14-Cre^{ERT}mice. The female K14-Cre^{ERT} mice lost a higher percentage of weight in the first 3 weeks after 4-NQO termination than the female K14iSema3FKO mice (**Figure 41 C**); but male mice were similar in their rate of weight of loss in both groups (**Figure 41 D**) and no group lost more than 20% of body mass.

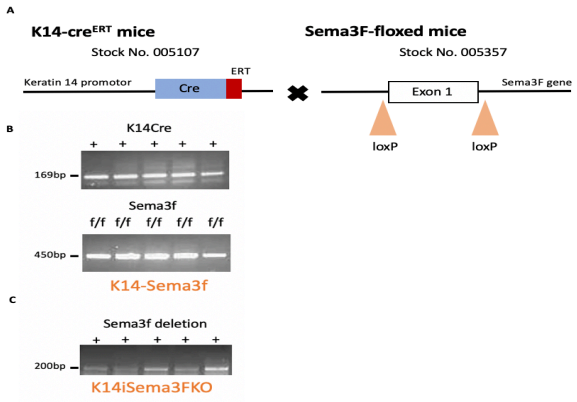

Figure 40: A. Genetic strategy used to study the role of Sema3F in keratinocytes during OSCC tumorigenesis. **B.** Representative agarose gels of K14-Sema3F genotyping. Agarose gel illustrates a band size of 169 bp indicating Cre is present (top panel). Agarose gel illustrates a band size of 450 bp indicating Sema3F gene is floxed (bottom panel). **C.** Agarose gel illustrates a band size of 200 bp, which confirms that the *Sema3F* gene was recombined (loss of exon 1) after 4-OHT administration.

At the end of the 9-week observation period, mice were sacrificed, necropsied and their tongues were harvested from K14Cre^{ERT} and K14iSema3FKO. Grossly, all K14Cre^{ERT} mice showed formation of one or more tumors, as well as white plaques of the tongue, gingiva and palatal mucosa (**Figure 42 A-B**). Surprisingly, none of K14iSema3FKO mice showed gross evidence of tumor formation, however one female showed a small white, keratinized plaque on the tongue, which is more consistent with benign epithelial hyperplasia (**Figure 42 C-D**).

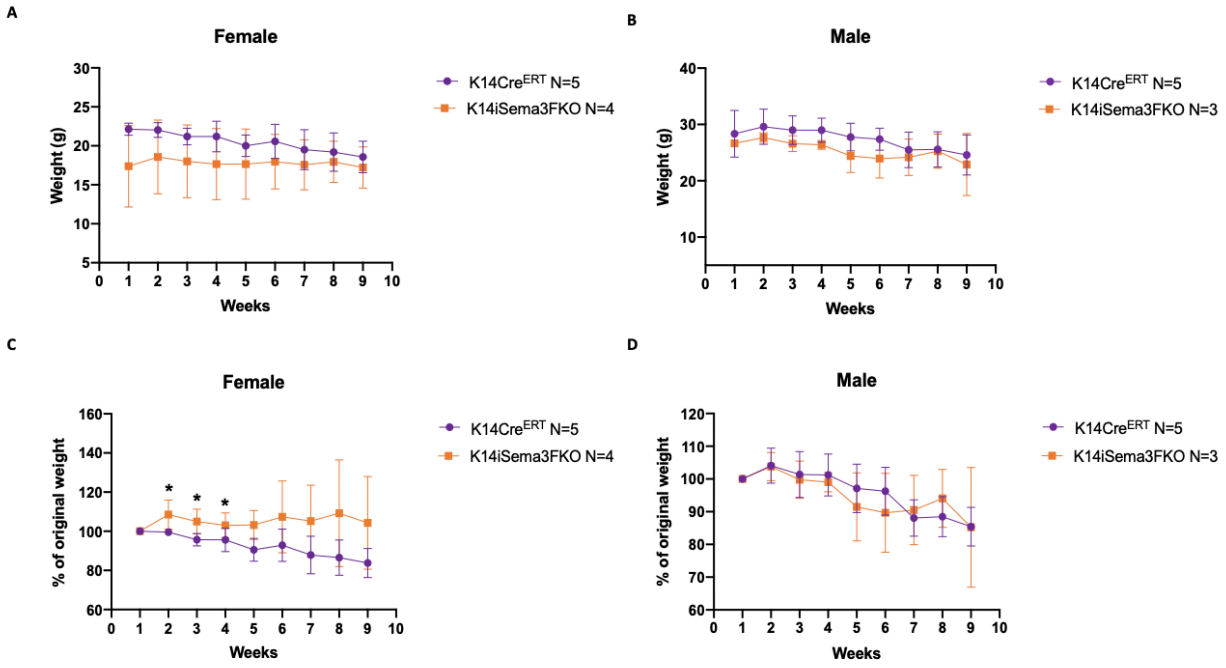

Figure 41: Quantification of mice weight following carcinogen treatment. **A-B.** K14Cre^{ERT} (purple) and K14iSema3FKO (orange) mice were followed for 9 weeks after 4NQO termination and weights were recorded weekly. Weights from each group were averaged for each time point (Mean; SD). **A, C.** Female mice. **B, D.** Male mice. **C-D.** The percent of original body weight was calculated for each group and averaged. Weight loss in female K14-Cre^{ERT} mice was significantly more than K14iSema3FKO mice from week 2 to week 4 (*p<0.05). None of the groups exceeded 20% loss in body mass during this observation period.

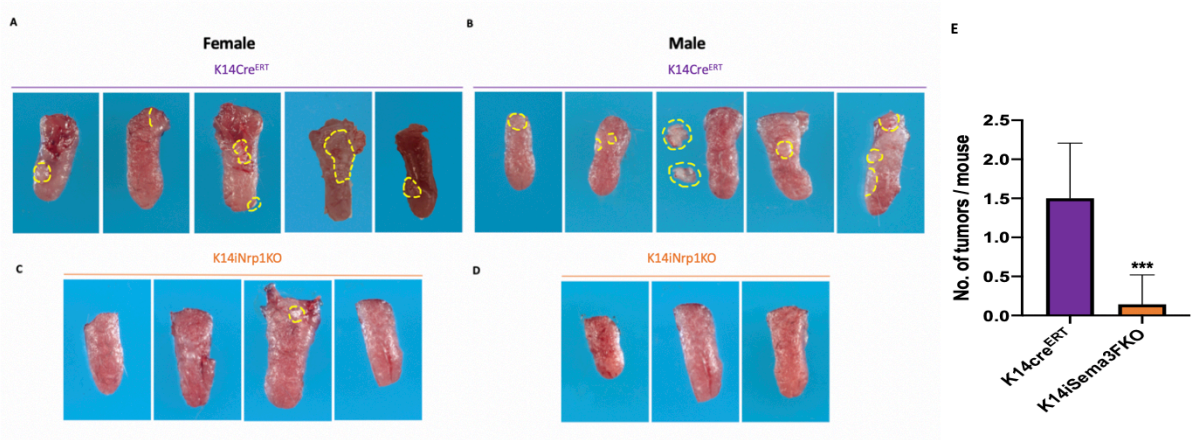

Figure 42: A. Gross images of female K14Cre^{ERT} tongues showing one or more tumors present in all mice. **B.** Gross images of male K14Cre^{ERT} tongues showing one or more tumors present in all mice, with 1 mouse exhibiting multiple lesions in the tongue as well as in the gingival and palatal mucosa. **C.** Gross imaging of female K14iSema3FKO tongues showing that one out of four mice developed a white plaque. **D.** Gross imaging of male K14iSema3FKO tongues are devoid of any plaque or tumor formation. **E.** The average number of tumors per mouse was graphed for each group; the mean number of tumors per mouse was significantly less in K14iSema3FKO mice (n=7) compared to K14Cre^{ERT} (n=10) (***p<0.001).

Histological examination of K14Cre^{ERT} tongues showed multiple histological changes in most of the mice and 6/6 exhibited carcinoma in situ (CIS) and/or invasive OSCC in examined specimens (**Figure 43 A, D**). To date, two K14iSema3FKO tongues have shown epithelial hyperplasia but there has been no evidence of dysplasia, CIS or OSCC in either examined (**Figure 43 B, D**). Note: At the writing of this thesis, 6/10 control tongues and 2/7 K14iSema3FKO tongues have been returned from the pathology core; as samples continue to arrive, graphs will be updated.

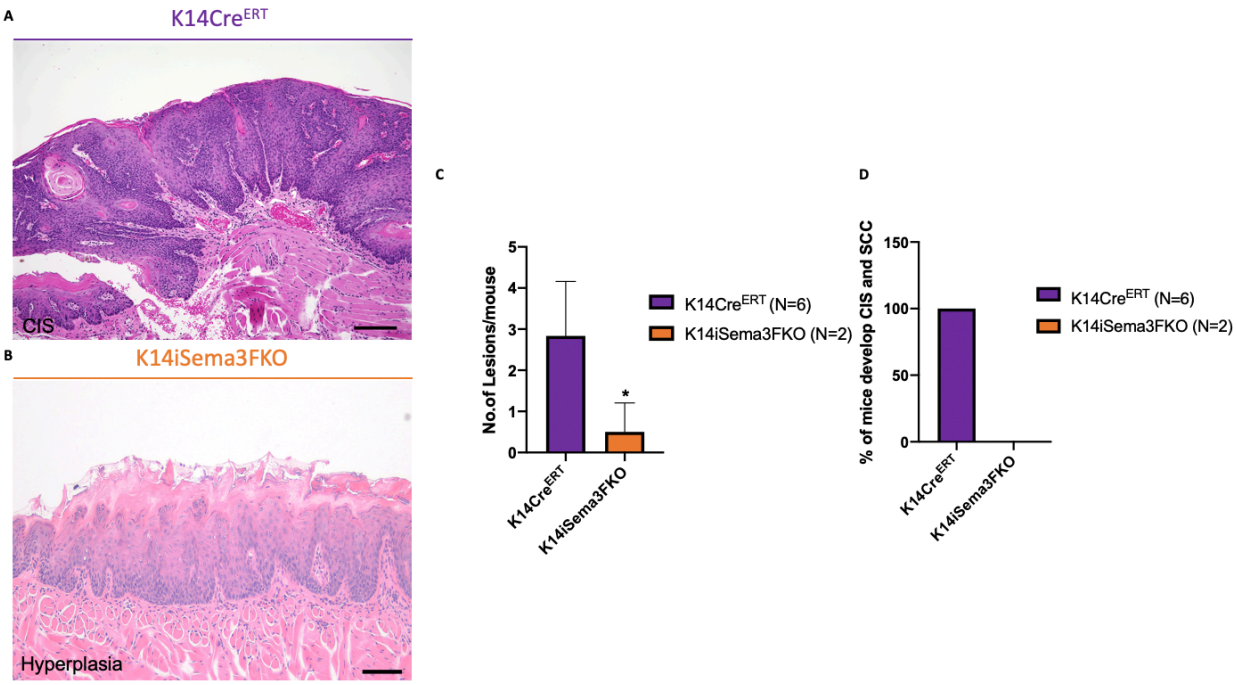

Figure 43: A. Representative hematoxylin and eosin stain of K14Cre^{ERT} tongue showing carcinoma in situ. **B.** Representative hematoxylin and eosin stain of K14iSema3FKO tongue showing hyperplastic epithelium. **C.** Number of lesions per mouse was graphed for each group; the mean numbers of CIS/OSCC per mouse was significantly less in K14iSema3FKO mice (n=2) compared to K14Cre^{ERT} (n=6) (*$p<0.05$). **D.** The percent of mice that developed CIS or OSCC was graphed for each group; K14iSema3FKO didn't develop any malignant tumors, while controls had 100% incidence of carcinoma.

Aim 3C:

In a dose-dependent manner, exogenous SEMA3F protein inhibited cell motility in Nrp2-expressing mouse OSCC cells (WT3-Luc) using *in vitro* migration (**Figure 44 A**) and invasion assays (**Figure 44 B**). However, the effect of SEMA3F on cellular proliferation after 48 hours appears to be insignificant (**Figure 44 C**).

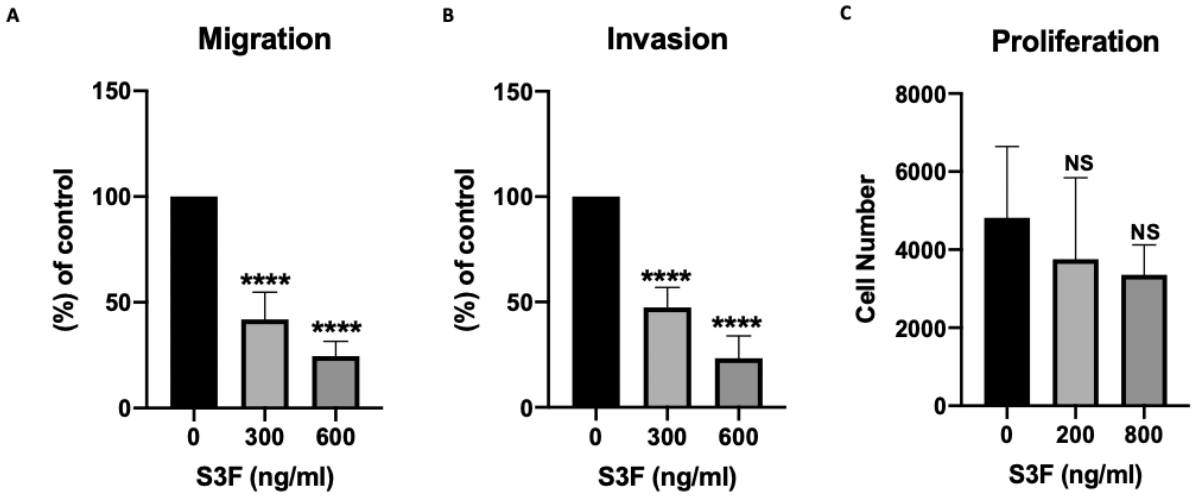

Figure 44: A. SEMA3F significantly (****p<0.0001) reduced WT3-Luc migration in a dose-dependent manner. **B.** SEMA3F significantly (****p<0.0001) reduced WT3-Luc invasion in a dose-dependent manner. **C.** After 48 hours incubation in SEMA3F, the average number of WT3-Luc cells counted per field was less than control; however, cell counts were quite variable and the cell proliferation was not significantly different between the groups.

We next examined the anti-tumor activity of exogenous SEMA3F protein in a series of preclinical trials in human or mouse OSCC models in immuno-competent or –deficient mice. The SEMA3F protein was always delivered via slow-release mini-osmotic pumps at a dose of 0.3 mg/kg/day and mice in the control group received the same pumps filled with HBSS vehicle.

In the first (pilot) preclinical trial, HSC3 human OSCC cells that express high levels of NRP2 protein (**Figure 45 A**) were injected orthotopically into immunodeficient nude mice

tongues (N=6 mice in total) (**Figure 45 C)**. The experimental timeline is illustrated in **Figure 45 B**. After one week, established tongue tumors were confirmed by visual inspection (**Figure 45 D**), mice were randomized, and control or SEMA3F pumps (n=3 mice/group) were surgically implanted in the peritoneal cavity (**Figure 45 E**). Twenty-one days after tumor injection (14 days after drug delivery), the mice were euthanized and necropsied. Tongue tumors were fixed, paraffin embedded, and analyzed histologically. H&E staining of sagittal sections of each tongue tumor are shown in **Figure 46 A-B**, and tumor cross-sectional areas were calculated and graphed in **Figure 46 D.** The mean tumor area was smaller in SEMA3F-treated tumors compared to the vehicle-treated group but was not statistically significant ($p<0.1$) due to the variability in tumors and the small sample size. However, higher magnifications of tumor borders demonstrate phenotypic differences in SEMA3F-treated tumors with less infiltrative and well-circumscribed borders (**Figure 46 C2**); while control tumors exhibited invasive borders and perineural invasion (**Figure 46 C1**). The *in vivo* effects of SEMA3F on HSC3 cell motility and invasion but not proliferation are consistent with the *in vitro* effects of SEMA3F on WT3-Luc cells shown above.

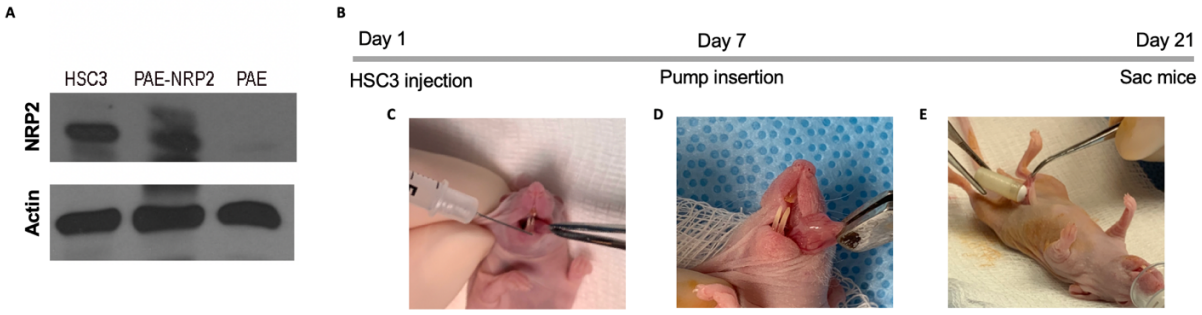

Figure 45: A. Immunoblotting confirms HSC3 express NRP2. Porcine aortic endothelial cells (PAE) served as a negative control and PAE transfected with NRP2 (PAE-NRP2) served as a positive control. **B.** Experimental timeline. **C.** HSC3 cells ($1x10^6$/mouse) were injected into the tongue on day 1. **D.** After 7 days, established tongue tumors were confirmed by visual examination. **E.** Tumor-bearing mice were randomized and implanted with slow-release osmotic pumps containing SEMA3F (0.3 mg/kg/day) or vehicle (HBSS), N=3 mice/ group, on Day 7. Mice were euthanized and necropsied on Day 21 after 2 weeks of systemic drug delivery.

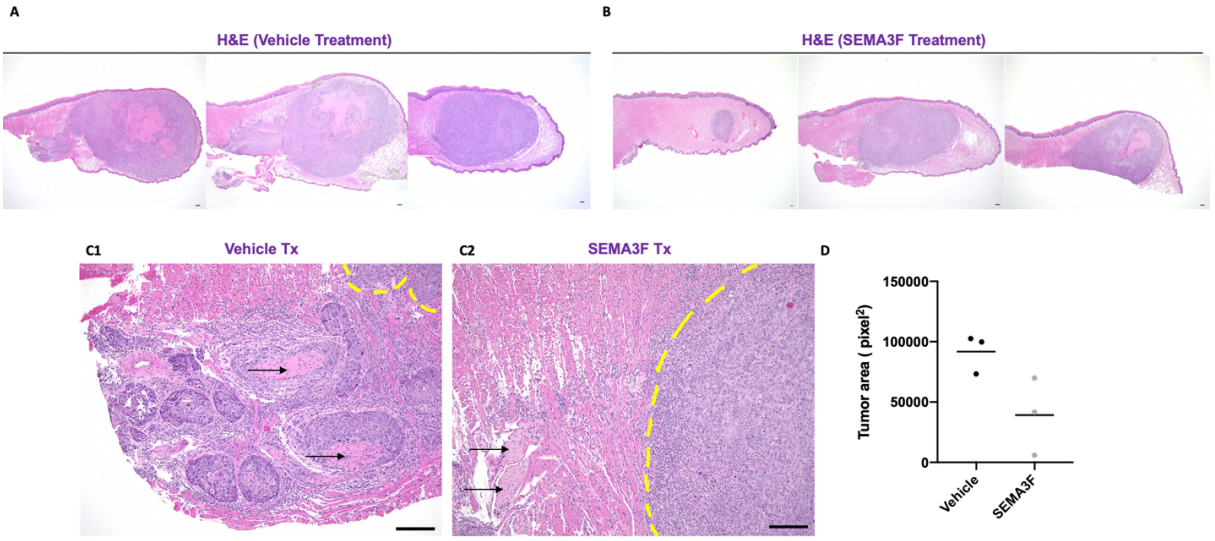

Figure 46: A. Hematoxylin and eosin stain of nude mouse tongues with HSC3 tumor in vehicle treatment group. **B.** Hematoxylin and eosin stain of nude mouse tongues with HSC3 tumor in SEMA3F treatment group. **C.** Higher magnification of hematoxylin and eosin stain of mouse tongues of HSC3 tumor in vehicle treatment group exhibiting infiltrative borders and peri-neural invasion **(C1)** while HSC3 tumor in SEMA3F group showed well-defined border **(C2)** (black arrows point to the nerve bundles). **D.** Tumor area per mouse was calculated and graphed for each group; mean tumor area was lower in SEMA3F treatment but not significantly different ($p<0.1$). Scale bar =100 μm.

Although systemic treatment of SEMA3F had little effect on the overall tumor volume, IHC studies revealed more than 60% reduction in tumor angiogenesis (CD31-positive vessels; **Figures 47 A**), lymphangiogenesis (podoplanin-positive vessels; **Figures 47 B**), and Nrp2-positive stromal cells (identified using a mouse-specific anti-Nrp2 antibody that did not react with the human HSC3 cells; **Figures 48 A**) in the SEMA3F-treated tumors compared to the vehicle-treated group. Cellular proliferation (mainly in tumor cells), identified using antibodies to Ki67, was slightly lower in mice treated with SEMA3F compared to controls but the data did not reach statistical significance (**Figure 48 B**).

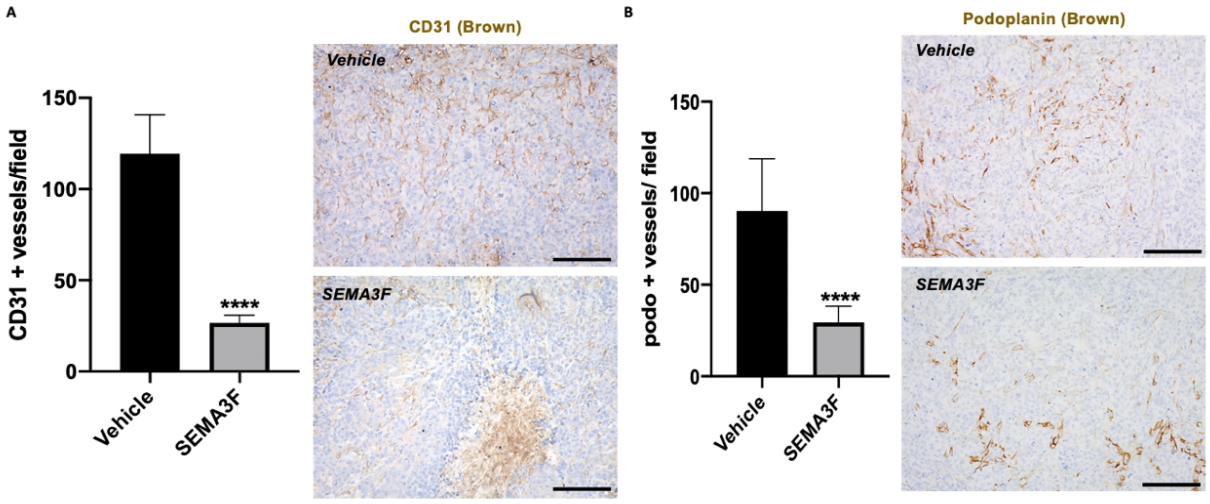

Figure 47: A. Intra-tumoral blood vessel numbers per field were significantly lower (****p<0.0001) in SEMA3F-treated tumors compared to vehicle-treated tumors. Representative IHC of CD31 for both vehicle and SEMA3F groups are shown to the right of the graph. **B.** Intra-tumoral lymphatic vessel numbers per field were significantly lower (****p<0.0001) in SEMA3F-treated tumors compared to vehicle-treated tumors. Representative IHC of podoplanin for both vehicle and SEMA3F treatment groups are shown to the right of the graph. Scale bar =100 μm.

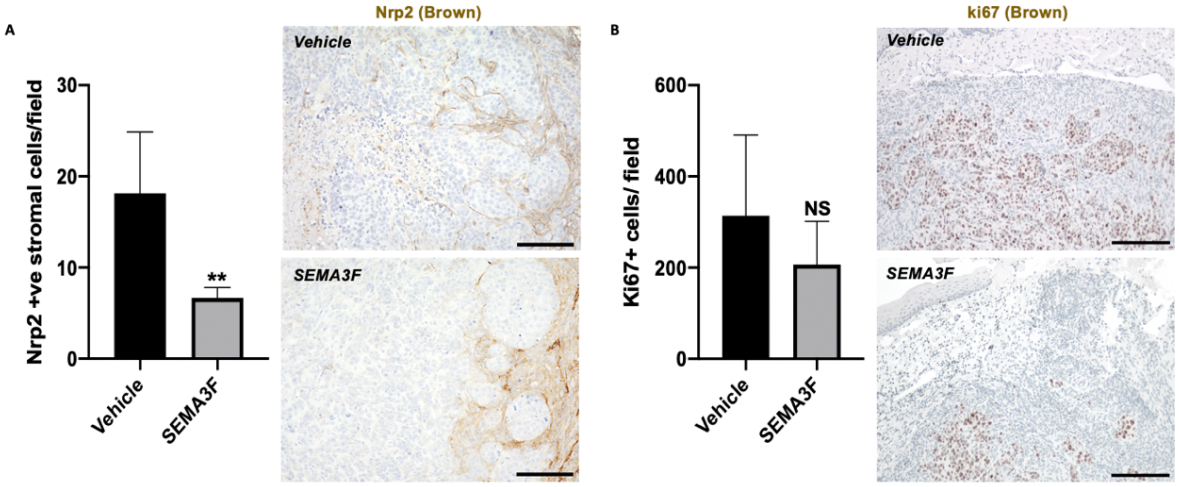

Figure 48: A. The number of mouse Nrp2-positive stroma cells (including endothelial cells and inflammatory cells) per field were significantly lower (**p<0.01) in SEMA3F-treated tumors compared to vehicle-treated tumors. Representative IHC of mouse Nrp2 for both vehicle and SEMA3F treatment groups are shown to the right of the graph. **B.** Cellular proliferation, identified as ki67-positive cells per field, was reduced in SEMA3F-treated tumors compared to vehicle-treated tumors but the difference was not statistically significant. Representative IHC of ki67 for both vehicle and SEMA3F treatment groups are shown to the right of the graph. Scale bar =100 μm.

Since our pilot preclinical trial above using exogenous SEMA3F protein to treat human OSCC in nude mice showed a clear inhibitory effect on tumor angiogenesis (**Figure 47 A**), suggesting that our SEMA3F protein was biologically active in vivo and working systemically, we were encouraged to expand to a larger cohort using syngeneic OSCC models. WT3-Luc mouse OSCC cells that express high levels of Nrp2 protein (**Figure 35 A**) were injected orthotopically into immunocompetent, syngeneic C57Bl/6 mice tongues (N=24 mice in total) (**Figure 49)**. The experimental timeline is illustrated in **Figure 49 A**. After one week, established tongue tumors were confirmed by luciferase bioluminescence (representative images are shown in **Figure 49, top panels**), mice were randomized, and control or SEMA3F pumps (n=11-12 mice/group) were surgically implanted in the peritoneal cavity. One mouse showed no bioluminescence at 7 days and was therefore not used in the trial. Twenty-one days after tumor injection (14 days with drug), the mice were again examined using the Xenogen IVIS system and bioluminescent images revealed a dramatic anti-tumor effect in SEMA3F-treated mice compared to controls (representative images are shown in **Figure 49 B, bottom panels**). Total radiance values (a surrogate for tumor volume) were graphed for each tumor in both groups. Results demonstrate a complete regression of established OSCC tumors in 66.7% (8/12) of mice treated systemically with SEMA3F (**Figure 49 C**). Mice were euthanized and necropsied on day 21 after imaging. Tongues were photographed (representative images are shown in **Figure 50 A**) and gross tumor dimensions (width and length) were measured externally with calipers. Calculated tumor areas were graphed for each tumor and treatment group. A reduction in average tumor area (and complete regression in some mice) was observed in the SEMA3F-treated mice compared to control mice but the difference was not

statistically significant (p=0.06) (**Figure 50 B)**. Tongues were then fixed, paraffin embedded, and analyzed histologically. H&E staining of sagittal sections of each tongue were examined, and indeed, tumors that appeared to regress after SEMA3F treatment showed no evidence of tumor histologically (representative images are shown in **Figure 51 A-B)**. Results from IVIS imaging, gross examination, and histological examination were all consistent. Since the majority of tumors in the SEMA3F treatment group completely regressed, we did not compare tumor-associated blood vessel density between the groups.

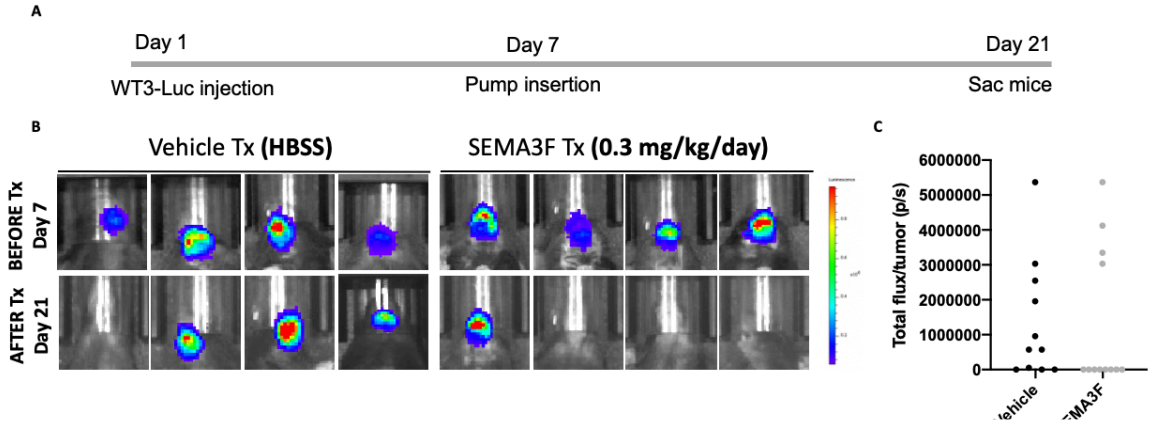

Figure 49: A. A. Experimental timeline. WT3-Luc tumor bearing C57BL6 mice were randomized 1 week after injection and implanted with slow-release osmotic pumps containing SEMA3F (0.3 mg/kg/day) or vehicle (HBSS), N=11-12 mice/group. **B.** Representative images of tumor incidence; tumors were visualized using bioluminescence imaging (Day 7 and Day 21). **C.** Total radiance or flux per tumor was graphed for each group.

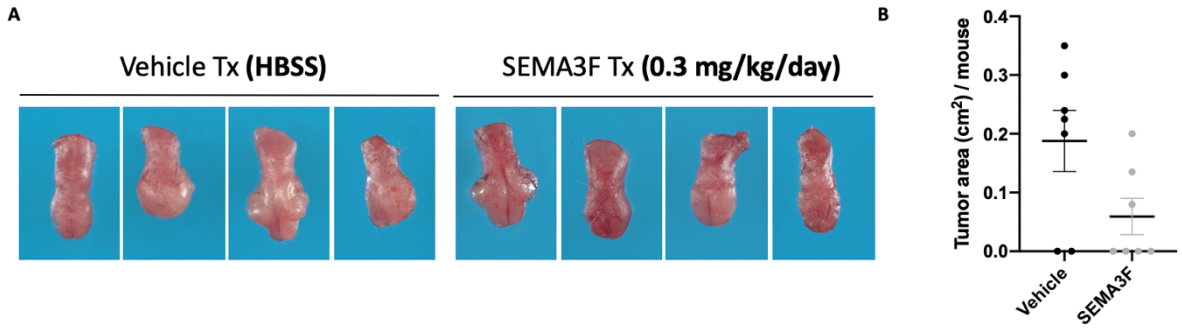

Figure 50: A. Representative images of final gross tongues in both vehicle and SEMA3F treatment groups (Day 21). **B.** Tumor area per mouse for each group (N=7/group) were graphed. The mean tumor area was smaller in the SEMA3F treatment group compared to the control group but the data did not reach significance (p =0.06).

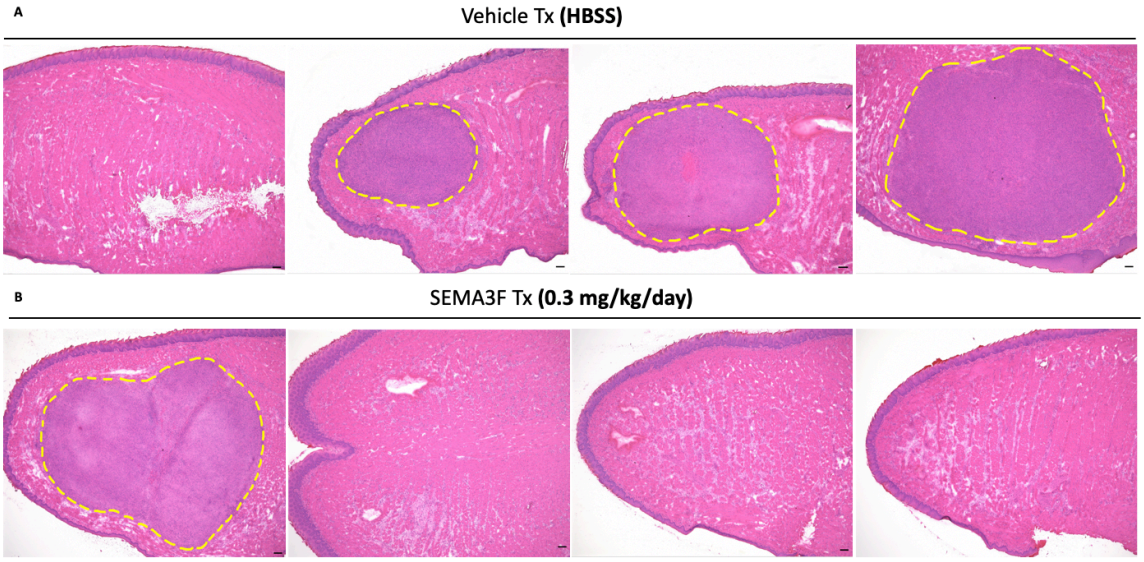

Figure 51: A. Representative hematoxylin and eosin stain of mouse tongues of WT3-Luc in vehicle treatment group. **B.** Representative hematoxylin and eosin stain of mouse tongues of WT3-Luc in SEMA3F treatment group. Scale bar =100 μm.

Since we observed complete regression in the majority of mice receiving SEMA3F protein in immunocompetent mice with syngeneic OSCC but not in immunodeficient (nude) mice with human OSCC, we repeated our previous preclinical trial using exogenous SEMA3F treatment in immunodeficient mice (N=5/group) with WT3-Luc OSCC cells. All mice had established tumors on day 7 confirmed by imaging (**Figure 52 A-B, top panels**) before vehicle- or SEMA3F-containing pumps were implanted. On day 21 (after 2 weeks of drug treatment), mice were imaged again and all mice showed luciferase signal (**Figure 52 A-B, bottom panels**). None of the immunodeficient mice showed regression of OSCC when treated with SEMA3F (**Figure 52 C-E**), which was a stark contrast from the results using immunocompetent mice (**Figure 49 B-C**). Although mean tumor radiance was similar in both groups (**Figure 52 C**), the SEMA3F treatment group had smaller tumors (lower median tumor radiance) than the control group (**Figure 52 D**), and 3/5 mice showed stable disease or no tumor growth on SEMA3F therapy (**Figure 52 E**).

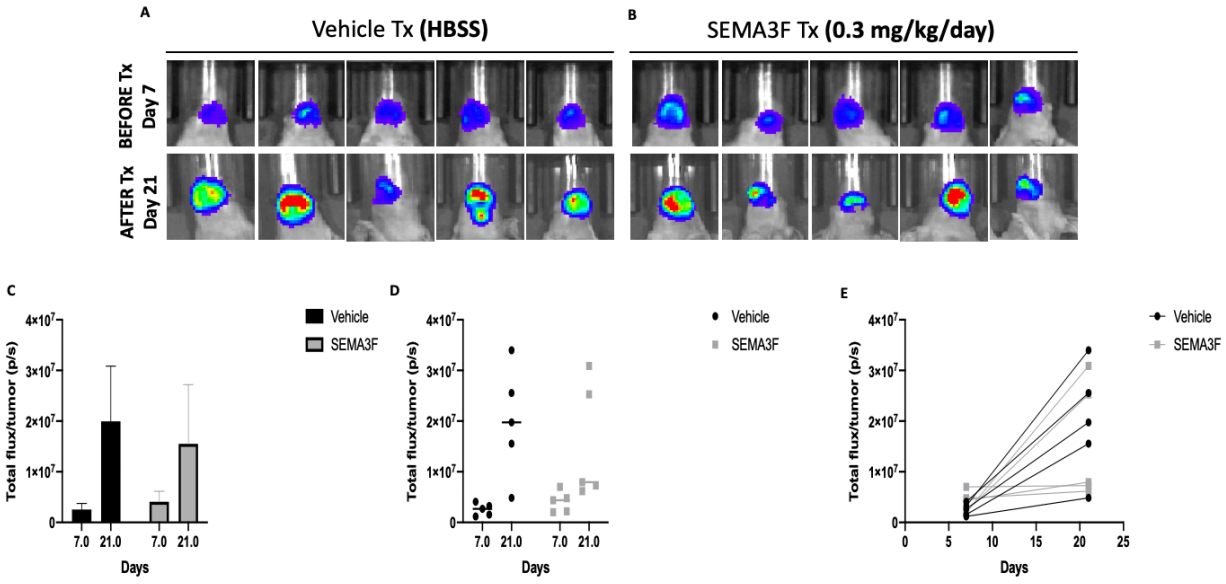

Figure 52: A. Images of tumor incidence of all mice (N=5/group); tumors were visualized using bioluminescence imaging (Day 7 and Day 21). **B.** The mean of total flux per tumor for each group were graphed at day 7 and day 21. **C.** The median of total flux per tumor for each group were graphed at day 7 and day 21. **D.** The total flux per tumor for each mouse for both groups were graphed at day 7 and day 21. The majority of mice treated with SEMAF (3/5) had stable disease or no increase in tumor radiance, whereas the tumor radiance increased in all control tumors.

Discussion:

NRP1 expression in oral mucosa, oral epithelial dysplasia and OSCC was first described by our laboratory in 2016.(51) More specifically, normal oral mucosa expresses NRP1 in differentiated keratinocytes in the suprabasal layers of the epithelium. However, NRP1 expression is upregulated during oral dysplasia and OSCC to include all epithelial layers. One other group has confirmed NRP1 expression in OSCC and correlated its expression with tumor aggressiveness.(67) To our knowledge, no publications have explored the role or function of Nrp1 in OSCC tumorigenesis. Thus, in order to understand the role of Nrp1 in OSCC, we used the Cre-Lox system to delete the *Nrp1* gene in K14-expressing cells (all layers of oral and skin epithelium). The cre enzyme in our models is tamoxifen-inducible, meaning that the *Nrp1* gene (in this case) was intact until tamoxifen is given. We did not introduce 4-OHT until at least 5 weeks of age, therefore normal development was not affected in our models. To our knowledge, our mice are the first inducible K14-Nrp1KO mice ever developed as previous publications that depleted *Nrp1* in keratinocytes used constitutive promoter-driven cre enzymes and lacked Nrp1 expression in K14-positive cells from birth and focused on cutaneous biology and not the oral cavity.(68, 127) Our data show that mice lacking Nrp1 in their keratinocytes did not develop CIS or OSCC in the 4-NQO carcinogenesis model. This finding strongly suggests that the Nrp1 receptor is crucial for the initiation and progression of oral carcinogenesis. The lack of any cancers in the K14iNrp1KO mice suggests that Nrp1 is a key regulator in these cells and suggests that VEGF (or another growth promoting ligand of Nrp1 such as PlGF2 or HGF) may provide autocrine growth signaling via Nrp1 to initiate carcinogenesis or override growth control mechanisms. As 4-NQO is known to mimic the effects of UV

irradiation, it is likely that this chemical caused DNA mutations in the dividing basal keratinocytes in all our mouse models. In control mice, these mutated cells likely grew uncontrollably and progressed through the stages of carcinogenesis from hyperplasia to dysplasia to CIS to OSCC. In the K14Cre^{ERT} control mice, the keratinocytes were able to upregulate Nrp1 in the basal cells undergoing mutation and enable VEGF/Nrp1 autocrine signaling (or potentially HGF/NRP1/C-met signaling,(128)) to promote the growth and survival of the cells. In contrast, basal cells mutated from 4-NQO in Nrp1iKO mice are not able to upregulate Nrp1 receptor or signal via its ligands and these cells did not progress through subsequent carcinogenesis stages. Our results are consistent with a previous carcinogenesis model using DMBA and TPA to induce skin carcinoma in K14-NRP1KO mice compared to control mice. The authors report a 75% reduction in skin tumors in mice lacking Nrp1 in the epidermis.(68) Additionally, this study compared VEGF overexpression in wildtype versus K14Nrp1KO mice and even with the addition of VEGF, mice lacking Nrp1 in epithelial cells had smaller tumors than controls suggesting that VEGF mediates tumor cell growth directly through Nrp1.(68) One possibility is that a small subset of tumor cells with stem cell proprieties express VEGFR in addition to NRP1 and therefore the VEGFR/VEGF/NRP1 complex can signal and initiate tumor formation and growth.(129) To be fair, one third (3/9) of the Nrp1iKO mice did develop epithelial hyperplasia and a single mouse (1/9) developed benign papilloma suggesting that there are mechanisms independent of the NRP1 pathway in oral mucosa that mediate cellular proliferation and growth.

As our results *in vivo* suggested that Nrp1 signals directly within keratinocytes to promote survival or growth, likely in an autocrine fashion, via one of its known ligands such as VEGFA, we explored this mechanism using *in vitro* studies in human and mouse OSCC cell lines. We found that silencing NRP1 (using siRNA) in human HSC3 cells reduced cell viability and dramatically inhibited 3D colony formation in soft agar, as compared to controls. This data suggests that Nrp1 promotes growth, likely via ligand-induced downstream signaling in human carcinoma cells (**Figure 20**). Additional assays examining migration and invasion are needed to confirm the cellular function of NRP1 in OSCC. Furthermore, it would be enlightening to examine the downstream signaling pathways of NRP1 in OSCC cells and/or normal keratinocytes in future experiments. Recently, two groups explored the mechanistic action of NRP1 in human SCC of the epidermis mediated by VEGF. Both found that VEGF signals through NRP1 and that the cytoplasmic domain of NRP1 (the last 3 amino acids, S-E-A) interacts with a scaffold protein called GIPC1 via its PDZ domain; GIPC1 (also called synectin) associates with Syx (synectin-binding RhoA exchange factor) to activate RhoA/ROCK and cause phosphorylation of MEK3/6, p27 and p38—which promote tumor growth and aggressiveness.(69, 130)

To our knowledge, this is the first study of NRP2 expression in normal oral mucosa and early stages of oral carcinogenesis in both human and mouse models. Previously published studies were only focused on NRP2 expression in the setting of invasive OSCC and its clinicopathological correlation.(80, 82) Our results found that NRP2 expression was not observed in keratinocytes or endothelium in normal oral mucosa; this is in agreement with the absence of NRP2 in adult mouse normal skin. (47) NRP1 and NRP2 typically have non-overlapping patterns of expression in normal tissues and this holds true in the normal epithelium as well with NRP1 expressed in normal epithelium but not NRP2.(51)

Interestingly, during the earliest phases of oral epithelial dysplasia NRP2 up-regulation was first seen in local endothelial cells but not keratinocytes. This is likely due to a dysplasia-associated inflammatory response, as even acute inflammation up-regulates Nrp2 expression in endothelium.(48) Furthermore, upregulation of NRP2 expression in keratinocytes was observed in late dysplasia along with endothelial cells. In general, there is a lack of agreement and significant interobserver variability in oral dysplasia grading among oral pathologists and there is a need for a standardized grading system to reliably predict dysplasia progression and prognosis.(131) Our data suggests that NRP2 is only upregulated in keratinocytes in advanced stages of oral dysplasia, and therefore NRP2 could potentially be a diagnostics marker, as well as a predictive marker, for cancer progression. However, further clinicopathological studies with larger sample sizes and long term follow up are needed to validate the diagnostic and prognostic value of NRP2. Both human and mice OSCC models exhibited high NRP2 expression regardless of tumor

differentiation, and within OSCC tumors NRP2 expression was observed in carcinoma cells, endothelial cells, and inflammatory cells. It was previously reported that NRP2 expression in OSCC correlated with lymph node metastasis and poor overall survival, similar to many other carcinomas expressing NRP2.(132, 133) NRP2 function in tumor cells mainly depends on the other receptors expressed by the tumor cells. It is highly unlikely that epithelial or carcinoma cells expresses VEGF receptors. However, some highly metastatic carcinomas have the ability to up-regulate VEGFR2, suggesting an autocrine function of NRP2 via VEGFR/VEGF.(134, 135) One study showed Nrp2 expression in esophageal carcinoma (closely related to OSCC) can signal within carcinoma cells via ERK MAP kinase, which in turn increase the activity of MMP2 and MMP9 to induce E-cadherin degradation and loss of E-cadherin implies more invasive and metastatic phenotype.(136)

Our results from the 4NQO model suggest that NRP2 does not play a role in tumor initiation as NRP1 does but rather plays a key role in OSCC progression. All K14Cre mice that have been examined histologically to date developed either CIS or OSCC (6/6 mice), while 4/10 K14Cre tongues have not been received from the pathology core as of yet. In contrast, all (9/9) K14iNrp2KO mice tongues have been analyzed histologically and the breakdown of the resulting lesions in these mice range across all stages of OSCC progression: 1/9 was normal, 1/9 developed hyperplasia, 1/9 developed dysplasia, 1/9 had a benign papilloma, 1/9 developed CIS, and 1/9 developed OSCC. Since only 22% of mice lacking Nrp2 expression in the oral mucosa developed CIS/OSCC, we can conclude that NRP2 is important for the advancement

of the disease from dysplasia to carcinoma. Yet, there is still so much to learn about the role and function of NRP2 in tumor cells. For instance, does NRP2 signal directly upon binding VEGF ligands in OSCC tumor cells? And if VEGF/NRP2 can signal without VEGFR cooperation, then what is the result of this signaling—increased proliferation or migration? In Aim 1, silencing of NRP1 in OSCC reduced colony formation in OSCC cells; in future experiments, we plan to similarly silence NRP2 in OSCC and examine proliferation, motility, and invasion. Alternately, NRP2 in OSCC may act indirectly to increase tumor angiogenesis. I hypothesized in the introduction of this thesis that tumor-derived NRP2 may also act to sequester VEGF in the tumor microenvironment to recruit neovessels to the tumor (illustrated in **Figure 9**). When NRP2 was silenced in pancreatic carcinoma cells, the resulting tumors had decreased microvessel density compared to control tumors expressing NRP2.(137) In future experiments, we plan to examine the MVD in the few tumors that did develop in K14iNrp2KO mice (papilloma and OSCC) and compare to the MVD in control tumors.

WT and Nrp2-KO mice had similar blood vessel counts and area in adult mouse tongues. However, OSCC isografts in Nrp2-KO mice showed a 46% reduction in tumor-associated blood vessel density compared to OSCC in WT littermates. Nrp2-KO mice have 25% fewer lymphatic capillaries in the normal adult tongue than WT mice. Therefore, one may expect that tumor-associated lymphangiogenesis in OSCC in Nrp2-KO mice may be reduced to a similar percentage when compared to OSCC in WT mice, but in actuality the reduction in tumor LVD in Nrp2-KO was much greater at 74% less than WT. Taken together, these results suggest that Nrp2 is essential for tumor

angiogenesis and lymphangiogenesis in OSCC and to a lesser extent Nrp2 is essential for lymphangiogenesis in the tongue during normal development. Thus, targeting NRP2 in OSCC may inhibit blood and lymphatic vessels within the tumor, hence reducing OSCC dissemination. Lastly, NRP2 may be an excellent target for cancer drug development since it is expressed on the surface (membrane) of multiple cell types found in the OSCC tumor microenvironment, but it is rarely found in adult normal epithelial cells or endothelial cells.

Our results confirmed that SEMA3F protein is expressed in the epithelium and mainly in the suprabasal layers. This is consistent with the published literature; our group and Uchida et. Al., found keratinocytes to be the primary cells to secrete SEMA3F in adult and embryonic epidermis.(48, 103) In addition, a recent study published in 2020 showed that tissues with highest SEMA3F gene expression were suprabasal epidermis and the squamous epithelial cells of tongue using Affymetrix human Genome U133 Plus 2.0 Array.(138) In contrast, Doci et. Al., analyzed 10 cases of normal mucosa from the head and neck region using IHC and reported SEMA3F expression mainly in the basal cells of the epithelium.(107) The difference in SEMA3F expression patterns between our findings and Doci et. al., may be due to: 1) different primary antibodies used to detect SEMA3F. Doci et. Al., did not disclose which primary antibody they used in their study. We tested all commercially available anti-SEMA3F antibodies and found none to be specific and then designed our own peptide based on the amino acid sequence unique to the Sema domain in SEMA3F and contracted GeneScript to immunize 3 rabbits. Although our SEMA3F antibody is polyclonal, we have tested its specificity under many conditions

described in Aim 3.GeneScript anti-SEMA3F can detect human or mouse SEMA3F, binds SEMA3F but not SEMA3A-E,G, (126) binds SEMA3F under reducing or non-reducing conditions in western blots, neutralizes SEMA3F activity in bioassays, and detects SEMA3F protein via IHC in FFPE sections in a pattern overlapping with *Sema3F* mRNA patterns detected via in situ hybridization. One downside of this antibody is that it binds to SEMA3F via its SEMA domain which is present in both the active SEMA3F protein (95kD) as well as in the cleaved, inactive protein (65kD). Therefore, one cannot conclude based on IHC detection that the endogenous SEMA3F protein localized in the oral epithelium is capable of binding to Nrp2. 2) Another difference between our study and Doci et. Al., is the type of tissue stained. Half of their cases were from pharyngeal and laryngeal mucosa, which makes it hard to compare with our results that are mainly from tongue oral mucosa. Our preliminary results suggest that keratinocytes progressively lose SEMA3F protein expression as dysplasia progresses to OSCC with complete loss of SEMA3F protein in carcinoma cells. It has been shown that more than 70% of head and neck cancers have heterozygous loss of the *SEMA3F* gene. In fact, *SEMA3F* is one of the top down-regulated genes in head and neck cancer.(107)

As previously mentioned, *SEMA3F* was first discovered as a tumor suppressor gene in lung carcinoma and to date, the descriptive and *in vitro* studies in OSCC suggest that SEMA3F plays a tumor suppressor role in oral carcinogenesis. (107, 108) Based on these reports, we predicted that K14iSema3FKO mice would exhibit rapid tumor formation following 4NQO with increased incidence of CIS and OSCC. To our surprise, we discovered that mice deficient in *Sema3F* in keratinocytes did not develop any dysplasia,

CIS or OSCC. In fact, our findings support a pro-tumorigenic role for endogenous SEMA3F. Based on our results in Aim 2 showing that normal oral epithelium lacks NRP2 expression, it makes sense that SEMA3F cannot act as an autocrine tumor suppressor in epithelial cells because they cannot bind SEMA3F protein. NRP2 is the only functional receptor for SEMA3F. Therefore, SEMA3F is likely acting in a paracrine fashion to influence some cell type in the oral mucosa that expresses NRP2. Possible cell types could include dendritic cells,(139) T cells(140), macrophages,(141) and melanocytes.(142) Dendritic cells are antigen-presenting cells in the epithelial compartment that act as messengers between the innate and adaptive immune systems and maintain immune tolerance. Dendritic cells express NRP2, and SEMA3 signaling, either by direct downstream effects on F-actin polymerization and cell motility or by repulsive mechanisms, may guide dendritic cell entry into lymphatics where T cells are activated.(143, 144) Additionally, subsets of T cells express NRP2, and SEMA3F/NRP2 blocks T cell migration.(140) Taken together, our data, from the lack of tumor development in the K14iSema3FKO mice, would support a model in which SEMA3F expression by wild-type keratinocytes is normally regulating immune tolerance via NRP2 expression in dendritic cells and T cells. When *Sema3F* is depleted, we hypothesize that immune surveillance is enhanced and that any basal epithelial cell that is transformed by 4NQO is detected and eradicated. Preliminary results from the Briscoe Laboratory in collaboration with the Bielenberg Laboratory support this hypothesis: Using a mismatched, allograft heart transplant model, systemic delivery of SEMA3F prolonged graft survival to 26.2 days compared to 6.5 days for vehicle treated mice.(145) These

results support a novel immunomodulatory function for SEMA3F/NRP2 and will require further studies.

Previous studies using SEMA3F therapy in cancer models have all relied on transfection of SEMA3F plasmids into tumor cells prior to implantation or transduction of SEMA3F-encoding virus.(105, 108) Our preclinical trials are the first to evaluate SEMA3F therapy delivered as a purified protein. Biologically active SEMA3F protein is not commercially available. The Bielenberg laboratory has purified large amounts of active SEMA3F protein that made these trials possible. In Aim 3, exogenous SEMA3F as a therapeutic drug showed outstanding response in different *in vitro* and *in vivo* models. SEMA3F inhibited human OSCC cell motility *in vitro*, consistent with the observations of a well-circumscribed and less infiltrative tumor border in the SEMA3F-treated group in human OSCC xenografts in immunodeficient mice. In this model, there was also significant reduction in blood and lymphatic vessel density with SEMA3F treatment compared to controls--suggesting that SEMA3F is a potential anti-angiogenic and anti-lymphangiogenic drug. In contrast, exogenous SEMA3F appears to have no direct effect on tumor growth as we observed no difference in tumor cell proliferation between control and treatment group in both *in vivo* and *in vitro* studies. Remarkably, two-thirds of SEMA3F-treated syngeneic OSCC (WT3-Luc) tumors showed a complete tumor regression in C57BL/6 mice. This excellent response can be attributed to the multiple targetable cells expressing NRP2 including epithelial cells, endothelial cells as well as immune cells. The profound tumor regression seen in C57Bl/6 mice may be attributed to the immune response mediated by SEMA3F protein. Tumor associated macrophages (TAMs), also known as M2

macrophages, express NRP2 and secrete a series of anti-inflammatory cytokines, which in turn suppress anti-tumoral immunity.(141) A recent study showed that deletion of *Nrp2* in TAMs results in increased apoptotic debris accumulation, T cell infiltration and enhanced anti-tumoral immune response.(141) One possible explanation is that exogenous SEMA3F protein targeted TAMs in our models. In fact, SEMA3F treatment showed significant reduction in Nrp2-positive stromal cells in human OSCC xenografts in nude mice, which have macrophages but lack T cells. In the immunocompetent C57Bl/6 mice, which have both macrophage and T cells, SEMA3F may be targeting Nrp2 in the TAMs to increase phagocytosis or promote anti-tumoral immunity by recruiting T cells and at least partly explain why we saw tumor regression. In contrast, in nude mice SEMA3F treatment of syngeneic OSCC showed no regression although tumors were smaller. Taken together, we suggest that SEMA3F is a powerful anti-angiogenic drug but also has potent effects on anti-tumor immunity.

Yet, in our trials approximately 33.3% of the mice were outliers in that they still had large tumor burden after SEMA3F treatment. Our future goals will explore the mechanistic action of SEMA3F treatment and look into the subset of tumors that did not regress. Histological examination will reveal whether the remaining tumors were necrotic inside or have reduced MVD in response to the SEMA3F. If these tumors show no phenotypic difference with control tumors, we will look into the possibility that some of our alzet pumps may become clogged and not secrete SEMA3F as expected. Our laboratory is working on ways to measure the systemic levels of exogenous SEMA3F in the serum using ELISA to detect the recombinant his-tagged SEMA3F protein. In conclusion, our exogenous

SEMA3F preclinical trial results are very promising as no other drugs reported, to our knowledge, can induce tumor regression in established OSCC or HNSCC.

References:

1. Shield KD, Ferlay J, Jemal A, Sankaranarayanan R, Chaturvedi AK, Bray F, et al. The global incidence of lip, oral cavity, and pharyngeal cancers by subsite in 2012. CA Cancer J Clin. 2017;67(1):51-64.
2. Chi AC, Day TA, Neville BW. Oral cavity and oropharyngeal squamous cell carcinoma--an update. CA Cancer J Clin. 2015;65(5):401-21.
3. Bray F, Ferlay J, Soerjomataram I, Siegel RL, Torre LA, Jemal A. Global cancer statistics 2018: GLOBOCAN estimates of incidence and mortality worldwide for 36 cancers in 185 countries. CA Cancer J Clin. 2018;68(6):394-424.
4. Siegel RL, Miller KD, Jemal A. Cancer statistics, 2020. CA Cancer J Clin. 2020;70(1):7-30.
5. Mohideen K, Krithika C, Jeddy N, Bharathi R, Thayumanavan B, Sankari SL. Meta-analysis on risk factors of squamous cell carcinoma of the tongue in young adults. J Oral Maxillofac Pathol. 2019;23(3):450-7.
6. Chang CP, Chang SC, Chuang SC, Berthiller J, Ferro G, Matsuo K, et al. Age at start of using tobacco on the risk of head and neck cancer: Pooled analysis in the International Head and Neck Cancer Epidemiology Consortium (INHANCE). Cancer Epidemiol. 2019;63:101615.
7. WHO Classification of Head and Neck Tumours 4th ed2017.
8. bin-Woo S. Oral Pathology: A comprehensive atlas and text. 2nd ed2016.
9. Brad Neviile DDD, Carl Allen, Angela Chi. Oral and Maxillofacial Pathology 4th ed2015.
10. Farah CS, Woo SB, Zain RB, Sklavounou A, McCullough MJ, Lingen M. Oral cancer and oral potentially malignant disorders. Int J Dent. 2014;2014:853479.
11. Silverman S, Jr., Gorsky M, Lozada F. Oral leukoplakia and malignant transformation. A follow-up study of 257 patients. Cancer. 1984;53(3):563-8.
12. Dost F, Le Cao K, Ford PJ, Ades C, Farah CS. Malignant transformation of oral epithelial dysplasia: a real-world evaluation of histopathologic grading. Oral Surg Oral Med Oral Pathol Oral Radiol. 2014;117(3):343-52.
13. AJCC Cancer Staging Manual. 8th ed2017.
14. Bernier J, Cooper JS, Pajak TF, van Glabbeke M, Bourhis J, Forastiere A, et al. Defining risk levels in locally advanced head and neck cancers: a comparative analysis of concurrent postoperative radiation plus chemotherapy trials of the EORTC (#22931) and RTOG (# 9501). Head Neck. 2005;27(10):843-50.
15. Cohen EEW, Bell RB, Bifulco CB, Burtness B, Gillison ML, Harrington KJ, et al. The Society for Immunotherapy of Cancer consensus statement on immunotherapy for the treatment of squamous cell carcinoma of the head and neck (HNSCC). J Immunother Cancer. 2019;7(1):184.
16. Noone AM HN, Krapcho M, Miller D, Brest A, Yu M, Ruhl, Tatalovich Z, Mariotto A, Lewis DR, Chen DR, Feuer EJ, Cronin KD. SEER Cancer Statistic Reivew, 1975-2015. National Cancer Institute. Bethesda, MD; 2019.
17. Noone AM HN, Krapcho M, Miller D, Brest A, Yu M, Ruhl J, Tatalovich Z, Mariotto A, Lewis DR, Chen HS, Feuer EJ, Cronin KA (eds). SEER Cancer Statistics Review, 1975-2015. National Cancer Institute Bethesda, MD.
18. Massano J, Regateiro FS, Januario G, Ferreira A. Oral squamous cell carcinoma: review of prognostic and predictive factors. Oral Surg Oral Med Oral Pathol Oral Radiol Endod. 2006;102(1):67-76.

19. Kowalski LP, Medina JE. Nodal metastases: predictive factors. Otolaryngol Clin North Am. 1998;31(4):621-37.
20. Lieng H, Gebski VJ, Morgan GJ, Veness MJ. Important prognostic significance of lymph node density in patients with node positive oral tongue cancer. ANZ J Surg. 2016;86(9):681-6.
21. Patel SG, Amit M, Yen TC, Liao CT, Chaturvedi P, Agarwal JP, et al. Lymph node density in oral cavity cancer: results of the International Consortium for Outcomes Research. Br J Cancer. 2013;109(8):2087-95.
22. Gil Z, Carlson DL, Boyle JO, Kraus DH, Shah JP, Shaha AR, et al. Lymph node density is a significant predictor of outcome in patients with oral cancer. Cancer. 2009;115(24):5700-10.
23. Prabhu RS, Hanasoge S, Magliocca KR, Hall WA, Chen SA, Higgins KA, et al. Lymph node ratio influence on risk of head and neck cancer locoregional recurrence after initial surgical resection: implications for adjuvant therapy. Head Neck. 2015;37(6):777-82.
24. Hida K, Maishi N, Torii C, Hida Y. Tumor angiogenesis--characteristics of tumor endothelial cells. Int J Clin Oncol. 2016;21(2):206-12.
25. Folkman J. Is angiogenesis an organizing principle in biology and medicine? J Pediatr Surg. 2007;42(1):1-11.
26. Folkman J. Tumor angiogenesis: therapeutic implications. N Engl J Med. 1971;285(21):1182-6.
27. Folkman J, Merler E, Abernathy C, Williams G. Isolation of a tumor factor responsible for angiogenesis. J Exp Med. 1971;133(2):275-88.
28. Hurwitz H, Fehrenbacher L, Novotny W, Cartwright T, Hainsworth J, Heim W, et al. Bevacizumab plus irinotecan, fluorouracil, and leucovorin for metastatic colorectal cancer. N Engl J Med. 2004;350(23):2335-42.
29. Hasina R, Lingen MW. Angiogenesis in oral cancer. J Dent Educ. 2001;65(11):1282-90.
30. Kyzas PA, Cunha IW, Ioannidis JP. Prognostic significance of vascular endothelial growth factor immunohistochemical expression in head and neck squamous cell carcinoma: a meta-analysis. Clin Cancer Res. 2005;11(4):1434-40.
31. Williamson SK, Moon J, Huang CH, Guaglianone PP, LeBlanc M, Wolf GT, et al. Phase II evaluation of sorafenib in advanced and metastatic squamous cell carcinoma of the head and neck: Southwest Oncology Group Study S0420. J Clin Oncol. 2010;28(20):3330-5.
32. Cohen EE, Davis DW, Karrison TG, Seiwert TY, Wong SJ, Nattam S, et al. Erlotinib and bevacizumab in patients with recurrent or metastatic squamous-cell carcinoma of the head and neck: a phase I/II study. Lancet Oncol. 2009;10(3):247-57.
33. Argiris A, Kotsakis AP, Hoang T, Worden FP, Savvides P, Gibson MK, et al. Cetuximab and bevacizumab: preclinical data and phase II trial in recurrent or metastatic squamous cell carcinoma of the head and neck. Ann Oncol. 2013;24(1):220-5.
34. Adkins D, Mehan P, Ley J, Siegel MJ, Siegel BA, Dehdashti F, et al. Pazopanib plus cetuximab in recurrent or metastatic head and neck squamous cell carcinoma: an open-label, phase 1b and expansion study. Lancet Oncol. 2018;19(8):1082-93.
35. Chau NG, Haddad RI. Antiangiogenic agents in head and neck squamous cell carcinoma: Tired of going solo. Cancer. 2016;122(23):3592-5.
36. Breiteneder-Geleff S, Soleiman A, Horvat R, Amann G, Kowalski H, Kerjaschki D. [Podoplanin--a specific marker for lymphatic endothelium expressed in angiosarcoma]. Verh Dtsch Ges Pathol. 1999;83:270-5.

37. Wigle JT, Oliver G. Prox1 function is required for the development of the murine lymphatic system. Cell. 1999;98(6):769-78.
38. Banerji S, Ni J, Wang SX, Clasper S, Su J, Tammi R, et al. LYVE-1, a new homologue of the CD44 glycoprotein, is a lymph-specific receptor for hyaluronan. J Cell Biol. 1999;144(4):789-801.
39. Karpanen T, Egeblad M, Karkkainen MJ, Kubo H, Yla-Herttuala S, Jaattela M, et al. Vascular endothelial growth factor C promotes tumor lymphangiogenesis and intralymphatic tumor growth. Cancer Res. 2001;61(5):1786-90.
40. Yanai Y, Furuhata T, Kimura Y, Yamaguchi K, Yasoshima T, Mitaka T, et al. Vascular endothelial growth factor C promotes human gastric carcinoma lymph node metastasis in mice. J Exp Clin Cancer Res. 2001;20(3):419-28.
41. He Y, Rajantie I, Pajusola K, Jeltsch M, Holopainen T, Yla-Herttuala S, et al. Vascular endothelial cell growth factor receptor 3-mediated activation of lymphatic endothelium is crucial for tumor cell entry and spread via lymphatic vessels. Cancer Res. 2005;65(11):4739-46.
42. Migliozzi MT, Mucka P, Bielenberg DR. Lymphangiogenesis and metastasis--a closer look at the neuropilin/semaphorin3 axis. Microvasc Res. 2014;96:68-76.
43. Miyahara M, Tanuma J, Sugihara K, Semba I. Tumor lymphangiogenesis correlates with lymph node metastasis and clinicopathologic parameters in oral squamous cell carcinoma. Cancer. 2007;110(6):1287-94.
44. Franchi A, Gallo O, Massi D, Baroni G, Santucci M. Tumor lymphangiogenesis in head and neck squamous cell carcinoma: a morphometric study with clinical correlations. Cancer. 2004;101(5):973-8.
45. Hwang-Bo J, Bae MG, Park JH, Chung IS. 3-O-Acetyloleanolic acid inhibits VEGF-A-induced lymphangiogenesis and lymph node metastasis in an oral cancer sentinel lymph node animal model. BMC Cancer. 2018;18(1):714.
46. Hwang-Bo J, Park JH, Bae MG, Chung IS. Recombinant canstatin inhibits VEGF-A-induced lymphangiogenesis and metastasis in an oral squamous cell carcinoma SCC-VII animal model. Cancer Med. 2016;5(10):2977-88.
47. Bielenberg DR, Pettaway CA, Takashima S, Klagsbrun M. Neuropilins in neoplasms: expression, regulation, and function. Exp Cell Res. 2006;312(5):584-93.
48. Mucka P, Levonyak N, Geretti E, Zwaans BMM, Li X, Adini I, et al. Inflammation and Lymphedema Are Exacerbated and Prolonged by Neuropilin 2 Deficiency. Am J Pathol. 2016;186(11):2803-12.
49. Rossignol M, Beggs AH, Pierce EA, Klagsbrun M. Human neuropilin-1 and neuropilin-2 map to 10p12 and 2q34, respectively. Genomics. 1999;57(3):459-60.
50. Soker S, Takashima S, Miao HQ, Neufeld G, Klagsbrun M. Neuropilin-1 is expressed by endothelial and tumor cells as an isoform-specific receptor for vascular endothelial growth factor. Cell. 1998;92(6):735-45.
51. Shahrabi-Farahani S, Gallottini M, Martins F, Li E, Mudge DR, Nakayama H, et al. Neuropilin 1 Receptor Is Up-Regulated in Dysplastic Epithelium and Oral Squamous Cell Carcinoma. Am J Pathol. 2016;186(4):1055-64.
52. Kurschat P, Bielenberg D, Rossignol-Tallandier M, Stahl A, Klagsbrun M. Neuron restrictive silencer factor NRSF/REST is a transcriptional repressor of neuropilin-1 and diminishes the ability of semaphorin 3A to inhibit keratinocyte migration. J Biol Chem. 2006;281(5):2721-9.

53. Takagi S, Tsuji T, Amagai T, Takamatsu T, Fujisawa H. Specific cell surface labels in the visual centers of Xenopus laevis tadpole identified using monoclonal antibodies. Dev Biol. 1987;122(1):90-100.
54. Fujisawa H, Takagi S, Hirata T. Growth-associated expression of a membrane protein, neuropilin, in Xenopus optic nerve fibers. Dev Neurosci. 1995;17(5-6):343-9.
55. Takagi S, Kasuya Y, Shimizu M, Matsuura T, Tsuboi M, Kawakami A, et al. Expression of a cell adhesion molecule, neuropilin, in the developing chick nervous system. Dev Biol. 1995;170(1):207-22.
56. Kitsukawa T, Shimono A, Kawakami A, Kondoh H, Fujisawa H. Overexpression of a membrane protein, neuropilin, in chimeric mice causes anomalies in the cardiovascular system, nervous system and limbs. Development. 1995;121(12):4309-18.
57. Kawasaki T, Kitsukawa T, Bekku Y, Matsuda Y, Sanbo M, Yagi T, et al. A requirement for neuropilin-1 in embryonic vessel formation. Development. 1999;126(21):4895-902.
58. Migdal M, Huppertz B, Tessler S, Comforti A, Shibuya M, Reich R, et al. Neuropilin-1 is a placenta growth factor-2 receptor. J Biol Chem. 1998;273(35):22272-8.
59. Seifi-Alan M, Shams R, Bandehpour M, Mirfakhraie R, Ghafouri-Fard S. Neuropilin-1 expression is associated with lymph node metastasis in breast cancer tissues. Cancer Manag Res. 2018;10:1969-74.
60. Cao Y, Wang L, Nandy D, Zhang Y, Basu A, Radisky D, et al. Neuropilin-1 upholds dedifferentiation and propagation phenotypes of renal cell carcinoma cells by activating Akt and sonic hedgehog axes. Cancer Res. 2008;68(21):8667-72.
61. Miao HQ, Lee P, Lin H, Soker S, Klagsbrun M. Neuropilin-1 expression by tumor cells promotes tumor angiogenesis and progression. FASEB J. 2000;14(15):2532-9.
62. Wang G, Shi B, Fu Y, Zhao S, Qu K, Guo Q, et al. Hypomethylated gene NRP1 is co-expressed with PDGFRB and associated with poor overall survival in gastric cancer patients. Biomed Pharmacother. 2019;111:1334-41.
63. Yang L, Liu L, Zhu YH, Wang BB, Chen YN, Zhang F, et al. Neuropilin-1 is associated with the prognosis of cervical cancer in Henan Chinese population. Onco Targets Ther. 2019;12:2911-20.
64. Zhang Y, Liu P, Jiang Y, Dou X, Yan J, Ma C, et al. High Expression of Neuropilin-1 Associates with Unfavorable Clinicopathological Features in Hepatocellular Carcinoma. Pathol Oncol Res. 2016;22(2):367-75.
65. Caponegro MD, Moffitt RA, Tsirka SE. Expression of neuropilin-1 is linked to glioma associated microglia and macrophages and correlates with unfavorable prognosis in high grade gliomas. Oncotarget. 2018;9(86):35655-65.
66. Shahrabi-Farahani S, Wang L, Zwaans BM, Santana JM, Shimizu A, Takashima S, et al. Neuropilin 1 expression correlates with differentiation status of epidermal cells and cutaneous squamous cell carcinomas. Lab Invest. 2014;94(7):752-65.
67. Chu W, Song X, Yang X, Ma L, Zhu J, He M, et al. Neuropilin-1 promotes epithelial-to-mesenchymal transition by stimulating nuclear factor-kappa B and is associated with poor prognosis in human oral squamous cell carcinoma. PLoS One. 2014;9(7):e101931.
68. Beck B, Driessens G, Goossens S, Youssef KK, Kuchnio A, Caauwe A, et al. A vascular niche and a VEGF-Nrp1 loop regulate the initiation and stemness of skin tumours. Nature. 2011;478(7369):399-403.

69. Yoshida A, Shimizu A, Asano H, Kadonosono T, Kondoh SK, Geretti E, et al. VEGF-A/NRP1 stimulates GIPC1 and Syx complex formation to promote RhoA activation and proliferation in skin cancer cells. Biol Open. 2015;4(9):1063-76.
70. Chen H, Chedotal A, He Z, Goodman CS, Tessier-Lavigne M. Neuropilin-2, a novel member of the neuropilin family, is a high affinity receptor for the semaphorins Sema E and Sema IV but not Sema III. Neuron. 1997;19(3):547-59.
71. Kolodkin AL, Levengood DV, Rowe EG, Tai YT, Giger RJ, Ginty DD. Neuropilin is a semaphorin III receptor. Cell. 1997;90(4):753-62.
72. He Z, Tessier-Lavigne M. Neuropilin is a receptor for the axonal chemorepellent Semaphorin III. Cell. 1997;90(4):739-51.
73. Gluzman-Poltorak Z, Cohen T, Herzog Y, Neufeld G. Neuropilin-2 is a receptor for the vascular endothelial growth factor (VEGF) forms VEGF-145 and VEGF-165 [corrected]. J Biol Chem. 2000;275(24):18040-5.
74. Yuan L, Moyon D, Pardanaud L, Breant C, Karkkainen MJ, Alitalo K, et al. Abnormal lymphatic vessel development in neuropilin 2 mutant mice. Development. 2002;129(20):4797-806.
75. Walz A, Rodriguez I, Mombaerts P. Aberrant sensory innervation of the olfactory bulb in neuropilin-2 mutant mice. J Neurosci. 2002;22(10):4025-35.
76. Yasuoka H, Kodama R, Tsujimoto M, Yoshidome K, Akamatsu H, Nakahara M, et al. Neuropilin-2 expression in breast cancer: correlation with lymph node metastasis, poor prognosis, and regulation of CXCR4 expression. BMC Cancer. 2009;9:220.
77. Keck B, Wach S, Taubert H, Zeiler S, Ott OJ, Kunath F, et al. Neuropilin-2 and its ligand VEGF-C predict treatment response after transurethral resection and radiochemotherapy in bladder cancer patients. Int J Cancer. 2015;136(2):443-51.
78. Dong X, Guo W, Zhang S, Wu T, Sun Z, Yan S, et al. Elevated expression of neuropilin-2 associated with unfavorable prognosis in hepatocellular carcinoma. Onco Targets Ther. 2017;10:3827-33.
79. Xu W, Liu Y, Jia C, Miao N, Xu H, Wang Y, et al. [Correlation between the expression of neuropilin-2 and tumor-associated lymphangiogenesis in gastric cancer and clinicopathological parameters]. Zhonghua Yi Xue Za Zhi. 2014;94(14):1067-70.
80. Zhang B, Gao Z, Sun M, Li H, Fan H, Chen D, et al. Prognostic significance of VEGF-C, semaphorin 3F, and neuropilin-2 expression in oral squamous cell carcinomas and their relationship with lymphangiogenesis. J Surg Oncol. 2015;111(4):382-8.
81. Wild JR, Staton CA, Chapple K, Corfe BM. Neuropilins: expression and roles in the epithelium. Int J Exp Pathol. 2012;93(2):81-103.
82. Ong HS, Gokavarapu S, Xu Q, Tian Z, Li J, Ji T, et al. Cytoplasmic neuropilin 2 is associated with metastasis and a poor prognosis in early tongue cancer patients. Int J Oral Maxillofac Surg. 2017;46(10):1205-19.
83. Stacker SA, Hughes RA, Achen MG. Molecular targeting of lymphatics for therapy. Curr Pharm Des. 2004;10(1):65-74.
84. Achen MG, Stacker SA. Molecular control of lymphatic metastasis. Ann N Y Acad Sci. 2008;1131:225-34.
85. Stacker SA, Caesar C, Baldwin ME, Thornton GE, Williams RA, Prevo R, et al. VEGF-D promotes the metastatic spread of tumor cells via the lymphatics. Nat Med. 2001;7(2):186-91.

86. White JD, Hewett PW, Kosuge D, McCulloch T, Enholm BC, Carmichael J, et al. Vascular endothelial growth factor-D expression is an independent prognostic marker for survival in colorectal carcinoma. Cancer Res. 2002;62(6):1669-75.
87. Nakamura Y, Yasuoka H, Tsujimoto M, Yang Q, Imabun S, Nakahara M, et al. Prognostic significance of vascular endothelial growth factor D in breast carcinoma with long-term follow-up. Clin Cancer Res. 2003;9(2):716-21.
88. Yokoyama Y, Charnock-Jones DS, Licence D, Yanaihara A, Hastings JM, Holland CM, et al. Vascular endothelial growth factor-D is an independent prognostic factor in epithelial ovarian carcinoma. Br J Cancer. 2003;88(2):237-44.
89. Morita Y, Morita N, Hata K, Nakanishi M, Kimoto N, Omata T, et al. Cyclooxygenase-2 expression is associated with vascular endothelial growth factor-c and lymph node metastasis in human oral tongue cancer. Oral Surg Oral Med Oral Pathol Oral Radiol. 2014;117(4):502-10.
90. Yoshimatsu Y, Miyazaki H, Watabe T. Roles of signaling and transcriptional networks in pathological lymphangiogenesis. Adv Drug Deliv Rev. 2016;99(Pt B):161-71.
91. Dieterich LC, Detmar M. Tumor lymphangiogenesis and new drug development. Adv Drug Deliv Rev. 2016;99(Pt B):148-60.
92. Xu Y, Yuan L, Mak J, Pardanaud L, Caunt M, Kasman I, et al. Neuropilin-2 mediates VEGF-C-induced lymphatic sprouting together with VEGFR3. J Cell Biol. 2010;188(1):115-30.
93. Favier B, Alam A, Barron P, Bonnin J, Laboudie P, Fons P, et al. Neuropilin-2 interacts with VEGFR-2 and VEGFR-3 and promotes human endothelial cell survival and migration. Blood. 2006;108(4):1243-50.
94. Klagsbrun M, Takashima S, Mamluk R. The role of neuropilin in vascular and tumor biology. Adv Exp Med Biol. 2002;515:33-48.
95. Neufeld G, Mumblat Y, Smolkin T, Toledano S, Nir-Zvi I, Ziv K, et al. The role of the semaphorins in cancer. Cell Adh Migr. 2016;10(6):652-74.
96. Alto LT, Terman JR. Semaphorins and their Signaling Mechanisms. Methods Mol Biol. 2017;1493:1-25.
97. Miao HQ, Soker S, Feiner L, Alonso JL, Raper JA, Klagsbrun M. Neuropilin-1 mediates collapsin-1/semaphorin III inhibition of endothelial cell motility: functional competition of collapsin-1 and vascular endothelial growth factor-165. J Cell Biol. 1999;146(1):233-42.
98. Geretti E, Shimizu A, Kurschat P, Klagsbrun M. Site-directed mutagenesis in the B-neuropilin-2 domain selectively enhances its affinity to VEGF165, but not to semaphorin 3F. J Biol Chem. 2007;282(35):25698-707.
99. Gaur P, Bielenberg DR, Samuel S, Bose D, Zhou Y, Gray MJ, et al. Role of class 3 semaphorins and their receptors in tumor growth and angiogenesis. Clin Cancer Res. 2009;15(22):6763-70.
100. Guttmann-Raviv N, Shraga-Heled N, Varshavsky A, Guimaraes-Sternberg C, Kessler O, Neufeld G. Semaphorin-3A and semaphorin-3F work together to repel endothelial cells and to inhibit their survival by induction of apoptosis. J Biol Chem. 2007;282(36):26294-305.
101. Kessler O, Shraga-Heled N, Lange T, Gutmann-Raviv N, Sabo E, Baruch L, et al. Semaphorin-3F is an inhibitor of tumor angiogenesis. Cancer Res. 2004;64(3):1008-15.
102. Nakayama H, Bruneau S, Kochupurakkal N, Coma S, Briscoe DM, Klagsbrun M. Regulation of mTOR Signaling by Semaphorin 3F-Neuropilin 2 Interactions In Vitro and In Vivo. Sci Rep. 2015;5:11789.

103. Uchida Y, James JM, Suto F, Mukouyama YS. Class 3 semaphorins negatively regulate dermal lymphatic network formation. Biol Open. 2015;4(9):1194-205.
104. Roche J, Boldog F, Robinson M, Robinson L, Varella-Garcia M, Swanton M, et al. Distinct 3p21.3 deletions in lung cancer and identification of a new human semaphorin. Oncogene. 1996;12(6):1289-97.
105. Bielenberg DR, Hida Y, Shimizu A, Kaipainen A, Kreuter M, Kim CC, et al. Semaphorin 3F, a chemorepulsant for endothelial cells, induces a poorly vascularized, encapsulated, nonmetastatic tumor phenotype. J Clin Invest. 2004;114(9):1260-71.
106. Mishra R, Kumar D, Tomar D, Chakraborty G, Kumar S, Kundu GC. The potential of class 3 semaphorins as both targets and therapeutics in cancer. Expert Opin Ther Targets. 2015;19(3):427-42.
107. Doci CL, Mikelis CM, Lionakis MS, Molinolo AA, Gutkind JS. Genetic Identification of SEMA3F as an Antilymphangiogenic Metastasis Suppressor Gene in Head and Neck Squamous Carcinoma. Cancer Res. 2015;75(14):2937-48.
108. Liu Y, Li R, Yin K, Ren G, Zhang Y. The crucial role of SEMA3F in suppressing the progression of oral squamous cell carcinoma. Cell Mol Biol Lett. 2017;22:32.
109. Bielenberg DR, Klagsbrun M. Targeting endothelial and tumor cells with semaphorins. Cancer Metastasis Rev. 2007;26(3-4):421-31.
110. Parikh AA, Fan F, Liu WB, Ahmad SA, Stoeltzing O, Reinmuth N, et al. Neuropilin-1 in human colon cancer: expression, regulation, and role in induction of angiogenesis. Am J Pathol. 2004;164(6):2139-51.
111. Vasioukhin V, Degenstein L, Wise B, Fuchs E. The magical touch: genome targeting in epidermal stem cells induced by tamoxifen application to mouse skin. Proc Natl Acad Sci U S A. 1999;96(15):8551-6.
112. Gu C, Rodriguez ER, Reimert DV, Shu T, Fritzsch B, Richards LJ, et al. Neuropilin-1 conveys semaphorin and VEGF signaling during neural and cardiovascular development. Dev Cell. 2003;5(1):45-57.
113. Bielenberg DR, Seth A, Shimizu A, Pelton K, Cristofaro V, Ramachandran A, et al. Increased smooth muscle contractility in mice deficient for neuropilin 2. Am J Pathol. 2012;181(2):548-59.
114. Sekido Y, Bader S, Latif F, Chen JY, Duh FM, Wei MH, et al. Human semaphorins A(V) and IV reside in the 3p21.3 small cell lung cancer deletion region and demonstrate distinct expression patterns. Proc Natl Acad Sci U S A. 1996;93(9):4120-5.
115. Bielenberg DR, Shimizu A, Klagsbrun M. Semaphorin-induced cytoskeletal collapse and repulsion of endothelial cells. Methods Enzymol. 2008;443:299-314.
116. Patnaik A, LoRusso PM, Messersmith WA, Papadopoulos KP, Gore L, Beeram M, et al. A Phase Ib study evaluating MNRP1685A, a fully human anti-NRP1 monoclonal antibody, in combination with bevacizumab and paclitaxel in patients with advanced solid tumors. Cancer Chemother Pharmacol. 2014;73(5):951-60.
117. Sahay A, Molliver ME, Ginty DD, Kolodkin AL. Semaphorin 3F is critical for development of limbic system circuitry and is required in neurons for selective CNS axon guidance events. J Neurosci. 2003;23(17):6671-80.

118. Chang SE, Foster S, Betts D, Marnock WE. DOK, a cell line established from human dysplastic oral mucosa, shows a partially transformed non-malignant phenotype. Int J Cancer. 1992;52(6):896-902.
119. Momose F, Araida T, Negishi A, Ichijo H, Shioda S, Sasaki S. Variant sublines with different metastatic potentials selected in nude mice from human oral squamous cell carcinomas. J Oral Pathol Med. 1989;18(7):391-5.
120. Rheinwald JG, Beckett MA. Tumorigenic keratinocyte lines requiring anchorage and fibroblast support cultured from human squamous cell carcinomas. Cancer Res. 1981;41(5):1657-63.
121. Lin CJ, Grandis JR, Carey TE, Gollin SM, Whiteside TL, Koch WM, et al. Head and neck squamous cell carcinoma cell lines: established models and rationale for selection. Head Neck. 2007;29(2):163-88.
122. Cherng JM, Shieh DE, Chiang W, Chang MY, Chiang LC. Chemopreventive effects of minor dietary constituents in common foods on human cancer cells. Biosci Biotechnol Biochem. 2007;71(6):1500-4.
123. Lewis MP, Lygoe KA, Nystrom ML, Anderson WP, Speight PM, Marshall JF, et al. Tumour-derived TGF-beta1 modulates myofibroblast differentiation and promotes HGF/SF-dependent invasion of squamous carcinoma cells. Br J Cancer. 2004;90(4):822-32.
124. Lombardi AJ, Hoskins EE, Foglesong GD, Wikenheiser-Brokamp KA, Wiesmuller L, Hanenberg H, et al. Acquisition of Relative Interstrand Crosslinker Resistance and PARP Inhibitor Sensitivity in Fanconi Anemia Head and Neck Cancers. Clin Cancer Res. 2015;21(8):1962-72.
125. Foy JP, Tortereau A, Caulin C, Le Texier V, Lavergne E, Thomas E, et al. The dynamics of gene expression changes in a mouse model of oral tumorigenesis may help refine prevention and treatment strategies in patients with oral cancer. Oncotarget. 2016;7(24):35932-45.
126. Coma S, Amin DN, Shimizu A, Lasorella A, Iavarone A, Klagsbrun M. Id2 promotes tumor cell migration and invasion through transcriptional repression of semaphorin 3F. Cancer Res. 2010;70(9):3823-32.
127. Riese A, Eilert Y, Meyer Y, Arin M, Baron JM, Eming S, et al. Epidermal expression of neuropilin 1 protects murine keratinocytes from UVB-induced apoptosis. PLoS One. 2012;7(12):e50944.
128. Hu B, Guo P, Bar-Joseph I, Imanishi Y, Jarzynka MJ, Bogler O, et al. Neuropilin-1 promotes human glioma progression through potentiating the activity of the HGF/SF autocrine pathway. Oncogene. 2007;26(38):5577-86.
129. Benitah SA. Tumour biology: Skin-cancer stem cells outwitted. Nature. 2011;478(7369):329-30.
130. Grun D, Adhikary G, Eckert RL. NRP-1 interacts with GIPC1 and SYX to activate p38 MAPK signaling and cancer stem cell survival. Mol Carcinog. 2019;58(4):488-99.
131. Kujan O, Khattab A, Oliver RJ, Roberts SA, Thakker N, Sloan P. Why oral histopathology suffers inter-observer variability on grading oral epithelial dysplasia: an attempt to understand the sources of variation. Oral Oncol. 2007;43(3):224-31.
132. Kawakami T, Tokunaga T, Hatanaka H, Kijima H, Yamazaki H, Abe Y, et al. Neuropilin 1 and neuropilin 2 co-expression is significantly correlated with increased vascularity and poor prognosis in nonsmall cell lung carcinoma. Cancer. 2002;95(10):2196-201.

133. Gray MJ, Van Buren G, Dallas NA, Xia L, Wang X, Yang AD, et al. Therapeutic targeting of neuropilin-2 on colorectal carcinoma cells implanted in the murine liver. J Natl Cancer Inst. 2008;100(2):109-20.
134. Li M, Jiang D, Barnhart TE, Cao T, Engle JW, Chen W, et al. Immuno-PET imaging of VEGFR-2 expression in prostate cancer with (89)Zr-labeled ramucirumab. Am J Cancer Res. 2019;9(9):2037-46.
135. Migliozzi MT, Hida Y, Seth M, Brown G, Kwan J, Coma S, Panigrahy D, Adam RM, Banyard J, Shimizu A, Bielenberg DR. VEGF/VEGFR2 Autocrine Signaling Stimulates Metastasis in Prostate Cancer Cells. Current Angiogenesis. 2014;3(4):231-44.
136. Fung TM, Ng KY, Tong M, Chen JN, Chai S, Chan KT, et al. Neuropilin-2 promotes tumourigenicity and metastasis in oesophageal squamous cell carcinoma through ERK-MAPK-ETV4-MMP-E-cadherin deregulation. J Pathol. 2016;239(3):309-19.
137. Dallas NA, Gray MJ, Xia L, Fan F, van Buren G, 2nd, Gaur P, et al. Neuropilin-2-mediated tumor growth and angiogenesis in pancreatic adenocarcinoma. Clin Cancer Res. 2008;14(24):8052-60.
138. Zhang H, Vreeken D, Junaid A, Wang G, Sol W, de Bruin RG, et al. Endothelial Semaphorin 3F Maintains Endothelial Barrier Function and Inhibits Monocyte Migration. Int J Mol Sci. 2020;21(4).
139. Roy S, Bag AK, Singh RK, Talmadge JE, Batra SK, Datta K. Multifaceted Role of Neuropilins in the Immune System: Potential Targets for Immunotherapy. Front Immunol. 2017;8:1228.
140. Mendes-da-Cruz DA, Brignier AC, Asnafi V, Baleydier F, Messias CV, Lepelletier Y, et al. Semaphorin 3F and neuropilin-2 control the migration of human T-cell precursors. PLoS One. 2014;9(7):e103405.
141. Roy S, Bag AK, Dutta S, Polavaram NS, Islam R, Schellenburg S, et al. Macrophage-Derived Neuropilin-2 Exhibits Novel Tumor-Promoting Functions. Cancer Res. 2018;78(19):5600-17.
142. Rushing EC, Stine MJ, Hahn SJ, Shea S, Eller MS, Naif A, et al. Neuropilin-2: a novel biomarker for malignant melanoma? Hum Pathol. 2012;43(3):381-9.
143. Curreli S, Wong BS, Latinovic O, Konstantopoulos K, Stamatos NM. Class 3 semaphorins induce F-actin reorganization in human dendritic cells: Role in cell migration. J Leukoc Biol. 2016;100(6):1323-34.
144. Takamatsu H, Takegahara N, Nakagawa Y, Tomura M, Taniguchi M, Friedel RH, et al. Semaphorins guide the entry of dendritic cells into the lymphatics by activating myosin II. Nat Immunol. 2010;11(7):594-600.
145. Kochupurakkal NN, H. Demirci, G.; Macleaod, K.; Bielenberg, D.; Klagsbrun, M.; Briscoe, D. A Novel Immunomodulatory Function for Semaphorin3F and Neuropilin-2 in Allograft Rejection.: Abstract# 1491. THE WORLD TRANSPLANT CONGRESS: Transplatation 2014.